REALISTIC CALCULATIONS OF EXCITATIONS IN NUCLEAR MATTER

Thesis by

Nai-Hang Kwong

In Partial Fulfillment of the Requirements

for the Degree of

Doctor of Philosophy

California Institute of Technology

Pasadena, California

1983

(Submitted September 24, 1982)

ACKNOWLEDGEMENTS

I would like to express my gratitude to my advisers, Prof. S. Koonin and Prof. D. Sandler. Prof. Koonin introduced me to nuclear theory research and has always been a source of valuable insights and advice on methodology. Prof. Sandler initiated the project and has provided pivotal guidance throughout this work. The FHNC inputs have been provided by E. Krotscheck. His and Prof. J. Clark's advice on this subject is gratefully acknowledged. This work has benefitted from discussions with Y. Alhassid, H. Friedrichs, K. Sandhya-Devi, S. Trentalange and R. Williams. I am indebted to Mrs. A. Yeung and Mr. B. Cook for their help in typing.

Thanks are due to my parents and all my family for their encouragements.

This work was supported by National Science Foundation Grant #PHY77-21602A3 and teaching assistantships from the California Institute of Technology.

ABSTRACT

A numerical method has been developed to solve the RPA equation, exchange term included, in nuclear matter. The dynamic form factor $S(q,\omega)$ is extracted for several v4 and v6 phenomenological potentials, including the d1-potential of Gogny *et al*. The limits of validity of the long-wavelength (Landau) approximation and the often adopted local-kernel approximation are discussed. Substantial disagreements with the exact results are found for the latter. The method is then applied to solve a Jastrow-correlated extension of the RPA equation, using the hard-core OMY potential. Results of calculations performed in two-body cluster approximation and Fermi-Hypernetted-Chain (FHNC) approximation are compared. The two-body results predict an instability against density fluctuations, which disappears at the FHNC level. The validity and consequences of employing the FHNC effective potential within the self-consistent HF/RPA framework are discussed. Future developments include applying the method to other Fermi systems such as liquid ^{3}He and the microscopic calculation of Landau parameters.

CONTENTS

CONTENTS

(contd.)

Introduction

At near-zero temperature, the excitation spectra of many-body Fermi systems are often dominated by long-wavelength, high-energy peaks. Led by the E1 photonuclear resonance, the large number of giant resonances ($\lesssim$20 MeV) are now common phenomena in intermediate-energy nuclear spectroscopy [Sp81]. A travelling mode in liquid ^{3}He dubbed zero sound was predicted [La56] and eventually measured (speed $\approx$ 194 m/s) [Sk76]. The old example of plasma oscillation in the electron gas may also be cited [e.g. Fe71, Pi66]. Despite the vast difference in scale, they share a common physical interpretation: density fluctuations caused by the coherent motion of the constituent particles. Since all these systems are made up of fermions interacting via an essentially strong two-body force, a unified microscopic approach (i.e. in terms of the properties of the constituent particles and their interactions) to these fluctuations should and does exist. Basic to this framework are the so-called 'Random-Phase-Approximation (RPA)' equation and its extensions. The work reported here is devoted to a better understanding of realistic and phenomenological models through providing a reliable numerical method of solving these equations in infinite systems. An early overview can be found in [Sa80].

0.1. A Brief Overview of RPA

In its modern formulation, the RPA assumes that the lowest-energy states are predominantely individual excitations of single particles. The collective wave is a superposition of these excitations. In the thermodynamic limit, i.e., the limit where the number of particles A and the volume Ω grow very large with the density ρ kept constant, a linear integral eigenvalue problem (see (2.1)) over an oddly-shaped region (Figure 1) in momentum space has to be solved. The discrete part of the spectrum gives the frequencies of the collective modes, and

the eigenvectors give the amplitude of excitation from the ground state. The Green-function formalism [Fe71] has helped to derive the equation without much regard for the representation of the ground state. As a result, one has some freedom in choosing the single-particle wavefunction used in calculating the kernel. A typical term illustrates what this means :

$$<ph'|V(|\vec{r}_1-\vec{r}_2|)|hp'>$$

where p (particle) denotes the wavefunction of the excited particle and h (hole) is its wavefunction in the ground state. It is the virtual scattering amplitude between an excited particle and another particle in the medium. Because of the translational symmetry of the infinite system, the plane wave is often adequate for p and h. For the finite nucleus, however, such a simple choice as this does not exist, and one can only rely on the knowledge of the structure of the ground state. The successful independent-particle models such as the Hartree-Fock (HF) or the more phenomenological shell model are crucial here. As formulated by Thouless [Th60], the HF equations define the set of single-particle orbitals, a Slater determinant of which extremizes the energy expectation value. A particle being raised to an unoccupied orbital is then an 'elementary' excitation described above. This leads naturally to the time-dependent HF (TDHF) derivation of the RPA [Ro70, Ke76]. Constrained to a Slater determinant, the TDHF wavefunction is allowed to evolve via the full Hamiltonian. The RPA equation is obtained as the first order deviation from the static HF state. A third derivation in the nuclear context may also be mentioned. Called the Equation-of-Motion method [Ro70], it is based on an approximation that treats the product of a p-creating operator and an h-annihilating operator as a boson operator.

Since its introduction by Bohm and Pines [Bo51], the RPA has become the major tool in describing plasma oscillations and incorporating polarization

effects in the ground state of the electron gas [Fe71]. It has also helped to affirm the position of independent-particle models in nuclear physics by adequately describing various photoabsorption and particle-scattering resonances (but see next section). For low-temperature normal liquid ^{3}He, the closely-related Landau theory and its extensions also score phenomenological successes [Pi81]. This theory [La58] postulates that at very long wavelengths, the excitations can be described by weakly-interacting quasiparticles obeying Fermi statistics. Landau parametrized their dynamical properties by an effective mass and a set of interaction parameters -- the 'Landau parameters'. The theory conveniently correlates many dynamical and thermal data of ^{3}He, and the calculation of the parameters from microscopic quantities remains a major topic in many-body physics (see Chapter 5 for the connection with our work). Coherent density fluctuations come into the theory through the collisionless transport equation of these quasiparticles, which is formally identical to the RPA equation at the infinite-wavelength limit.

In this thesis we consider low-lying excitations in nuclear matter: a hypothetical infinite system composed of an equal number of protons and neutrons with the Coulomb force switched off. We study the relation between the underlying two-nucleon interaction and the properties of the excitations. Macroscopic models for the giant resonances exist in which one imposes boundary conditions on the travelling waves in this system [Bl80]. The determination of these boundary conditions is a separate problem and will not concern us here. Other many-body consequences of the two-nucleon force are often more directly manifest in nuclear matter. Most notably, the bulk-dependence of the binding energy and the interior density of heavy nuclei can be separated from finite-range effects. Microscopic studies of nuclear matter will also shed light on the physics of highly-compressed hadronic matter, supposedly produced in high-

energy heavy-ion collisions, and present in neutron stars. Because of its effectively lower density than ^{3}He (see below), it is often used to test many-body techniques, which is the case here. A bonus to the TDHF approach is its close relation with the stability problem of the HF state (see Chapter 1 and [Th60]). Recently there has been much interest in the possible occurrence of pion condensation in nucleonic matter. One mechanism of spontaneous generation of neutral pions is a large-amplitude wave in nuclear matter with both spin and isospin equal to 1 (spin-up protons oscillating against spin-down neutrons). If the dynamical parameters (strength and range of force ; mass) are allowed to vary, such a wave will start to appear at the onset of instability of the plane-wave state we choose for our HF state (Section 3.3).

0.2. The Problem of the Core

Choosing the plane waves of HF orbitals in the construction of the kernel presupposes a weak interaction. For nucleons and helium atoms, however, the free-space two-particle potentials (Lennard-Jones, Reid-soft-core, etc.) have strong, short-ranged, repulsive cores which make the above matrix element : $\langle ph' | V(|\vec{r}_1-\vec{r}_2|) | hp' \rangle$ either infinite or too large for RPA to be useful. This difficulty of RPA had precluded any theory for ^{3}He more fundamental than the Landau model. In the nuclear problem, the HF model has been preserved by the following arguments [Th72]. At low energy, the nucleons are kept apart and so nuclear properties are quite insensitive to the short-range details of the interaction. Furthermore, if only few-body observables,such as binding energy and electromagnetic transition strengths, are of interest, the many-body correlation effects can be packaged into the definitions of a set of effective single-particle wavefunctions and a weak effective two-body potential. The Pauli principle also helps by making it energetically costly for most particles to scatter virtually out

of their assigned orbitals. In short, the framework of weakly-interacting mean-fields may still be viable in calculating matrix elements of few-body operators for a many-nucleon system. To determine the effective interaction, one adopts a self-consistent approach. A parametrized form of the interaction is first chosen by physical insight and for convenience of calculation. The parameters are fitted, through HF, to ground state empirical data and are then used in RPA (and low-energy reaction) calculations. For infinite matter, there are relatively few data to use: typically binding energy, saturation density, isothermal compressibility etc.[†]. Fits to finite nuclei are more stringent, and satisfactory results are not obtained unless density-dependent and momentum-dependent terms are added to the interaction. These terms are supposed to mimic many-body correlations and dynamical effects due to the core. A density-dependent RPA (DDRPA) has also been developed to accommodate this extension. As mentioned above, satisfactory results have been obtained by these calculations.

Successful as these models are, they leave a gap in our theoretical edifice : can we really understand these density waves from the empirical data of two particles in free-space ? This problem of confronting the core directly has been taken up for years for the ground state of nuclear matter. Short of Monte Carlo simulations, two approaches have reached maturity [Cl79a, Da81] : the Brückner G-matrix theory and the Jastrow-variational theory. Both start with single-particle models and keep the bare, strong nucleon-nucleon force. In the Brückner theory (see [Be71] for a review), one expresses the correlations among plane-wave orbitals as a perturbation series in $V(ij)$ and resums approximately certain classes of diagrams to all orders. These classes are labelled by the

[†]The binding energy can be deduced from the volume term of the semi-empirical mass formula and the saturation density from elastic electron-scattering data (see, e.g., [Be71] and references therein). The compressibility can be deduced through the hydrodynamic model from the frequency of the density breathing mode of heavy nuclei [Bi80].

number of particles, starting from two, which are scattered virtually out of the Fermi sea. One can hope to achieve convergence relative to this parameter rapidly if the system is not too dense. Essentially this theory derives an effective DDHF interaction for the ground state which can then be used in DDRPA.

Our main concern is the RPA-extension of the Jastrow-variational theory [Cl80, Sa80, Ch82, Sa82]. This is achieved within the Correlated-Basis-Function framework initiated by Feenberg [Fe69]. For the ground state, one correlates the Fermi gas state by an A-body operator $F = \prod_{i<j}^{A} \mathrm{f}(r_{ij})$. The function f($r$), healing to 1 smoothly as r goes to infinity, modulates the overlap of two one-body wavefunctions. Specifically, f is set to zero where $V(ij)$ is infinite. Varying f to minimize the expectation value of the Hamiltonian, one hopes to obtain a useful upper bound to the ground-state energy of the system. This and other expectation values are calculated through cluster expansions, which are usually generated by the logarithm of the normalization integral, $\xi_0 = \langle \Phi_0 | F^2 | \Phi_0 \rangle$. We can write $\eta(r_{12}) = \mathrm{f}^2(r_{12}) - 1$ as a measure of the dynamical correlation. In configuration space, then

$$\ln \xi_0 = \ln \int d\vec{r}_1 \cdots d\vec{r}_A \; |\Phi_0|^2 \prod_{i<j}^{A} [1+\eta(r_{ij})]$$

Defining $\frac{A}{\nu} l(k_F r_{12}) = \sum_{k}^{k_F} e^{i\vec{k}\cdot\vec{r}_{12}}$, where ν is the degeneracy of the momentum orbital, we see that $|\Phi_0|^2$ is a series of products of two-body, Fermi-statistical correlations. The first terms are

$$1 - \frac{1}{\nu} \sum_{i<j} l^2(k_F r_{ij}) + \frac{1}{\nu^2} \sum_{i<j<k} l(k_F r_{ij}) l(k_F r_{jk}) l(k_F r_{ki}) \cdots$$

The structural similarity of ln ξ_0 with the configurational integral in the equilibrium theory of classical fluids (e.g. [Hu63]) prompted the development of

Fermi-extensions of resummation procedures based on integral equations there. Of these the most widely used are the so-called Fermi-Hypernetted-Chain (FHNC) equation [Kr75, Fa75]. The upper-bound property of $\xi_0^{-1}<\Phi_0|F\hat{H}F|\Phi_0>$ is very likely to be preserved by these approximate methods of evaluation [Cl79a]. The performance of both Brückner and Jastrow theories presumably depends on the ratio of the effective core-radius and the average separation of the particles. Their conclusions for nuclear matter seem to converge at present [Da81]. In ^{3}He this ratio is three times that of nuclear matter, disqualifying the Brückner theory as a feasible theory for the ground state and thus also for zero sound. For Jastrow-correlated RPA (CRPA), $|\Phi_0>$ is replaced by other Fermi-gas states and the same F is imposed. Despite the infinite character of the system, the theory must be based on a wavefunction model of the ground state. This makes the TDHF route the most natural way to generalize the RPA within this framework. The resulting equation is almost structurally the same as the ordinary RPA equation. Made up of A-body matrix elements instead of the two-body ones shown above, the kernel can again be evaluated to FHNC accuracy. The less dense system nuclear matter is used to test the theory.

We first solved the RPA and DDRPA equations with effective smooth potentials to obtain a general understanding of the behavior of the solution. While doing this, we found that the RPA equation for infinite matter had always been solved only in the Landau ($q \to 0$) limit, and often with the kernel averaged over the domain (Section 2.2). It is therefore also interesting to set the ranges of validity to these limits and study the finite-q behavior of the solution in terms of the inputs. For unity of exposition, we derive the RPA, DDRPA, CRPA equations through TDHF in Chapter 1. The method of solution is described in Chapter 2. Results using effective forces are reported in Chapter 3. Chapter 4 briefly summarizes the calculation of the CRPA-kernel to FHNC accuracy and presents

results from a hard-core potential, the OMY [Oh56]. The same FHNC inputs as those in [Kr81a] are used here. A final survey chapter of future plans concludes this report.

We would like to start addressing the problem of interpretation of the CRPA-eigenvectors here. We have to resort again to a parallel with RPA. In the TDHF derivation, this interpretive supplement is conventionally provided by a pedestrian version of linear response theory in the density matrix formalism [Bl80]. This we will paraphrase in wavefunction language and then generalize to serve CRPA (Section 1.4). In the next section, we formulate the general theory of linear response, with the exact eigenstates of the system's Hamiltonian, in a way that facilitates comparison with the (C)RPA-versions.

0.3. The Physics

All the results in this thesis, in situations where our representation of the ground state is stable, are to be interpreted within the framework laid down in this section.

Suppose the many-body system, with Hamiltonian $\hat{H}$, has been prepared in the distant past in the ground state $|\Psi_0>$. At $t = 0$, a weak, possibly time-dependent, external field is turned on, which couples to and excites the system. The perturbation operator for this 'probe' is denoted by $\lambda(t)\hat{P}$, where $\hat{P}$ is an operator in the system's Hilbert space and $\lambda(t)$, carrying the coupling to the probe, acts as the small parameter. The dynamical problem is then

$$i\hbar\frac{\partial}{\partial t}|\Psi(t)> = [\hat{H}+\lambda(t)\hat{P}\vartheta(t)]\ |\Psi(t)>, \tag{0.1}$$

$$|\Psi(t)> = |\Psi_0> e^{-i\frac{E_0}{\hbar}t}, \qquad t\leq 0,$$

where E_0 is the exact ground-state energy, and $\vartheta(t)$ is the step function. The *linear* response of the system is measured by the change to $O(\lambda)$ in the expectation values of the observables after $t = 0$. We will write this for an arbitrary operator $\hat{Q}$ below in a form readily linked to experimental quantities.

First $|\Psi(t)>$ can be written as $|\Psi(t)> = (|\Psi_0>+|\varphi(t)>)e^{-i\frac{E_0}{\hbar}t}$ with $<\varphi(t)|\Psi_0> = 0$ and $|\varphi(t)> = 0$ for $t = 0$. Substitution into (0.1) produces the equation for the 'response' part:

$$[i\hbar\frac{\partial}{\partial t}-(\hat{H}-E_0)]|\varphi(t)> = \lambda(t)\hat{P}\vartheta(t)|\Psi_0> + \lambda(t)\hat{P}\vartheta(t)|\varphi(t)>$$

Defining $|\tilde{\varphi}(\omega)> \equiv \int_0^\infty dt\ e^{i(\omega+i\eta)t}|\varphi(t)>$, we Fourier-analyze this equation. The positive, infinitesimal η guarantees convergence of the integral. An integration by parts with $|\varphi(0)> = 0$ gives $\int_0^\infty dt\ e^{i(\omega+i\eta)t}\frac{\partial}{\partial t}|\varphi(t)> = -i(\omega+i\eta)|\tilde{\varphi}(\omega)>$, and a convolution theorem holds for the last term. The result is

$$|\tilde{\varphi}(\omega)> = [\hbar\omega-(\hat{H}-E_0)+i\eta]^{-1}\left(\tilde{\lambda}(\omega)\hat{P}|\Psi_0>+\frac{1}{2\pi}\int_{-\infty}^{\infty}d\omega'\,\tilde{\lambda}(\omega-\omega'+i\eta)\hat{P}|\tilde{\varphi}(\omega')>\right).$$

While this is iteratively solvable, we are interested for the linear response only in the first term. Thus,

$$|\tilde{\varphi}(\omega)> = [\hbar\omega-(\hat{H}-E_0)+i\eta]^{-1}\tilde{\lambda}(\omega)\hat{P}|\Psi_0> \qquad (0.2)$$

We can see in retrospect that the omission of the normalization constant $<\Psi(t)|\Psi(t)> = 1+<\varphi(t)|\varphi(t)>$ introduces errors only of $O(\lambda^2)$. With (0.2), the first-order measured change for an arbitrary hermitian operator $\hat{Q}$ is

$$\delta_t<\hat{Q},\hat{P}> \equiv <\Psi(t)|\hat{Q}|\Psi(t)>-<\Psi(0)|\hat{Q}|\Psi(0)>$$

$$= \langle\Psi_0|\hat{Q}|\varphi(t)\rangle + \langle\varphi(t)|\hat{Q}|\Psi_0\rangle \qquad t > 0 .$$

The frequency response is

$$\tilde{\delta}_\omega\langle\hat{Q},\hat{P}\rangle \equiv \int_0^\infty dt\ e^{i(\omega+i\eta)t}\ \delta_t\langle\hat{Q},\hat{P}\rangle$$

$$= \langle\Psi_0|\hat{Q}|\tilde{\varphi}(\omega)\rangle + \langle\tilde{\varphi}(-\omega)|\hat{Q}|\Psi_0\rangle^\dagger$$

$$= \tilde{\lambda}(\omega)\langle\Psi_0|\hat{Q}\frac{1}{\hbar\omega-(\hat{H}-E_0)+i\eta}\hat{P}|\Psi_0\rangle - \tilde{\lambda}^*(-\omega)\langle\Psi_0|\hat{P}\frac{1}{\hbar\omega+(\hat{H}-E_0)+i\eta}\hat{Q}|\Psi_0\rangle$$

$$= \sum_n \tilde{\lambda}(\omega)\frac{\langle\Psi_0|\hat{Q}|\Psi_n\rangle\langle\Psi_n|\hat{P}|\Psi_0\rangle}{\hbar\omega-(E_n-E_0)+i\eta} - \tilde{\lambda}^*(-\omega)\frac{\langle\Psi_0|\hat{P}|\Psi_n\rangle\langle\Psi_n|\hat{Q}|\Psi_0\rangle}{\hbar\omega+(E_n-E_0)+i\eta} . \quad (0.3)$$

The last line is obtained by inserting the complete set of eigenstates of $\hat{H}$, $\hat{I} = \sum_n |\Psi_n\rangle\langle\Psi_n|$. A very important case is when $\lambda(t)$ is real ($\tilde{\lambda}(\omega) = \tilde{\lambda}^*(-\omega)$) and both $\hat{P}$ and $\hat{Q}$ are density operators, say, at $\vec{r}$ and $\vec{r}'$ respectively : $\hat{P} = \sum_{i=1}^{A}\delta(\vec{r}-\vec{r}_i)$, $\hat{Q} = \sum_{i=1}^{A}\delta(\vec{r}'-\vec{r}_i)$. For translationally invariant systems, we take the spatial Fourier transform $\frac{1}{\Omega}\int d(\vec{r}-\vec{r}')\ e^{i\vec{q}\cdot(\vec{r}-\vec{r}')}\tilde{\delta}_\omega\langle\hat{\rho}(\vec{r}'),\hat{\rho}(\vec{r})\rangle$, the ratio of which to $\tilde{\lambda}$ is the so-called 'retarded' particle-hole propagator :

$$\tilde{\Pi}^R(\omega,\vec{q}) = \frac{1}{\Omega}\sum_n \left(\frac{|\langle\Psi_n|\hat{\rho}(\vec{q})|\Psi_0\rangle|^2}{\hbar\omega-(E_n-E_0)+i\eta} - \frac{\langle\Psi_n|\hat{\rho}(-\vec{q})|\Psi_0\rangle|^2}{\hbar\omega-(E_n-E_0)+i\eta} \right) \quad (0.4)$$

Here $\hat{\rho}(\vec{q}) \equiv \sum_{i=1}^{A} e^{i\vec{q}\cdot\vec{r}_i}$ acts to change the system's momentum by $\vec{q}$. As is customarily pointed out, all the poles of $\tilde{\Pi}^R(\omega,\vec{q})$ lie just below the real axis of the

† Note that $\int_0^\infty dt\ e^{i(\omega+i\eta)t}\,|\varphi(t)\rangle^\dagger = [\int_0^\infty dt\ e^{i(-\omega+i\eta)t}\,|\varphi(t)\rangle]^\dagger = \langle\tilde{\varphi}(-\omega)|$.

complex ω-plane. When we transform back to the time domain, the contour of the integral $\frac{1}{2\pi}\int_{-\infty}^{\infty} d\omega\, e^{-i\omega t}\tilde{\Pi}^R(\omega,\vec{q})$ can be completed in the lower(upper) half-plane when $t>0$ ($t<0$). The integral thus vanishes for negative t, and we denote it by $\vartheta(t)\Pi(t,\vec{q})$. This, in convolution with $\tilde{\lambda}(\omega)$, gives the differential expectation value :

$$\delta_t\langle\hat{\rho}(\vec{r}'),\hat{\rho}(\vec{r})\rangle = \int d\vec{q}\; e^{i\vec{q}\cdot(\vec{r}'-\vec{r})}\int_0^{\infty} dt'\,\vartheta(t-t')\Pi(t-t',\vec{q})\lambda(t')\,.$$

At any t, $\delta_t\langle\hat{\rho}(\vec{r}'),\hat{\rho}(\vec{r})\rangle$ collects the effects of only that part of $\lambda(t)$ in the past; hence the name 'retarded' for $\tilde{\Pi}^R(\omega,\vec{q})$.

The imaginary part of $\tilde{\Pi}^R$ is, up to a constant, the double-differential cross-section of the inelastic scattering of the probe off the medium [Fe71]. Here q is the momentum transfer and $\hbar\omega$ is the energy absorbed. In the literature, it is often called the dynamic form factor :

$$S(q,\omega) = \frac{1}{\hbar A}\sum_n |\langle\Psi_n|\hat{\rho}(\vec{q})|\Psi_0\rangle|^2\delta(\hbar\omega-E_n+E_0)$$

since the proportionality constant relating $S(q,\omega)$ and the cross-section is essentially the elastic scattering cross-section of the probe off one particle in free-space. In photoabsorption reactions, an important observable is the total cross-section [Sp81], which in heavy nuclei is proportional to the low-q limit of the ratio of the energy-weighted sum of the dynamic form factor to q^2 : $\frac{1}{q^2}\sum_n (E_n-E_0)|\langle\Psi_n|\hat{\rho}(\vec{q})|\Psi_0\rangle|^2$. This expression can be calculated as a ground-state expectation value by inserting E_n-E_0 into the matrix element and replacing it by $\hat{H}$. Invoking the closure property of the excited states, we write it as

$$\frac{1}{2A}\langle\Psi_0|[\hat{\rho}(-\vec{q}),[\hat{H},\hat{\rho}(\vec{q})]]|\Psi_0\rangle = \sum_n (E_n-E_0)|\langle\Psi_n|\hat{\rho}(\vec{q})|\Psi_0\rangle|^2\,. \qquad (0.5)$$

The double commutator of the kinetic energy with $\hat{\rho}(q)$ gives $\frac{\hbar^2 A}{2m}$. Additional contributions will be obtained if both the potential energy and the excitation operator contain spin (isospin) operators. In this case, the double commutator is usually written as $\frac{\hbar^2 A}{2m}(1+\kappa)$ where κ is called an enhancement factor. Started by Levinger and Bethe [Le51] the calculation of this enhancement factor for the E1-photoabsorption resonance still remains an ongoing problem, the most recent attempt being taken in the Variational approach [Sa79].

0.4. The Ideal Fermi Gas at Zero Temperature

The success of independent-particle models convinces one of the prominent role played by statistics in the low-lying states of Fermi systems. For infinite systems at least, then, the ideal Fermi gas will serve as a useful reference point for discussing the effects of the interaction. Exactly solvable, it will also help to evaluate numerical procedures in Chapter 2. In what follows, we summarize the calculation of the dynamic form factor for this system as treated for example, in [Fe71].

Any eigenstate of the Fermi gas is defined by a Slater determinant of the set of occupied plane-wave orbitals. The energy is equal to $\sum_{i=1}^{A} \frac{\hbar^2 k_i^2}{2m}$, where $\vec{k}_i$ is the momentum of the i-th particle. With periodic boundary conditions, the 'distance' between two states is $\Delta\vec{k} = \frac{(2\pi)^3}{\Omega}$. Therefore, in the thermodynamic limit, the ground state is represented in momentum space by a spherical continuum -- the so-called Fermi sea -- of radius $k_F = \left(\frac{6\pi^2\rho}{\nu}\right)^{\frac{1}{3}}$. In second quantization, since $\langle \vec{k} | e^{i\vec{q}\cdot\vec{r}} | \vec{l} \rangle = \delta_{\vec{k},\vec{l}+\vec{q}}$, we have $\hat{\rho}(\vec{q}) = \sum_{\vec{k}} a^{\dagger}_{\vec{k}+\vec{q}} a_{\vec{k}}$. Thus $\hat{\rho}(\vec{q})$ can excite only those states in which exactly one particle, when given an extra momentum $\vec{q}$, is

expelled from the Fermi sea. A state may then be labelled by the 'active' orbital, with excitation energy $E_{\vec{k}}-E_0=\frac{\hbar^2}{2m}(|\vec{k}+\vec{q}|^2-k^2)=\frac{\hbar^2}{2m}(q^2+2\vec{k}\cdot\vec{q})$ and amplitude $\langle\Psi_{\vec{k}}|\hat{\rho}(\vec{q})|\Psi_0\rangle=1$. These yield

$$S(q,\omega)=\frac{\nu}{A}\sum_{\vec{k}}\vartheta(|\vec{k}+\vec{q}|-k_F)\vartheta(k_F-k)\delta(\hbar\omega-E_{\vec{k}}+E_0)$$

Defined by the theta functions, the excitable region is a polar cap of thickness q as shown in Figure 1. Replacing the sum by an integral, $\sum_{\vec{k}}\to\frac{\Omega}{(2\pi)^3}\int d\vec{k}$ and choosing cylindrical coordinates with the z-axis parallel to $\vec{q}$, we have, for $q<2k_F$,

$$S(q,\omega)=\frac{\nu}{(2\pi)^2\rho}\int_{-\frac{q}{2}}^{k_F}dk_z\ \frac{1}{2}\int_{\max(k_F^2-(q+k_z)^2,0)}^{k_F^2-k_z^2}dk_\rho^2\ \frac{m}{\hbar^2 q}\delta\left(\frac{m\omega}{\hbar q}-\frac{q}{2}-k_z\right)$$

This integral is clearly the cross-sectional area of the cap at a certain $k_z=\frac{m\omega}{\hbar q}-\frac{q}{2}$, or the number of degenerate states at that frequency ω allowed by the Pauli principle. The final result is more compactly expressed in the dimensionless variable $\lambda\equiv\frac{m}{\hbar^2 k_F q}\hbar\omega$.

$$S(q,\omega)=\begin{cases}\frac{3}{2}\cdot\frac{m}{\hbar^2 k_F^2}\lambda & 0<\lambda<1-\frac{q}{2k_F}\\ \frac{3}{4}\cdot\frac{m}{\hbar^2 q k_F}\left[1-\left(\lambda-\frac{q}{2k_F}\right)^2\right] & 1-\frac{q}{2k_F}<\lambda<1+\frac{q}{2k_F}\\ 0 & \text{elsewhere}\end{cases}\qquad(0.6)$$

This function is displayed in Figure 4 (solid curve with a kink) for a typical value of q : $q=.1k_F$ with $k_F=1.4$ fm^{-1}.

Chapter 1

In this chapter, we sketch the derivation of the ordinary Random-Phase Approximation (RPA) equation, the density-dependent RPA (DDRPA) equation, and the Jastrow-correlated RPA (CRPA) equation. The derivations are general at this stage, and occasional specializations to infinite systems are stated. Normalization condition, prototype linear response functions and sum rules are also derived.

1.1. The Derivation of The RPA Equation

As advertised in the introductory chapter, we will proceed within the TDHF framework. We choose as our starting point the currently fashionable 'time-dependent variational principle' [Ke76] for its formal advantages. The principle is formulated as follows : Let us take the 'action'

$$S = \int_{t_1}^{t_2} L\,(\Psi,\Psi^*)\,dt\,,$$

where the 'Lagrangian' is

$$L = \langle\Psi|\, i\hbar\frac{\partial}{\partial t} - \hat{H}\,|\Psi\rangle.$$

S must be stationary with respect to variation of $|\Psi\rangle$ ($\langle\Psi|$) with fixed endpoints t_1 and t_2 :

$$\delta S = 0. \tag{1.1}$$

With the space of variation of $|\Psi\rangle$ defined, standard calculus-of-variation procedures will bring us to an Euler-Lagrange (EL) equation

$$\frac{d}{dt}\left(\frac{\delta L}{\delta|\dot{\Psi}\rangle}\right) = \frac{\delta L}{\delta|\Psi\rangle},$$

and its adjoint. If this space is the full many-body Hilbert space, the EL equation is just the many-body Schrödinger equation

$$i\hbar\frac{\partial}{\partial t}|\Psi>=\hat{H}\,|\Psi>.$$

As stressed in [Ke76], various approximate solutions to the Schrödinger equation can then be considered as the result of applying (1.1) with $|\Psi>$ parametrized in terms of a few time-dependent parameters. The TDHF equation is the EL equation for one such parametrization in which $|\Psi>$ is allowed to vary in the set of Slater determinants of single-particle states. If each particle has n degrees of freedom, this approximation brings an nA-dimensional differential equation into a set of A coupled, non-linear, n-dimensional equations. In the RPA limit, these equations are further reduced to linear ones. Each of the modified RPA's listed above (i.e. DDRPA and CRPA) will also come from (1.1) with a similar parametrization, which will be stated below.

In the ordinary RPA, we take as a basis a set of orthonormal single-particle states (orbitals), to be specified later, and fill A of these with identical fermions. We denote the resulting normalised Slater determinant by $|\Phi_0>$. Then by Thouless' theorem [Th60], any vector $|\Phi>$ in the space of Slater determinants of A arbitrary single particle orbitals not orthogonal to $|\Phi_0>$ (i.e. the space of variation of the TDHF parametrization) can be written as

$$|\Phi(t)> = \exp\left(\sum_{ph} C_{ph}(t)a_p^\dagger a_h\right)|\Phi_0>. \qquad (1.2)$$

The labels p and h refer to particle (unoccupied) and hole (occupied) orbitals, respectively. The basic idea is that each of the orbitals that make up $|\Phi>$ can be written as a linear combination of the basis orbitals we have chosen at the beginning. Thus

$$|\Phi> = \prod_{\alpha=1}^{A} a_\alpha^\dagger \, |vacuum> = \prod_{\alpha=1}^{A} \left[\sum_{h=1}^{A} f_{\alpha h} a_h^\dagger + \sum_{p=A+1}^{\infty} f_{\alpha p} a_p^\dagger \right] |vacuum>.$$

Since any term with more than one identical creation operators vanishes, the expression reduces to a superposition of (multi-) particle-hole states with respect to our basis. The same is true of (1.2). The identification of the two expressions then works out in such a way that the C_{ph}'s are consistently and uniquely determined. If $|\Phi_0>$ is some representation of the ground state, the form (1.2) is particularly useful for the anticipated reduction to the RPA, which will then be linear in the C_{ph}'s.

Now we invoke the variational principle (1.1). With (1.2), the Lagrangian becomes a function of $C_{ph}(t)$, $C_{ph}^*(t)$, $\dot{C}_{ph}(t)$, $\dot{C}_{ph}^*(t)$:

$$L\,(C_{ph}, C_{ph}^*, \dot{C}_{ph}, \dot{C}_{ph}^*) = <\Psi(t)\,|\, i\hbar \frac{\partial}{\partial t} - \hat{H}\,|\,\Psi(t>,$$

where $\quad |\Psi(t)> = \xi^{-\frac{1}{2}} |\,\Phi(t)>,$

and $\quad |\Phi(t)> = \exp\,(\sum_{ph} C_{ph}(t) a_p^\dagger a_h)\,|\Phi_0> \;,\; \xi = <\Phi(t)\,|\,\Phi(t)>.$

Straightforward algebra gives

$$<\Psi(t)\,|\,\frac{\partial}{\partial t}|\,\Psi(t)> = \frac{1}{2}\xi^{-1}\left[<\Phi\,|\,\frac{\partial \Phi}{\partial t}> - <\frac{\partial \Phi}{\partial t}\,|\,\Phi>\right],$$

and, with

$$|\,\frac{\partial \Phi}{\partial t}> = \sum_{ph} \dot{C}_{ph} a_p^\dagger a_h \,|\,\Phi(t)>,$$

we extract the explicit dependence of L on $\dot{C}_{ph}\,(\dot{C}_{ph}^*)$:

$$L = \frac{i\hbar}{2}\xi^{-1} \sum_{ph} \left[\dot{C}_{ph} <\Phi\,|\,a_p^\dagger a_h\,|\,\Phi> + \text{c.c.}\right] - \xi^{-1} <\Phi\,|\,\hat{H}\,|\,\Phi>.$$

In terms of these new dynamical variables, the Euler-Lagrange equations are

$$\frac{d}{dt}\left(\frac{\partial L}{\partial \dot{C}_{ph}}\right) = \frac{\partial L}{\partial C_{ph}} \; ; \; \frac{d}{dt}\left(\frac{\partial L}{\partial \dot{C}^{*}_{ph}}\right) = \frac{\partial L}{\partial C^{*}_{ph}}. \tag{1.3}$$

We need to look at only one of these as the other is its complex conjugate. The second equation, when expanded , reads

$$i\hbar \sum_{p'h'} \dot{C}_{p'h'} \left[<\Phi | a_h^{\dagger} a_p \, a_{p'}^{\dagger} a_{h'} | \Phi> - \xi^{-1} <\Phi | a_{p'}^{\dagger} a_{h'} | \Phi> <\Phi | a_h^{\dagger} a_p | \Phi> \right] \tag{1.3a}$$

$$= <\Phi | a_h^{\dagger} a_p \hat{H} | \Phi> - \xi^{-1} <\Phi | a_h^{\dagger} a_p | \Phi> <\Phi | \hat{H} | \Phi>,$$

which is actually a form of the TDHF equation. We now expand the equation in terms of the C_{ph}'s and $\dot{C}_{ph}$'s and retain terms only up to first order. Two simplifying facts are: $<\Phi_0 | a_p^{\dagger} a_h | \Phi_0> = 0$ and $\xi = <\Phi|\Phi> = 1 + O(C^2)$. The zeroth-order equation is easily seen to be

$$<\Phi_0 | a_h^{\dagger} a_p \hat{H} | \Phi_0> = 0, \tag{1.4}$$

which, as we shall see, determines $|\Phi_0>$ to be the static Hartree-Fock state. The linear equation is, again by inspection,

$$i\hbar \dot{C}_{ph} = \sum_{p'h'} <\Phi_{ph} | \hat{H} | \Phi_{p'h'}> C_{p'h'} - <\Phi_0 | \hat{H} | \Phi_0> C_{ph} + \sum_{p'h'} <\Phi_{php'h'} | \hat{H} | \Phi_0> C^{*}_{p'h'}. \tag{1.5}$$

From here on, $|\Phi_{ph}> \equiv a_p^{\dagger} a_h |\Phi_0>$, $|\Phi_{php'h'}> \equiv a_p^{\dagger} a_h \, a_{p'}^{\dagger} a_{h'} |\Phi_0>$. The periodic, time-reversal-symmetric solutions†, or 'normal modes', are usually obtained by inserting the ansatz

$$C_{ph}(t) = X_{ph} e^{-i\omega t} + Y^{*}_{ph} e^{i\omega t}, \tag{1.6}$$

†By this we mean the solution set is invariant under $t \rightarrow -t$ in contrast with the Tamm-Dancoff solutions; it is equivalent to stating $X_{ph}(\omega) = Y^{*}_{ph}(-\omega)$.

and separating the terms involving $e^{i\omega t}$ from those with $e^{-i\omega t}$. More rigorous is, of course, Fourier-transforming (1.5), in which case, $X_{ph}(\omega) = C_{ph}(\omega)$ and $Y_{ph}(\omega) = C^{*}_{ph}(-\omega)$. Either way, an eigenvalue problem emerges :

$$\hbar\omega X_{ph} = \sum_{p'h'} \left[<\Phi_{ph}|\hat{H}|\Phi_{p'h'}> - \delta_{pp'}\delta_{hh'}<\Phi_0|\hat{H}|\Phi_0> \right] X_{p'h'} + \sum_{p'h'} <\Phi_{php'h'}|\hat{H}|\Phi_0> Y_{p'h'}$$

$$-\hbar\omega Y^{*}_{ph} = \sum_{p'h'} \left[<\Phi_{ph}|\hat{H}|\Phi_{p'h'}> - \delta_{pp'}\delta_{hh'}<\Phi_0|\hat{H}|\Phi_0> \right] Y^{*}_{p'h'} + \sum_{p'h'} <\Phi_{php'h'}|\hat{H}|\Phi_0> X^{*}_{p'h'}$$

The coefficients can be expressed more explicitly by taking the usual form of the Hamiltonian:

$$\hat{H} = \sum_{k,l=1}^{\infty} <k|T|l> a_k^{\dagger} a_l + \frac{1}{2} \sum_{klmn=1}^{\infty} <kl|V|mn> a_l^{\dagger} a_k^{\dagger} a_m a_n .$$

When the tedious anticommutator algebra is carried out, we have the following equation :

$$\begin{bmatrix} A & B \\ B^{*} & A^{*} \end{bmatrix} \begin{bmatrix} X \\ Y \end{bmatrix} = \hbar\omega \begin{bmatrix} X \\ -Y \end{bmatrix}, \qquad (1.7)$$

where X, Y are column vectors with elements X_{ph} and Y_{ph} respectively and A, B are matrices with

$$A_{ph,p'h'} = <\Phi_{ph}|\hat{H}|\Phi_{p'h'}> - \delta_{pp'}\delta_{hh'}<\Phi_0|\hat{H}|\Phi_0> = (\varepsilon_p - \varepsilon_h)\delta_{pp'}\delta_{hh'} + <hp'|V|ph'>_a$$

$$B_{ph,p'h'} = <\Phi_{php'h'}|\hat{H}|\Phi_0> = <pp'|V|hh'>_a$$

$$\varepsilon_p = <p|T|p> + \sum_{j \varepsilon K_F} <pj|V|pj>_a \quad \text{etc.}$$

and $\quad |ij>_a \equiv |ij> - |ji>$.

K_F is the set of occupied orbitals in the state $|\Phi_0>$. Some obvious properties of the equation are: (i) A is hermitian and B is symmetric, implying $\begin{pmatrix} A & B \\ B^* & A^* \end{pmatrix}$ is hermitian; (ii) taking the complex conjugate of (1.7) shows that if ω is an eigenvalue with eigenvector $\begin{pmatrix} X \\ Y \end{pmatrix}$ then $-\omega^*$ is also an eigenvalue, with eigenvector $\begin{pmatrix} Y^* \\ X^* \end{pmatrix}$. ε_p will be recognised below as the HF energy of a particle in state p. (1.7) is the RPA equation.

Let us digress to say more on static HF and its relationship with RPA. Equation (1.4) expands to

$$<p\,|\,T\,|h> + \sum_{j\varepsilon K_F} <pj\,|\,V\,|hj>_a = 0\,.$$

This separates the particle states from the hole states, and independent diagonalizations in the two subspaces lead to the more usual form of the static HF equations, as promised:

$$<h\,|\,T\,|h'> + \sum_{j\varepsilon K_F} <hj\,|\,V\,|h'j>_a = \varepsilon_h <h\,|h'>$$

$$<p\,|\,T\,|p'> + \sum_{j\varepsilon K_F} <pj\,|\,V\,|p'j>_a = \varepsilon_p <p\,|p'>.$$

$|\Phi_0>$ is the Slater determinant of the h (hole) states. Through the average interaction with all other particles, a particle in orbital p acquires an energy ε_p. The total energy is

$$E_0 = <\Phi_0|\,\hat{H}\,|\Phi_0> = \sum_{j\varepsilon K_F} <j\,|\,T\,|j> + \frac{1}{2}\sum_{j,k\varepsilon K_F} <jk\,|\,V\,|jk>_a\,.$$

The factor ½ avoids double-counting in the double sum over all orbitals. The physical content of the static HF state is more apparent if we derive (1.4) from a

time-independent variational principle. For this principle, the space of variation again contains only Slater determinants (1.2) with the time dependence removed. $|\Phi_0>$ is required to minimize the energy expectation value $E = \xi^{-1}<\Phi|\hat{H}|\Phi>$. Mathematically this condition says, at $|\Phi> = |\Phi_0>$,

$$\frac{\partial E}{\partial C_{ph}} = 0 \quad , \quad \frac{\partial E}{\partial C^{*}_{ph}} = 0, \qquad \text{for all p,h,} \tag{1.8a}$$

and the matrix

$$\begin{bmatrix} \dfrac{\partial^2 E}{\partial C^{*}_{ph} \partial C_{p'h'}} & \dfrac{\partial^2 E}{\partial C^{*}_{ph} \partial C^{*}_{p'h'}} \\ \dfrac{\partial^2 E}{\partial C_{ph} \partial C_{p'h'}} & \dfrac{\partial^2 E}{\partial C_{ph} \partial C^{*}_{p'h'}} \end{bmatrix} \tag{1.8b}$$

must be positive-definite. Carrying out the differentiations shows that (1.8a) is just (1.4) and the HF 'stability' matrix (1.8b) is nothing but that appearing on the LHS of the RPA equation (1.7). We can then anticipate the following theorem [Th61]: If the matrix (1.8b) is (semi-) positive-definite, then all eigenvalues of the RPA equation are real. Thus, in analogy to the classical small-oscillation problem, we can imagine an energy surface in the space of Slater determinants, with the solutions of the static HF equation being the 'flat' points on the surface. The stability condition (1.8b) picks out the relative minima to be approximations to the true ground state. Then by the above theorem, we can have stable small-amplitude oscillations (RPA) around these minima. The double-matrix structure of the RPA, in contrast to that of the classical problem, can be traced back to the fact that the Schrödinger equation contains only a first-order time derivative.

In principle, our interpretation of the RPA states as low-lying excitations is only valid when they are built around the absolute minimum among all stable solutions to the HF equation. Nevertheless considerations have been almost

exclusively confined to the most easily found solution. For infinite systems, because of the translational symmetry, it is trivially checked that the set of plane-wave orbitals $\{\Omega^{-\frac{1}{2}} e^{i\vec{k}\cdot\vec{r}}\}$ satisfies the HF equation. $|\Phi_0\rangle$ is then the 'Fermi sea' with the orbitals with lowest momenta filled†. In this study, we will use this state whenever it is stable. One last point: Our $|\Phi_0\rangle$ is constrained to be a HF state (and ε_p (ε_h) to be HF single-particle energies) because we chose the TDHF path. Indeed, if we take away the time dependence of $|\Phi\rangle$ in the original variational principle (1.1), the EL equation will become

$$0 = \frac{\partial L}{\partial C^*_{ph}} = \langle\Phi_0|a_h^\dagger a_p \hat{H}|\Phi_0\rangle.$$

In the Green function approach [Fe71], for example, we do not have to specify exactly our model for the ground state. We have complete freedom in choosing the amount of correlation, arising from interactions with the medium because we put in the single-particle energies $\varepsilon_p(\varepsilon_h)$. The HF is but one of these choices.

As mentioned in the Introduction, a Slater determinant is a good approximant to the many-body wave function only when the interaction potential $\hat{V}$ is weak and smooth. Indeed, with a smooth spatial matter distribution, a strong $V(ij)$ will give unrealistically large values for the matrix elements $\langle ph'|V|hp'\rangle$ etc. as well as $\langle\Phi_0|\hat{H}|\Phi_0\rangle$. In other words, the wavefunctions of two particles should not overlap too much in regions where the potential is strongly repulsive*. Two ways to handle this problem were also mentioned : density-dependent RPA and Jastrow-correlated RPA. We will derive both versions below, in parallel to the ordinary RPA as much as possible. Accordingly, only additional structures will be stressed.

† It turns out that, in most cases, the orbitals with the lowest momenta are also those with the lowest single-particle energies.

* An alternative is to have a localised particle distribution, like a solid, which, however, generates a zero-point kinetic energy unbearably large for quantum liquids.

1.2. The Density-Dependent RPA

The Lagrangian for DDRPA is

$$L = \langle\Psi(t)|i\hbar\frac{\partial}{\partial t} - \hat{H}|\Psi(t)\rangle,$$

where $\hat{H} = \hat{T} + \hat{V}$, $\hat{V} = \sum_{i<j} V(\vec{r}_{ij}, \rho(\vec{R}_{ij}))$, $\vec{R}_{ij} = \frac{1}{2}(\vec{r}_i + \vec{r}_j)$. $|\Psi(t)\rangle$ is the same as defined previously. $\rho(\vec{R})$ is the expectation value of the density at $\vec{R}$ in state $|\Psi(t)\rangle$:

$$\rho(\vec{R}) = \langle\Psi(t)|\sum_{j=1}^{A}\delta(\vec{r}_j - \vec{R})|\Psi(t)\rangle .$$

We assume that the density does not change appreciably over the very short range of the density-dependent part of the force. For specificity, we just take the value of the density at the center-of-mass of the two particles. In terms of a single-particle basis, which we choose to be the same as that for the parametrization (1.2) of $|\Phi(t)\rangle$, $\rho(\vec{R})$ can be written as

$$\rho(\vec{R}) = \sum_{kl}\rho_{kl}(\vec{R})\langle\Psi(t)|a_k^\dagger a_l|\Psi(t)\rangle$$

where $\rho_{kl}(\vec{R}) = \langle k|\delta(\vec{r} - \vec{R})|l\rangle$. This C_{ph}-dependence of $\hat{H}$ brings two extra terms to $\frac{\partial L}{\partial C_{ph}^*}$, the so-called rearrangement terms, giving the EL equation as:

$$i\hbar\sum_{p'h'}\dot{C}_{p'h'}\left[\langle\Phi|a_h^\dagger a_p\, a_{p'}^\dagger a_{h'}|\Phi\rangle - \xi^{-1}\langle\Phi|a_{p'}^\dagger a_{h'}|\Phi\rangle\langle\Phi|a_h^\dagger a_p|\Phi\rangle\right]$$

$$= \langle\Phi|a_h^\dagger a_p\hat{H}|\Phi\rangle - \xi^{-1}\langle\Phi|a_h^\dagger a_p|\Phi\rangle\langle\Phi|\hat{H}|\Phi\rangle + \xi^{-1}\sum_{kl}\langle\Phi|\delta_{kl}\hat{V}|\Phi\rangle\langle\Phi|a_h^\dagger a_p\, a_k^\dagger a_l|\Phi\rangle$$

$$- \xi^{-2}\sum_{kl}\langle\Phi|\delta_{kl}\hat{V}|\Phi\rangle\langle\Phi|a_k^\dagger a_l|\Phi\rangle\langle\Phi|a_h^\dagger a_p|\Phi\rangle.$$

$\delta_{st}\,\hat{V}$ is roughly the variation of $\hat{V}$ relative to the density fluctuation due to the transfer of a particle from orbital t to orbital s :

$$\delta_{st}\,\hat{V} \equiv \frac{1}{2}\sum_{klmn}^{\infty} <kl\,|\,\frac{\partial V}{\partial \rho}(\vec{r}_{12},\rho(\vec{R}_{12}))\rho_{st}(\vec{R}_{12})\,|\,mn>a_l^{\dagger}a_k^{\dagger}a_m a_n\ .$$

It is, implicitly through ρ, an operator-valued 'functional' of $|\Phi(t)>$. In the resulting equations of linearization below, $\delta_{st}\,\hat{V}\equiv\delta_{st}\,\hat{V}|_{|\Phi(t)>=|\Phi_0>}$ is to be understood. The zeroth-order approximant is the so-called density-dependent HF (DDHF):

$$<\Phi_0|\,a_h^{\dagger}a_p\,\hat{H}\,|\Phi_0> + <\Phi_0|\,\delta_{ph}\,\hat{V}\,|\Phi_0> = 0$$

which is readily shown to be (recalling that $\rho_{ph}(\vec{R}) = <p\,|\,\delta(\vec{r}-\vec{R})\,|\,h>$)

$$<p\,|\,T\,|h>+\sum_{k\varepsilon K_F}<pk\,|\,V\,|hk>_a+<p\,|\sum_{k,l\varepsilon K_F}<kl\,|\,\frac{\partial V}{\partial\rho}(\vec{r}_{12},\rho(\vec{R}_{12}))\delta(\vec{r}-\vec{R}_{12})\,|\,kl>_a\,|h> = 0$$

Again, diagonalization gives

$$<p\,|\,T\,|p'>+\sum_{k\varepsilon K_F}<pk\,|\,V\,|p'k>_a+\sum_{k,l\varepsilon K_F}<kl\,|\,\frac{\partial V}{\partial\rho}\rho_{pp'}\,|kl>_a = <p\,|p'>\varepsilon_p\,,\quad \text{etc.}\,, \qquad (1.9)$$

which is solved by a basis of plane waves for infinite matter. The first order DDRPA equation is

$$\begin{aligned} i\hbar\dot{C}_{ph} = \sum_{p'h'}\Big[& <\Phi_{ph}\,|\,\hat{H}\,|\,\Phi_{p'h'}>+<\Phi_0|\,\delta_{ph}\,\hat{V}\,|\,\Phi_{p'h'}>+<\Phi_{ph}\,|\,\delta_{p'h'}\,\hat{V}\,|\Phi_0>+<\Phi_0|\,\delta^2_{h'p',ph}\,\hat{V}\,|\Phi_0> \\ & -\delta_{pp'}\delta_{hh'}<\Phi_0|\,\hat{H}\,|\Phi_0>+\delta_{hh'}<\Phi_0|\,\delta_{pp'}\,\hat{V}\,|\Phi_0>-\delta_{pp'}<\Phi_0|\,\delta_{h'h}\,\hat{V}\,|\Phi_0>\Big]\,C_{p'h'} \\ & +\sum_{p'h'}\Big[<\Phi_{php'h'}\,|\,\hat{H}\,|\,\Phi_0>+<\Phi_{p'h'}\,|\,\delta_{ph}\,\hat{V}\,|\,\Phi_0>+<\Phi_{ph}\,|\,\delta_{p'h'}\,\hat{V}\,|\,\Phi_0> \\ & +<\Phi_0|\,\delta_{p'h',ph}\,\hat{V}\,|\,\Phi_0>\Big]\,C^{*}_{p'h'}\,, \end{aligned}$$

where $\delta^2_{p'h',ph}\hat{V} \equiv \frac{1}{2}\sum_{klmn}^{\infty} <kl \mid \frac{\partial^2 V}{\partial \rho^2}\rho_{p'h'}\rho_{ph} \mid mn> a_l^\dagger a_k^\dagger a_m a_n$.

With the previous ansatz, we again get a matrix equation, with

$$A_{ph,p'h'} = (\varepsilon_p - \varepsilon_h)\delta_{pp'}\delta_{hh'} + <hp' \mid V \mid ph'>_a + U_R(ph, h'p')$$

$$B_{ph,p'h'} = <pp' \mid V \mid hh'>_a + U_R(ph, p'h'),$$

where $U_R(ph, p'h') \equiv$

$$\sum_{k\varepsilon K_F}\left[<p'k \mid \frac{\partial V}{\partial \rho}\rho_{ph} \mid h'k>_a + <pk \mid \frac{\partial V}{\partial \rho}\rho_{p'h'} \mid hk>_a\right] + \frac{1}{2}\sum_{k,l\varepsilon K_F} <kl \mid \frac{\partial^2 V}{\partial \rho^2}\rho_{p'h'}\rho_{ph} \mid kl>_a ,$$

and the ε_p's are given by (1.9) with $p = p'$. The DDHF equation can be derived from a stationary variational principle, requiring $|\Phi_0>$ to minimize $<\Psi \mid \hat{H} \mid \Psi>$, and $\begin{pmatrix} A & B \\ B^* & A^* \end{pmatrix}$ is again the stability matrix. So the relation between energy minima and stable oscillations also applies here. The proofs of these statements, though algebraically tedious, should, by now, be straightforward and will not be shown.

1.3. The Jastrow Correlated RPA

For the CRPA, the trial wavefunction is $|\Psi(t)> = \xi^{-\frac{1}{2}} F \mid \Phi(t)>$, $|\Phi(t)> = \exp\left(\sum_{ph} C_{ph}(t) a_p^\dagger a_h\right)|\Phi_0>$, $\xi = <\Phi(t) \mid F^\dagger F \mid \Phi(t)>$. For the time being, consider F as a fixed, time-independent A-body operator having the properties: (i) it is translationally invariant; (ii) it is symmetric under interchange of any two particles; (iii) when n particles are far removed from the rest of the system, $F(1 \ldots A) = F(1 \ldots n)\ F(n+1, \ldots A)$. The $V(ij)$ in $\hat{H}$ typically contains a strongly repulsive core which is kept 'manageable' (i.e. L is kept finite) by F. To get the EL equation, we note that F and $F^\dagger$ commutes with the operations $\frac{\partial}{\partial t}$,

$\frac{\partial}{\partial \dot{C}^*_{ph}}$, $\frac{\partial}{\partial C^*_{ph}}$ etc. So we take the ordinary TDHF equation (1.3a) and insert a $F^\dagger F$ pair between each bra-ket pair $<\Phi(t)|\cdots|\Phi(t)>$ in the following way: replace $\hat{H}$ by $F^\dagger \hat{H} F$ and, where there is no $\hat{H}$, insert $F^\dagger F$ to the left of particle-hole creators ($a_p^\dagger a_h$) and to the right of particle-hole annihilators ($a_h^\dagger a_p$). The result is:

$$i\hbar \sum_{p'h'} \dot{C}_{p'h'} \Big[<\Phi|a_h^\dagger a_p F^\dagger F a_{p'}^\dagger a_{h'}|\Phi> - \xi^{-1} <\Phi|F^\dagger F a_{p'}^\dagger a_{h'}|\Phi><\Phi|a_h^\dagger a_p F^\dagger F|\Phi> \Big] \qquad (1.10)$$

$$= <\Phi|a_h^\dagger a_p F^\dagger \hat{H} F|\Phi> - \xi^{-1} <\Phi|a_h^\dagger a_p F^\dagger F|\Phi><\Phi|F^\dagger \hat{H} F|\Phi> .$$

At this formal level, the single most important difference between the linear approximation of (1.10) and the ordinary RPA equation is the non-orthogonality introduced by F in the particle-hole basis. Thus, for example, $<\Phi_0|F^\dagger F|\Phi_{ph}>$ may not be zero and $<\Phi_{ph}|F^\dagger F|\Phi_{p'h'}>$ is not diagonal in ph. ξ^{-1} also has a more complicated structure:

$$\xi^{-1} = [<\Phi_0|F^\dagger F|\Phi_0> + \sum_{ph} (<\Phi_{ph}|F^\dagger F|\Phi_0> C^*_{ph} + c.c.) + O(C^2)]^{-1}$$

$$= \xi_0^{-1} [1 - \xi_0^{-1} \sum_{ph} (<\Phi_{ph}|F^\dagger F|\Phi_0> C^*_{ph} + c.c.)] + O(C^2), \qquad (1.11)$$

where $\xi_0 \equiv <\Phi_0|F^\dagger F|\Phi_0>$. The two lowest-order equations can still be read by inspection. We have, respectively, the correlated Brillouin condition:

$$<\Phi_{ph}|F^\dagger \hat{H} F|\Phi_0> - \xi_0^{-1} <\Phi_{ph}|F^\dagger F|\Phi_0><\Phi_0|F^\dagger \hat{H} F|\Phi_0> = 0, \qquad (1.12)$$

and the CRPA equation:

$$i\hbar \sum_{p'h'} \dot{C}_{p'h'} \Big[<\Phi_{ph}|F^\dagger F|\Phi_{p'h'}> - \xi_0^{-1} <\Phi_0|F^\dagger F|\Phi_{p'h'}><\Phi_{ph}|F^\dagger F|\Phi_0> \Big]$$

$$= \sum_{p'h'} C_{p'h'} \Big[<\Phi_{ph}|F^\dagger \hat{H} F|\Phi_{p'h'}> - \xi_0^{-1} <\Phi_{ph}|F^\dagger F|\Phi_{p'h'}><\Phi_0|F^\dagger \hat{H} F|\Phi_0> \Big]$$

$$+\sum_{p'h'} C^{*}_{p'h'}\left[\langle\Phi_{php'h'}|F^{\dagger}\hat{H}F'|\Phi_0\rangle-\xi_0^{-1}\langle\Phi_{php'h'}|F^{\dagger}F'|\Phi_0\rangle\langle\Phi_0|F^{\dagger}\hat{H}F|\Phi_0\rangle\right].$$

The other first-order terms cancel out because they contain the LHS of (1.12) as factors. We can again use the periodic ansatz for $C_{ph}(t)$ and get a double-matrix equation. For clarity's sake, we adopt the following notation: $\xi_{ph} \equiv \langle\Phi_{ph}|F^{\dagger}F|\Phi_{ph}\rangle$, $\hat{O}_{ph,p'h'} \equiv \langle\Phi_{ph}|F^{\dagger}\hat{O}F|\Phi_{p'h'}\rangle\xi_{ph}^{-\frac{1}{2}}\xi_{p'h'}^{-\frac{1}{2}}$, where $\hat{O}$ is an operator. In particular, we denote the unit operator by $\hat{N}$: $\hat{N}_{ph,p'h'} \equiv \langle\Phi_{ph}|F^{\dagger}F|\Phi_{p'h'}\rangle\xi_{ph}^{-\frac{1}{2}}\xi_{p'h'}^{-\frac{1}{2}}$. The matrix equation is

$$\begin{pmatrix} A & B \\ B^{*} & A^{*} \end{pmatrix}\begin{pmatrix} X \\ Y \end{pmatrix} = \hbar\omega\begin{pmatrix} M & 0 \\ 0 & -M^{*} \end{pmatrix}\begin{pmatrix} X \\ Y \end{pmatrix}, \qquad (1.13)$$

where $A_{ph,p'h'} = z_{ph}z_{p'h'}\left(\hat{H}_{ph,p'h'}-\hat{H}_{00}\hat{N}_{ph,p'h'}\right)$,

$$B_{ph,p'h'} = z_{php'h'}\left(\hat{H}_{php'h',0}-\hat{H}_{00}\hat{N}_{php'h',0}\right),$$

$$M_{ph,p'h'} = z_{ph}z_{p'h'}\left(\hat{N}_{ph,p'h'}-\hat{N}_{ph,0}\hat{N}_{0,p'h'}\right) \text{ and}$$

$$z_{ph} = \left(\frac{\xi_{ph}}{\xi_0}\right)^{\frac{1}{2}}.$$

To date, algorithms for evaluating these matrix elements accurately exist only for the Jastrow ansatz $F = \prod_{i<j}^{A} f(r_{ij})$. A major topic in itself, these algorithms will not be introduced until Chapter 4.

We now turn our attention to the problem of determining F (or $f(r_{ij})$). For the ground state, one chooses a model Slater determinant $|\Phi_0\rangle$ and requires $f(r_{ij})$ to extremize the energy $E_0 = \xi_0^{-1}\langle\Phi_0|F^{\dagger}\hat{H}F|\Phi_0\rangle$. As expected, however, only when f is fixed does the correlated Brillouin condition (1.12) define the stationary points on the energy surface $E = \xi^{-1}\langle\Phi|F^{\dagger}\hat{H}F|\Phi\rangle$ in the space of Slater

determinants. Therefore, in contrast with HF/RPA, (1.12) is not equivalent to the ground-state problem. Rather, we have a double parametrization, f and $|\Phi>$, for the stationary wave-function, both of which must vary consistently with the other. To fix both, we first take a convenient single-particle basis which is consistent with (1.12) and the three general properties of F required earlier. With $|\Phi_0>$ thus chosen, we solve the variational ground-state problem for F (or f). Thus we see (1.12) is just a condition, much less restrictive on $|\Phi_0>$ than its uncorrelated counterpart, the HF equation. If we constrain $f(r)$ to be short-ranged (i.e. $\int d\vec{r}(f^2-1)$ to be finite), we are justified to use it in the CRPA equation, where the most important particle-hole excitations have long wavelengths. We can again investigate the stability of the variational ground state along the direction of $|\Phi>$, i.e. infinitesimal $C_{ph}(C^*_{ph})$ with f fixed. The stability matrix is $\begin{pmatrix} A & B \\ B^* & A^* \end{pmatrix}$ and its semi-positive-definiteness implies the reality of all eigenvalues of the CRPA equation . For infinite matter, because F is also translationally invariant, the free-Fermi-gas basis satisfies (1.12) trivially. With this choice, the density $\rho(\vec{r})=\xi_0^{-1}<\Phi_0|F^\dagger\sum_i^A\delta(\vec{r}-\vec{r}_i)F|\Phi_0>$ is constant over all space. Any slight deviation in the Slater determinant $(C_{ph}a_p^\dagger a_h)$ introduces non-uniformity. So the stability analysis mentioned above is interpreted as directed toward stability against infinitesimal density fluctuations.

1.4. Linear Response

As promised, the experimental relevance of the foregoing results is made clear through the theory of linear response. The notation used in Section 0.3 is followed here. We again focus more attention on the RPA approximate theory, treating the CRPA as a nonorthogonal version.

Our postulational starting point is still the variational principle (1.1), this time with the Lagrangian

$$L = \langle\Psi|i\hbar\frac{\partial}{\partial t} - \hat{H} - \lambda(t)\hat{P}\vartheta(t)|\Psi\rangle.$$

Obviously (0.1) and the ensuing exact linear response follow if $|\Psi\rangle$ is free to vary in the entire Hilbert space. To arrive at the RPA response we again restrict it to Slater determinants. $|\Phi_0\rangle$, when $|\Psi\rangle$ is expressed in the Thouless form (1.2), is taken to be the HF ground state, which must be stable for linear response to be meaningful. It is supposed to approximate the undisturbed $|\Psi\rangle$ adequately before the probe is switched on : $C_{ph}(t)=0$, $t<0$. For $t>0$, the same arguments and algebraic manipulations as those in Section 1.1 lead to the TDHF equation (1.3a) with two new terms on the RHS :

$$\lambda(t)\langle\Phi|a_h^\dagger a_p\hat{P}|\Phi\rangle - \xi^{-1}\lambda(t)\langle\Phi|a_h^\dagger a_p|\Phi\rangle\langle\Phi|\hat{P}|\Phi\rangle.$$

The terms independent of the C_{ph}'s and λ vanish by hypothesis. If $\hat{P}$ is a one-body operator, $\hat{P}=\sum_{kl}P_{kl}a_k^\dagger a_l$, there exists, among the driving terms, one of $O(C^0)$: $\lambda(t)P_{ph}$. Singling out the terms linear in the C_{ph}'s, we may formally write the equation as (cf. (1.5))

$$\begin{pmatrix} C_{ph}(t) \\ C_{ph}^*(t) \end{pmatrix} = -\begin{pmatrix} A-i\hbar\frac{\partial}{\partial t} & B \\ B^* & A^*+i\hbar\frac{\partial}{\partial t} \end{pmatrix}^{-1}\begin{pmatrix} \lambda(t)P_{ph} \\ \lambda^*(t)P_{hp} \end{pmatrix} + O(C^2,\lambda C)\ .$$

Solving this by iterating the first term reveals the fact that $O(\lambda)=O(C)$ and the terms summarised by $O(C^2,\lambda C)$ may be discarded when λ is small. We thus have a linear (in C_{ph}), inhomogeneous equation whose homogeneous counterpart is (1.5). It is the case of a driven harmonic oscillator in the classical analogy. Fourier analysis is employed as before, yielding

$$\begin{bmatrix} \tilde{C}_{ph}(\omega) \\ \tilde{C}^{*}_{ph}(-\omega) \end{bmatrix} = - \begin{bmatrix} A-\hbar\omega-i\eta & B \\ B^{*} & A^{*}+\hbar\omega+i\eta \end{bmatrix}^{-1} \begin{bmatrix} \tilde{\lambda}(\omega)P_{ph} \\ \tilde{\lambda}^{*}(-\omega)P_{hp} \end{bmatrix}. \qquad (1.14)$$

Evaluated with this wave function, the deviation to $O(\lambda)$ from the ground-state value of another one-body operator is

$$\tilde{\delta}_{\omega}<\hat{Q},\hat{P}> = \int_0^{\infty} dt e^{i(\omega+i\eta)t} (<\Phi_0|[1+\sum_{ph} C^{*}_{ph} a_h^{\dagger} a_p]\hat{Q}[1+\sum_{ph} C_{ph} a_p^{\dagger} a_h]|\Phi_0> - <\Phi_0|\hat{Q}|\Phi_0>)$$

$$= \sum_{ph} [\tilde{C}_{ph}(\omega) Q_{hp} + \tilde{C}^{*}_{ph}(-\omega) Q_{ph}]$$

$$= - [\ Q_{hp}\ Q_{ph}\ ] \begin{bmatrix} A-\hbar\omega-i\eta & B \\ B^{*} & A^{*}+\hbar\omega+i\eta \end{bmatrix}^{-1} \begin{bmatrix} \tilde{\lambda}(\omega)P_{ph} \\ \tilde{\lambda}^{*}(-\omega)P_{hp} \end{bmatrix}.$$

The computation of the inverse matrix, in parallel with finding $[\hbar\omega-(\hat{H}-E_0)+i\eta]^{-1}$ in the exact problem, involves the resolution of the unity by a complete set of orthonormal RPA eigenstates. It is easy to see that the RPA eigenvectors are orthogonal in the following way : $\sum_{ph} X^{n*}_{ph} X^{n'}_{ph} - Y^{n*}_{ph} Y^{n'}_{ph} = 0$ when $n \neq n'$. Furthermore, if all the eigenvalues are real, as we assume here, this 'inner product' for $n=n'$ has the same sign as the corresponding ω_n. To establish completeness, then, we merely note that if any $\begin{bmatrix} X^n \\ Y^n \end{bmatrix}$ can be expressed as a linear combination of the other eigenvectors, then 'dotting' both sides with the adjoint of $\begin{bmatrix} X^n \\ -Y^n \end{bmatrix}$ will lead to a contradiction. Armed with the above, we can use essentially the same eigenvector expansion for the Green function in hermitian linear algebra, modified to take care of the minus sign in our 'metric'. The result is : if the eigenvectors are normalised according to

$$[\ X^{n\dagger}\ Y^{n\dagger}\ ] \begin{bmatrix} X^{n'} \\ -Y^{n'} \end{bmatrix} = \mathrm{sign}(\omega_n)\delta_{nn'}, \qquad (1.15)$$

the required inverse matrix is given by

$$\begin{bmatrix} A-\hbar\omega-i\eta & B \\ B^* & A^*+\hbar\omega+i\eta \end{bmatrix}^{-1} = \sum_n \mathrm{sign}(\omega_n)\, \frac{1}{\hbar\omega_n-\hbar\omega-i\eta} \begin{bmatrix} X^n \\ Y^n \end{bmatrix} [\, X^{n\dagger}\ Y^{n\dagger}\,] \tag{1.16a}$$

$$= -\sum_{\omega_n>0} \frac{\begin{bmatrix} X^n \\ Y^n \end{bmatrix} [\, X^{n\dagger}\ Y^{n\dagger}\,]}{\hbar\omega-\hbar\omega_n+i\eta} - \frac{\begin{bmatrix} X^{n*} \\ Y^{n*} \end{bmatrix} [\, X^{nT}\ Y^{nT}\,]}{\hbar\omega+\hbar\omega_n+i\eta} \tag{1.16b}$$

The superscript T stands for the transpose of the column vector. It is readily checked that a product of the two matrices in question in (1.16a) does act as the identity when applied to any column vector expressed, consistently with completeness, as a superposition of the $\begin{bmatrix} X^n \\ -Y^n \end{bmatrix}$'s. Also interesting to note is that

$$\sum_{\omega_n>0} \begin{bmatrix} X^n \\ Y^n \end{bmatrix} [\, X^{n\dagger}\ -Y^{n\dagger}\,] - \begin{bmatrix} X^{n*} \\ Y^{n*} \end{bmatrix} [\, Y^{nT}\ -X^{nT}\,] = \begin{bmatrix} I & 0 \\ 0 & I \end{bmatrix}. \tag{1.17}$$

(1.16b) is substituted into the formula for $\tilde{\delta}_\omega\langle\hat{Q},\hat{P}\rangle$. With real $\lambda(t)$, comparison of the resulting expression with (0.3) identifies the RPA excitation amplitude

$$\langle\Psi_n\,|\,\hat{P}\,|\,\Psi_0\rangle = \sum_{ph}[X^{n*}_{ph}P_{ph} + Y^{n*}_{ph}P_{hp}]\,. \tag{1.18}$$

For nuclear matter, since $\langle\vec{p}\,|\,e^{i\vec{q}\cdot\vec{r}}\,|\,\vec{h}\rangle=\delta_{\vec{p},\vec{h}+\vec{q}}$, the retarded particle-hole propagator (0.4) is approximated by

$$\tilde{\Pi}^R(\omega,\vec{q}) \approx \frac{1}{\Omega} \sum_{\omega_n>0} \frac{|\sum_{\vec{h}}(X^{n*}_{\vec{h}+\vec{q},\vec{h}} + Y^{n*}_{\vec{h}-\vec{q},\vec{h}})|^2}{\hbar\omega-\hbar\omega_n+i\eta} - \frac{|\sum_{\vec{h}}(X^{n}_{\vec{h}-\vec{q},\vec{h}} + Y^{n}_{\vec{h}+\vec{q},\vec{h}})|^2}{\hbar\omega+\hbar\omega_n+i\eta} \tag{1.19}$$

before complications due to spin and isospin are brought in. Similarly qualified, the dynamic form factor is

$$S(q,\omega) \approx \frac{1}{\hbar A} \sum_{\omega_n>0} |\sum_{\vec{k}} (X^{n*}_{\vec{k}+\vec{q},\vec{k}} + Y^{n*}_{\vec{k}-\vec{q},\vec{k}})|^2 \delta(\omega-\omega_n) \tag{1.20}$$

Two points from the above results are worth noting. The response to a weak external potential is expected to be dominated by RPA resonances whenever the system is adequately described by the independent-particle model (or, technically, TDHF). If a two-(or higher-)body probe, say, $\hat{P}= \sum_{klmn} <kl\,|\,P\,|\,mn> a_k^\dagger a_l^\dagger a_n a_m$, is applied, a first-order driving term $\lambda(t) \sum_{j\varepsilon K_F} <pj\,|\,P\,|\,hj>_a$ can still be found to favor RPA over multi-particle-hole transitions. In this case, $\hat{P}$ is an 'effective' one-body excitation mechanism. The second point concerns the necessity of the linear response formalism. Starting by defining an RPA-state, the equations-of-motion method [Ro70] enables one to get the excitation amplitude (1.18) and, hence, $S(q,\omega)$ in one step. In contrast, there is no rigorous way to do the same in the TDHF approach. The culprit is the ansatz (1.6) which mixes the positive-energy and the negative-energy components in the representation of the 'excited' Slater determinant. The latter, then, cannot be used as an approximation to $|\Psi_n>$. Considering that the TDHF picture bears most resemblance to classical oscillations, the need for an interpretation based on resonances to a vibrating driving force rather than on quantal states should come as no surprise. Again this would have been a minor point but for our objective of obtaining a rigorous generalization to CRPA. The propagator is of course very rich in physics by itself, carrying information about the ground state in its real part.

Given the above, the extension to CRPA-response is quite straightforward and easy. We use the same Lagrangian with $|\Psi>$ being the correlated Slater determinant. Again we choose F and $|\Phi_0>$, representing the undisturbed state, to minimize the energy expectation value, satisfy the correlated Brillouin condition, and be stable against density fluctuations. In the corresponding Euler-

Lagrange equation, the zeroth-order terms duly vanish. The first-order driving term is $\lambda(t)z_{ph}[\hat{P}_{ph,0}-\hat{N}_{ph,0}\hat{P}_{00}] \equiv \lambda(t)z_{ph}\hat{P}'_{ph,0}$. The prime on the operator denotes this recurrent combination of matrix elements due to the non-orthogonality of the basis. Linearization with respect to C_{ph} is again justified, and Fourier transformation yields the following inhomogeneous matrix equation

$$\begin{pmatrix} \tilde{C}_{ph}(\omega) \\ \tilde{C}^{*}_{ph}(-\omega) \end{pmatrix} = - \begin{pmatrix} A-(\hbar\omega+i\eta)M & B \\ B^{*} & A^{*}+(\hbar\omega+i\eta)M^{*} \end{pmatrix}^{-1} \begin{pmatrix} \tilde{\lambda}(\omega)z_{ph}\hat{P}'_{ph,0} \\ \tilde{\lambda}^{*}(-\omega)z_{ph}\hat{P}'_{0,ph} \end{pmatrix}.$$

When evaluating $\delta_t<\hat{Q},\hat{P}>$, care must be taken to include the first-order contribution from the normalization constant ξ^{-1} (1.11). The frequency-response is

$$\tilde{\delta}_{\omega}<\hat{Q},\hat{P}> = \sum_{ph} [\tilde{C}_{ph}(\omega)z_{ph}\hat{Q}'_{0,ph} + \tilde{C}^{*}_{ph}(-\omega)z_{ph}\hat{Q}'_{ph,0}].$$

As expected, M acts as a metric matrix in the expression of orthogonality of the eigenvectors which can be normalised as

$$[\, X^{n\dagger}\; Y^{n\dagger}\,] \begin{bmatrix} M & 0 \\ 0 & -M^{*} \end{bmatrix} \begin{bmatrix} X^{n'} \\ Y^{n'} \end{bmatrix} = \mathrm{sign}(\omega_n)\delta_{nn'}, \tag{1.21}$$

to most conveniently invert the 'inhomogeneous' CRPA matrix :

$$\begin{pmatrix} A-(\hbar\omega+i\eta)M & B \\ B^{*} & A^{*}+(\hbar\omega+i\eta)M^{*} \end{pmatrix}^{-1} = - \sum_{\omega_n>0} \frac{\begin{bmatrix} X^{n} \\ Y^{n} \end{bmatrix}[\, X^{n\dagger}\; Y^{n\dagger}\,]}{\hbar\omega-\hbar\omega_n+i\eta} - \frac{\begin{bmatrix} X^{n*} \\ Y^{n*} \end{bmatrix}[\, X^{nT}\; Y^{nT}\,]}{\hbar\omega+\hbar\omega_n+i\eta} \tag{1.22}$$

This can be proved, as before, by resolving any column vector into a superposition of $\begin{pmatrix} MX^{n} \\ -M^{*}Y^{n} \end{pmatrix}$'s and then multiplying by the product of the two matrices. (1.21) ensures the completeness of this set of basis vectors. Substitution into the formula for $\tilde{\delta}_{\omega}<\hat{Q},\hat{P}>$ brings out the CRPA approximant to the transition

amplitude :

$$<\Psi_n|\hat{P}|\Psi_0> = \sum_{ph} z_{ph}[X^{n*}_{ph}\hat{P}'_{ph,0}+Y^{n*}_{ph}\hat{P}'_{0,ph}]. \tag{1.23}$$

An important special case is when $[\hat{P},F]=[\hat{Q},F]=0$, where

$$<\Psi_n|\hat{P}|\Psi_0> = [\ X^{n\dagger}_{ph}\ Y^{n\dagger}_{ph}\ ]\begin{bmatrix} M & 0 \\ 0 & M^* \end{bmatrix}\begin{bmatrix} P_{ph} \\ P_{hp} \end{bmatrix}. \tag{1.24}$$

When F is the Jastrow correlation factor, the density operator falls into this category. Further simplification is possible in our plane-wave-based infinite matter. $F^\dagger F=\prod_{i<j}^{A} f^2(\vec{r}_{ij})$ is invariant under translation of the center of mass or, equivalently, it conserves the total momentum of the system. Clearly the momentum of $|\Phi_{ph}>$ is $\vec{p}-\vec{h}$ and that of $|\Phi_0>$ is zero. Therefore referring to the definition of M in (1.13) we note $\hat{N}_{\vec{p}\vec{h},0}=0$ and $\hat{N}_{\vec{p}\vec{h},\vec{p}',\vec{h}'}\neq 0$ only when $\vec{p}-\vec{h}=\vec{p}'-\vec{h}'$. With $<\vec{p}\,|\rho(\vec{q})\,|\vec{h}>=\delta_{\vec{p},\vec{h}+\vec{q}}$ and the notation

$$\bar{X}^n_{\vec{h}+\vec{q},\vec{h}} = \sum_{\vec{h}'} M_{\vec{h}+\vec{q},\vec{h};\,\vec{h}'+\vec{q},\vec{h}'}\, X^n_{\vec{h}'+\vec{q},\vec{h}'}\ ,$$

the retarded propagator and the dynamic form factor assume the forms:

$$\tilde{\Pi}^R(\omega,\vec{q}) \approx \frac{1}{\Omega}\sum_{\omega_n>0}\frac{|\sum_{\vec{h}}(\bar{X}^{n*}_{\vec{h}+\vec{q},\vec{h}}+\bar{Y}^{n*}_{\vec{h}-\vec{q},\vec{h}})|^2}{\hbar\omega-\hbar\omega_n+i\eta} - \frac{|\sum_{\vec{h}}(\bar{X}^{n}_{\vec{h}-\vec{q},\vec{h}}+\bar{Y}^{n}_{\vec{h}+\vec{q},\vec{h}})|^2}{\hbar\omega+\hbar\omega_n+i\eta}, \tag{1.25}$$

$$S(q,\omega) \approx \frac{1}{\hbar A}\sum_{\omega_n>0}|\sum_{\vec{h}}(\bar{X}^{n*}_{\vec{h}+\vec{q},\vec{h}}+\bar{Y}^{n*}_{\vec{h}-\vec{q},\vec{h}})|^2\delta(\omega-\omega_n). \tag{1.26}$$

The CRPA-response theory is not an independent-particle model. Nevertheless the many-body correlations are assumed to be frozen in the ground-state F and not to interfere with the dynamical particle-hole excitations. This is justified when the wavelength of the excitation q^{-1} is long compared with the range of

$f(r)$. In some sense, we are considering an independent-'quasiparticle' model, and the remark following (1.20) still holds here.

We conclude this section with a discussion of the energy-weighted sum rule (EWSR) in the RPA context. Its usefulness for checking numerical accuracy stems from the following theorem by Thouless [Th61]: Equation (0.5) holds for RPA excitations if $\hat{P}$ is one-body and the double-commutator is evaluated with the static HF state :

$$\frac{1}{2A}\langle\Phi_{HF}|[\hat{P}^\dagger,[\hat{H},\hat{P}]]|\Phi_{HF}\rangle = \sum_{\omega_n>0}\hbar\omega|\langle\Psi_n|\hat{P}|\Psi_0\rangle_{RPA}|^2. \qquad (1.27)$$

As for the exact case, the key to the proof is to bring $\hbar\omega$ into the amplitude, replace it by the RPA matrix, and construct the 'completeness' combination (1.17) to get

$$[\,P_{ph} - P_{hp}\,]\begin{bmatrix}A & B\\ B^* & A^*\end{bmatrix}\begin{bmatrix}P_{ph}\\ -P_{hp}\end{bmatrix}.$$

Straightforward expansion of both sides will then show that they are indeed identical. If the double-commutator turns out to be a c-number, the HF value is exact, in which case the RPA is said to preserve the EWSR. Even in the general case, (1.27) is an exact identity and so is free from the uncertainties concerning the negligibility of non-RPA contributions. The natural candidate for the correlated counterpart of (1.27) is

$$\frac{1}{2A}\xi_0^{-1}\langle\Phi_0|F^\dagger[\hat{P}^\dagger,[\hat{H},\hat{P}]]F|\Phi_0\rangle = \sum_{\omega_n>0}\hbar\omega|\langle\Psi_n|\hat{P}|\Psi_0\rangle_{CRPA}|^2. \qquad (1.28)$$

Owing to our definition of the RPA wave function ($Fa_p^\dagger a_h|\Phi_0\rangle$ instead of $a_p^\dagger a_h F|\Phi_0\rangle$), (1.28) is <u>not</u> true in general, but, as probably expected, we can validate it by assuming that $\hat{P}$ commutes with F. To demonstrate this, note that

$$F^\dagger[\hat{P}^\dagger,[\hat{H},\hat{P}]]F = [\hat{P}^\dagger,[F^\dagger(\hat{H}-\hat{H}_{00}\hat{N})F,\hat{P}]]$$

if $[F,\hat{P}]=0$. Similar algebra to that above then reproduces (1.28). Our interest in this thesis is restricted to state-independent f($\boldsymbol{r}$) and (spin-isospin) density operators that satisfy (1.28). It has been agreed, though, that a realistic F should at least include tensor correlations in nuclear matter and momentum-dependence (backflow) in ^{3}He. The former fail to commute with the spin-density and the latter with any density. In these non-commutative cases, it is interesting to ask which of the two, the double-commutator or the CRPA sum, approximates the exact energy-weighted sum better. This question will concern us in future investigations.

Chapter 2

We consider models of nuclear matter which saturate at the Hartree-Fock level. The RPA-equation (1.7) becomes a coupled pair of integral equations in six dimensions. However, a massive reduction of the kernel into 'decoupled blocks' is allowed by the system's symmetries, which also provide the quantum numbers of the excitations. The 'irreducible' integral eigenvalue problem is then solved on a quadrature mesh, which is progressively refined until the suitably-smoothed dynamic form-factor $S(q,\omega)$ converges satisfactorily. This chapter contains the formal developments necessary for this problem. Numerical results for some model calculations will be presented in the next chapter.

2.1. The Equation In Momentum Space

Let us disregard spin and isospin for a moment (degeneracy ν=1) and assume $V(ij) = V(|\vec{r}_i - \vec{r}_j|)$. Translational symmetry then gives a conserved quantity for the excitations, the momentum $\hbar\vec{q}$, as shown explicitly below. With a set of plane waves $\{\Omega^{-\frac{1}{2}} e^{i\vec{k}\cdot\vec{r}}\}$ as the single-particle basis, the state label may just be the wave-vector (i.e. $p > k_F$, $h < k_F$). Also, as we shall see, all the matrix elements are real. In the thermodynamic limit we make the substitution $\sum_{\vec{p}\vec{h}} \to \frac{\Omega^2}{(2\pi)^6}\int d\vec{p}\,d\vec{h}$ in (1.7), obtaining the integral equations

$$[\hbar\omega - \Delta\varepsilon(\vec{h},\vec{p})]X(\vec{h},\vec{p}) = \frac{\Omega^2}{(2\pi)^6}\int d\vec{p}\,'d\vec{h}\,'[A(\vec{h},\vec{p},\vec{h}\,',\vec{p}\,')X(\vec{h}\,',\vec{p}\,') + B(\vec{h},\vec{p},\vec{h}\,',\vec{p}\,')Y(\vec{h}\,',\vec{p}\,')]$$

$$-[\hbar\omega + \Delta\varepsilon(\vec{h},\vec{p})]Y(\vec{h},\vec{p}) = \frac{\Omega^2}{(2\pi)^6}\int d\vec{p}\,'d\vec{h}\,'[A(\vec{h},\vec{p},\vec{h}\,',\vec{p}\,')Y(\vec{h}\,',\vec{p}\,') + B(\vec{h},\vec{p},\vec{h}\,',\vec{p}\,')X(\vec{h}\,',\vec{p}\,')] \qquad (2.1)$$

where the kernels are given by

$$A(\vec{h},\vec{p},\vec{h}',\vec{p}')=\langle\vec{h}'\vec{p}\mid V\mid\vec{p}'\vec{h}\rangle_a=\frac{(2\pi)^6}{\Omega^2}\delta(\vec{p}-\vec{h}-(\vec{p}'-\vec{h}'))[\tilde{V}(\vec{p}-\vec{h})-\tilde{V}(\vec{h}-\vec{h}')]\ ,$$

$$B(\vec{h},\vec{p},\vec{h}',\vec{p}')=\langle\vec{p}\vec{p}'\mid V\mid\vec{h}\vec{h}'\rangle_a=\frac{(2\pi)^6}{\Omega^2}\delta(\vec{p}-\vec{h}-(\vec{p}'-\vec{h}'))[\tilde{V}(\vec{h}-\vec{p})-\tilde{V}(\vec{p}'-\vec{h})]\ ,$$

and $\Delta\varepsilon(\vec{h},\vec{p})\equiv\varepsilon(\vec{p})-\varepsilon(\vec{h})$

$$=\frac{\hbar^2}{2m}(p^2-h^2)+\frac{2}{\pi}k_F^2\int_0^\infty dr\ rj_1(k_Fr)[j_0(hr)-j_0(pr)]V(r)\ .$$

$\tilde{V}(\vec{k})$ denotes the Fourier transform of $V(r)$ with the factor $\frac{1}{(2\pi)^3}$ included, and $p=|\vec{p}\,|,h=|\vec{h}\,|$. The delta functions, conserving the total momentum of the particle-hole pair ($\vec{q}=\vec{p}-\vec{h}$ for the X's and $\vec{q}=\vec{h}-\vec{p}$ for the Y's), are manifestations of the system's symmetry. On the practical side, they decouple (2.1) into an infinite set of 3-dimensional equations labelled by $\vec{q}$. We choose to retain the hole variables (hereafter denoted by $\vec{k}$ instead of $\vec{h}$) in the integrals. For each $\vec{q}$, the orbitals which are excitable to particle orbitals are restricted to a cap of thickness q on both sides of the Fermi sphere along the direction of $\vec{q}$ (Figure 1), defined by : $0<k<k_F$, $|\vec{k}+\vec{q}\,|\geq k_F$ for $X_q(\vec{k})$ and $0<k<k_F$, $|\vec{k}-\vec{q}\,|\geq k_F$ for $Y_q(\vec{k})$†. In polar coordinates with the z-axis parallel to $\vec{q}$, we have, for $X_q(\vec{k}_X)$, $|\vec{k}_X+\vec{q}\,|\geq k_F \Rightarrow (k_X^2+q^2+2k_Xq\cos\vartheta_X)=k_F^2$. Since $\cos\vartheta_X\leq 1$, k_X is limited to $max(0,k_F-q)\leq k_X\leq k_F$. For each allowed k_X, $\cos\vartheta_X\geq\frac{k_F^2-k_X^2-q^2}{2k_Xq}\equiv\alpha_0(k_X)$, and is thus limited to $max(-1,\alpha_0(k_X))\leq\cos\vartheta_X\leq 1$. For $Y_q(\vec{k}_Y)$, similar restrictions apply : $max(0,k_F-q)\leq k_Y\leq k_F$; $-1\leq\cos\vartheta_Y\leq min(1,-\alpha_0(k_Y))$. Clearly the allowed Y_q-subset is just the mirror image of the X_q-subset about the plane $\vartheta=\frac{\pi}{2}$, and so we may state the problem in just one polar-angle variable. Redefining $\alpha\equiv\cos\vartheta_X$

† It is clear that the problem is degenerate in the direction of $\vec{q}$; so we drop the arrow on labels.

and $cos\vartheta_Y \equiv -\alpha$, we check that $\int_{-1}^{-\alpha_0} d(cos\vartheta_Y) = -\int_{1}^{\alpha_0} d\alpha = \int_{\alpha_0}^{1} d\alpha$. The presence of $\vec{q}$ in the isotropic medium imposes a cylindrical symmetry which makes m, the z-projection (along $\vec{q}$) of the orbital angular momentum, a good quantum number. Anticipating separation, we write the excitation amplitudes as

$$X_q(k,\alpha,\varphi) = \sum_m X_{qm}(k,\alpha)e^{im\varphi}$$

$$Y_q(k,-\alpha,\varphi) = \sum_m Y_{qm}(k,-\alpha)e^{im\varphi} ,$$

and expect the kernels in (2.1) to conserve m. Being independent of $\vec{k},\vec{k}'$, the direct term $\tilde{V}(q)$ presents no problem. To demonstrate this property in the exchange term, we expand it in spherical harmonics $Y_{lm}(\alpha,\varphi)$. This choice over cylindrical Bessel functions is dictated by the spherical symmetry of the interaction $V(r)$ in $\vec{r}$-space. Thus φ is integrated out in favor of m. The end result of the above manipulations is a set of paired 2-dimensional integral equations, in the same form as (2.1), with $\frac{\Omega^2}{(2\pi)^6}\int d\vec{p}\,'d\vec{h}\,' \to \int_{max(0,k_F-q)}^{k_F} dk'k'^2 \int_{max(-1,\alpha_0)}^{1} d\alpha'$, variables (k,α) for the X's and $(k,-\alpha)$ for the Y's, and (q,m) as labels. The $\Delta\varepsilon$'s and the kernels are given by

$$\Delta\varepsilon_q(k,\alpha) = \Delta\varepsilon_q(k,-\alpha) \qquad (2.2)$$

$$= \frac{\hbar^2}{2m}(q^2+2qk\alpha)+\frac{2}{\pi}k_F^2\int_0^\infty dr\; rj_1(k_Fr)[j_0(kr)-j_0(pr)]V(r) ,$$

$$A_{qm}(k,\alpha,k',\alpha') = A_{qm}(k,-\alpha,k',-\alpha') = A_{qm}(k',\alpha',k,\alpha) = A_{qm}(k',-\alpha',k,-\alpha)$$

$$= \frac{1}{\pi}[\delta_{m0}V(q)-\sum_l(2l+1)\frac{(l-m)!}{(l+m)!}P_l^m(\alpha)P_l^m(\alpha')V_l(k,k')] ,$$

$$V(q) = \int_0^\infty dr\; r^2j_0(qr)V(r)\;;\; V_l(k,k') = \int_0^\infty dr\; r^2j_l(kr)j_l(k'r)V(r) ,$$

$$B_{qm}(k,\alpha,k',-\alpha') = B_{qm}(k,-\alpha,k',\alpha') = B_{qm}(k',-\alpha',k,\alpha) = B_{qm}(k',\alpha',k,-\alpha)$$

$$= \frac{1}{\pi}[\delta_{m0}V(q) - \sum_l (2l+1)\frac{(l-m)!}{(l+m)!}P_l^m(\alpha)P_l^m(-\alpha_p')V_l(k,p')],$$

$$p' = (k'^2+q^2+2qk'\alpha')^{1/2}\ ;\ \alpha_p' = \frac{k'\alpha'+q}{p'}.$$

This is as far as analytic techniques can carry us for an unspecified potential.

Discretizing the last equation on a double Legendre-Gaussian quadrature mesh, we change the problem back to one of matrix diagonalization. Each integral here is approximated by a weighted sum of the integrand over a set of 'nodes' :

$$\int_a^b f(t)dt = \frac{b-a}{2}\sum_{i=1}^n w_i f(t_i)\ \ ;\ \ t_i = \frac{b-a}{2}u_i + \frac{b+a}{2}.$$

The u_i's are the nodes when the integration range is from -1 to 1. The set $\{u_i, w_i, i=1,\ldots,n\}$ is given in standard numerical tables. [Ma69] may be consulted for a brief account of the theory. We only note here that the expression is exact for integrands which are polynomials of order up to $2n$. For our double integral, the quantities $\frac{b-a}{2}$, $\frac{b+a}{2}$ etc, are listed here :

	k	α
$\frac{b-a}{2}$:	$d_k = \frac{1}{2}min(k_F,q)$	$d_\alpha(k_i) = \frac{1}{2}[1-max(-1,\alpha_0(k_i))]$
$\frac{b+a}{2}$:	$s_k = \frac{1}{2}(k_F+\vartheta(k_F-q)(k_F-q))$	$s_\alpha(k_i) = \frac{1}{2}[1+max(-1,\alpha_0(k_i))]$
nodes(t) :	$k_i = d_k u_i + s_k$	$\alpha_j(k_i) = d_\alpha(k_i)u_j + s_\alpha(k_i)$

At this point we should clarify the notation for later convenience. The subscript-pairs (i,j) and (μ,ν) label the quadrature points, the latter assigned to dummy variables in the sums. For example, k_i is the value of the i-th k-

quadrature point. Subscripts (k,α) on quantities such as $d_\alpha(k_i)$ just indicate that the function d pertains to the variables α, but not to any particular α-quadrature points α_j.

Opting for polar coordinates and Legendre-Gaussian quadrature leads to an asymmetric factor in the discretized matrix :

$$\sum_{\mu=1}^{n_k}\sum_{\nu=1}^{n_\alpha(\mu)}[w_\mu k_\mu^2 d_\alpha(k_\mu)w_\nu(\mu)]A_{qm}(k_i,\alpha_j,k_\mu,\alpha_\nu)X_{qm}(k_\mu,\alpha_\nu)\ ,\ \text{etc.}$$

This asymmetry is, of course, artificial and is inconvenient from a numerical point of view. It can be removed by the similarity matrix $T_{ij,\mu\nu}=\delta_{ij,\mu\nu}(w_i k_i^2 d_\alpha(k_i)w_j)^{1/2}$. With this, and considerations of normalization, we now give the equation exactly as it is used in the computer for single-channel systems (hereafter the subscripts (q,m) are dropped) :

$$\hbar\omega\tilde{X}_{ij} = \Delta\varepsilon_{ij}\tilde{X}_{ij}+\sum_{\mu=1}^{n_k}\sum_{\nu=1}^{n_\alpha(\mu)}[\tilde{A}_{ij,\mu\nu}\tilde{X}_{\mu\nu}+\tilde{B}_{ij,\mu\nu}\tilde{Y}_{\mu\nu}]$$

$$-\hbar\omega\tilde{Y}_{ij} = \Delta\varepsilon_{ij}\tilde{Y}_{ij}+\sum_{\mu=1}^{n_k}\sum_{\nu=1}^{n_\alpha(\mu)}[\tilde{A}_{ij,\mu\nu}\tilde{Y}_{\mu\nu}+\tilde{B}_{ij,\mu\nu}\tilde{X}_{\mu\nu}]$$

$$\tilde{A}_{ij,\mu\nu} \equiv d_k k_i k_\mu[d_\alpha(k_i)d_\alpha(k_\mu)w_i w_\mu w_j(i)w_\nu(\mu)]^{1/2}A(k_i,\alpha_j,k_\mu,\alpha_\nu)$$

$$\tilde{B}_{ij,\mu\nu} \equiv d_k k_i k_\mu[d_\alpha(k_i)d_\alpha(k_\mu)w_i w_\mu w_j(i)w_\nu(\mu)]^{1/2}B(k_i,\alpha_j,k_\mu,\alpha_\nu)$$

$$\tilde{X}_{ij} \equiv \frac{k_i}{2\pi}[\Omega d_k d_\alpha(k_i)w_i w_j(i)]^{1/2}X(k_i,\alpha_j)$$

$$\tilde{Y}_{ij} \equiv \frac{k_i}{2\pi}[\Omega d_k d_\alpha(k_i)w_i w_j(i)]^{1/2}Y(k_i,-\alpha_j)\ .$$

The A's, B's, and $\Delta\varepsilon$'s are as defined in (2.2), and the normalization relation

$$\sum_{ij}\tilde{X}_{ij}^n\tilde{X}_{ij}^{n'} - \tilde{Y}_{ij}^n\tilde{Y}_{ij}^{n'} = \delta_{nn'}\ ,$$

with n,n' labelling the eigenvalues, holds. The dynamic form factor has the expression

$$S(q,\omega) = \delta_{m0}\frac{d_k}{(2\pi)^2\rho}\sum_{\omega_n>0}|\sum_{ij}k_i[d_\alpha(k_i)w_iw_j(i)]^{\frac{1}{2}}(\tilde{X}^n_{ij}+\tilde{Y}^n_{ij})|^2\delta(\omega-\omega_n)\ . \tag{2.3}$$

Since the range of α, $(\alpha_0(k)-1)$, depends on k, so does the number of α-quadrature points, so as to cover the integration region efficiently. A typical mesh used is displayed in Figure 2.

2.2. An Analytically Solvable Example

Before going further, we review the familiar [e.g., Pi66, Chapter 1], analytically solvable case of a 'local' kernel at the long wavelength (Landau) limit. In this very schematic model, one approximates the kernel by a constant F_0 and linearizes the equations with respect to q. The paired integral equations then reduce to an algebraic one. This model has played a central role in the RPA theory of infinite systems, so much so that to many it is synonymous with RPA itself. Despite its quantitative crudeness compared to our treatment, it helps set the framework and language for the discussion of the numerical results in later chapters.

Let us start with stability analysis. Take (2.1) and remove the minus sign in front of $\hbar\omega$ in the second equation. We express the limits of integration as step functions : $\vartheta(|\vec{k}\pm\vec{q}|-k_F)\vartheta(k_F-k)$. At $q\to 0$, (Reminder : upper sign for X and lower sign for Y),

$$\Delta\varepsilon(\vec{k},\vec{k}\pm\vec{q}) = \pm\frac{\hbar^2}{m}qk_F\alpha\pm\frac{2}{\pi}k_F^2q\,\alpha\int_0^\infty dr\ r^2\ V(r)[j_1(k_Fr)]^2 \tag{2.4}$$

$$= \pm\frac{\hbar^2}{m^*}q\,\alpha k_F\ ,$$

where $\frac{m^*}{m} = [1+\frac{2mk_F}{\hbar^2\pi}\int_0^\infty dr\ r^2\,[j_1(k_Fr)]^2V(r)]^{-1}$,

and $\vartheta(|\vec{k}\pm\vec{q}\,|-k_F)\vartheta(k_F-k) \approx \delta(k_F-k)\vartheta(\pm\alpha)q\,\alpha$.

Assume $m^*>0$ for the time being. Let the Fourier transforms of the potential in both A and B be approximated by a number : $\tilde{V}_0=\int d\vec{r}\,V(r)$+approximation of the exchange term. Then the integral reduces to $\frac{qk_F^2}{4\pi^2}\tilde{V}_0[\int_0^1 d\alpha\alpha X(\alpha)-\int_{-1}^0 d\alpha\alpha Y(\alpha)]$. Defining $u(\alpha)=\begin{cases} \alpha X(\alpha) & \alpha>0 \\ -\alpha Y(\alpha) & \alpha<0 \end{cases}$ combines the two equations, with proper scaling, into

$$(\lambda-|\alpha|)u(\alpha) = \frac{F_0}{2}|\alpha|\int_{-1}^1 d\alpha\, u(\alpha)$$

where $\lambda = \hbar\omega\frac{m^*}{\hbar^2qk_F}$ and $F_0 = \frac{m^*k_F}{2\pi^2\hbar^2}\tilde{V}_0$.

Since we are interested in the occurrence of negative λ's, we can disregard the interval $0<\lambda<1$. Then dividing both sides by $(\lambda-|\alpha|)$ and integrating yields the secular equation

$$1 = \frac{F_0}{2}\int_{-1}^1 d\alpha\frac{|\alpha|}{\lambda-|\alpha|} = F_0[\lambda\ln|\frac{\lambda}{\lambda-1}|-1]\,,$$

or $\chi_s(\lambda) \equiv \lambda\ln|\frac{\lambda}{\lambda-1}|-1 = \frac{1}{F_0}$.

$\chi_s(\lambda)$ is sketched in Figure 3a, from which we can see exactly one negative eigenvalue occurs, signalling instability of the uniform phase, if and only if $F_0<-1$.

Under the same approximation, the RPA equation reduces to the so-called collisionless Landau transport equation :

$$(\lambda-\alpha)u(\alpha) = \frac{F_0}{2}\alpha\int_{-1}^{1} d\alpha\, u(\alpha) \tag{2.5}$$

where λ may be complex. Consider first the case $F_0=0$. Recall that the free-fermion spectrum is, at $q\to 0$, a continuum extending from 0 to $\frac{\hbar^2 q k_F}{m}$. (2.4) shows that switching on the HF mean field amounts to rescaling the energy axis by $\frac{m}{m^*}$. The system responds as a collection of free fermions with the effective mass m^*. The more repulsive V is, the lighter these particles become. When V is sufficiently attractive, however, m^* may turn negative, whereupon the Fermi sea is unstable against spontaneous generation of particle-hole pairs. This instability is different in nature from that caused by $F_0<-1$, which is a coherent phenomenon among many positive-m^* particles.

Assume again $m^*>0$ and switch on the residual interaction. Consider first the eigenvalues outside the interval [-1,1] on the real line, thereby avoiding the singularity of $u(\alpha)$ at $\alpha=\lambda$. The eigenfunction is trivially solved by :

$$u(\alpha) = \frac{F_0}{2}\frac{\alpha}{\lambda-\alpha}\zeta \;\; ; \;\; \zeta \equiv \int_{-1}^{1} d\alpha\, u(\alpha) \tag{2.6}$$

Integrating as before gives the dispersion relation

$$\chi(\lambda) \equiv \frac{\lambda}{2}\ln\left(\frac{\lambda+1}{\lambda-1}\right)-1 = \frac{1}{F_0}. \tag{2.7}$$

Two sets of λ-values are easily checked to give a real χ : the real line excluding [-1,1] and the imaginary axis. For the latter, when the principal branches of the logarithm and the arctangent are taken,

$$\chi(i\lambda) = \frac{\lambda}{2}tan^{-1}\left(\frac{2\lambda}{\lambda^2-1}\right)-1 .$$

The sketches of χ over these sets (Figure 3b) divide the values of F_0 naturally into three regimes for discussion :

(i) $F_0<-1$. An imaginary eigenvalue occurs, in consistency with stability considerations above.

(ii) $-1<F_0<0$. No real solution to (2.7) is found. Only real solutions are allowed in this regime and the next by stability analysis.

(iii) $F_0>0$. A unique discrete eigenvalue λ_c stands out as a pole in $S(q,\omega)$[†]. To calculate $S(q,\omega)$ we note that the transition amplitude is [(1.17) and (1.18)]

$$<\Psi_c|\hat{\rho}(\vec{q})|\Psi_0> = \sum_{\vec{k}} [X^{\zeta *}_{\vec{k}+\vec{q},\vec{k}} + Y^{\zeta *}_{\vec{k}-\vec{q},\vec{k}}]$$

$$= \frac{\Omega}{(2\pi)^2} q k_F^2 \zeta^* ,$$

or, the residue at λ_c is

$$S_c = \frac{1}{A}\int_{\omega_c-\varepsilon}^{\omega_c+\varepsilon} d\omega S(q,\omega) = \frac{\Omega}{\rho}\left[\frac{qk_F}{2\pi^2}\right]^2 |\zeta|^2 .$$

In terms of $u(\alpha)$, the normalization condition (1.15) reads

$$\frac{\Omega}{2\pi^2} q k_F^2 \int_{-1}^{1} d\alpha \frac{|u(\alpha)|^2}{\alpha} = 1 . \tag{2.8}$$

Substituting (2.6) into this equation, we have

$$\Omega|\zeta|^2 = \frac{4(2\pi)^2}{qF_0^2 k_F^2 \zeta_1} \quad ; \quad \zeta_1 \equiv \int_{-1}^{1} \frac{\alpha}{(\lambda_c-\alpha)^2} d\alpha = \ln\left[\frac{\lambda_c-1}{\lambda_c+1}\right] + \frac{2\lambda_c}{\lambda_c^2-1},$$

$$\text{or} \quad S(q,\omega) = \frac{1}{\rho\zeta_1}\left[\frac{k_F}{\pi F_0}\right]^2 q\ \delta(\hbar\omega-\hbar\omega_c) \qquad \text{with} \quad \lambda>1 \tag{2.9}$$

[†] As usual, only the positive branch needs to be considered.

We now examine the possible solutions corresponding to λ within [0,1] when $F_0 > -1$. For any λ which is an eigenvalue, the solution is given by (2.6) at $\alpha \neq \lambda$. With ζ assumed finite, $u(\alpha)$ has a singularity at $\alpha=\lambda$. By virtue of this, the integrated version of (2.5),

$$\int_{-1}^{1} d\alpha\, (\lambda-\alpha)u(\alpha) = \frac{F_0\zeta}{2}$$

must also be satisfied. Let us look at the problem through perturbation theory. The R.H.S. of (2.5) is the unperturbed term. If the perturbed eigenvalues are expanded in a Rayleigh-Schroedinger series [e.g. Ba69], it is easily seen that all correction terms are of $O(A^{-1})$ in our case. This means the zeroth-order spectrum is unchanged by perturbation in an infinite system. The discrete eigenvalue outside [-1,1] can only be obtained non-perturbatively. Of $O(1)$, the eigenvectors demand more attention. We use the following trick of adding a small imaginary part to λ and letting it go to zero at the end. The ansatz is

$$u(\alpha) = -\frac{\zeta}{2} \cdot \frac{F_0\alpha}{\alpha-\lambda+i\eta} + b_\lambda \delta(\alpha-\lambda) \qquad (2.10)$$

b_λ is found by integrating both sides :

$$b_\lambda = \zeta[1 - F_0(\chi_1(\lambda) + \frac{i\pi\lambda}{2})]$$

where $$\chi_1(\lambda) \equiv \frac{\lambda}{2}\ln\left(\frac{1+\lambda}{1-\lambda}\right) - 1 \ .$$

Thus a consistent solution can be found for each $0<\lambda<1$. $S(q,\omega)$ is again calculated by invoking the normalization condition (2.8). Involving $|u(\alpha)|^2$, the normalization integral is dominated by the delta function :

$$\Omega \int_{-1}^{1} d\alpha \frac{|u(\alpha)|}{\alpha} = \Omega \frac{|b_\lambda|^2}{\lambda}\delta(\lambda-\lambda) = \frac{(2\pi)^2}{qk_F^2}$$

or $$\Omega|\zeta|^2\delta(\lambda-\lambda) = \frac{(2\pi)^2}{qk_F^2}\cdot\frac{\lambda}{[1-F_0\chi_1(\lambda)]^2+\frac{\pi^2\lambda^2}{4}F_0^2}.$$

With the energy delta function absorbed in $u(\alpha)$, $S(q,\omega)$ is a finite, continuous function in this region :

$$S(q,\omega) = \frac{1}{\rho}\left[\frac{1}{(2\pi)^2}qk_F^2\right]^2\Omega|\zeta|^2\delta(\lambda-\lambda)$$

$$= \frac{m^*k_F}{2\pi^3\rho\hbar^2}\cdot\frac{\frac{\pi}{2}\lambda}{[1-F_0\chi_1(\lambda)]^2+\frac{\pi^2\lambda^2}{4}F_0^2}, \qquad 0<\lambda<1\,. \tag{2.11}$$

(2.10) represents an essentially single particle-hole pair (delta function) mixed by F_0 with a small proportion of other pairs. In contrast, the discrete eigenvalue, called a collective excitation, is a coherent superposition of all members of the particle-hole basis. A sketch of $S(q,\omega)$ for typical values of $-1<F_0<0$ is displayed in Figure 5 (solid).

For positive F_0, considerations of the strong- and weak-coupling limits provide illuminating insights about the behavior of the resonance. When $F_0\ll 1$, λ_c tends to 1, and (2.7) reduces to $F_0\approx-\frac{2}{\ln(\lambda_c-1)}$. At the same time, $\zeta_1\approx\ln(\lambda_c-1)+\frac{1}{\lambda_c-1}$, giving

$$S_c \sim \frac{1}{F_0^2\zeta_1}\sim\frac{[\ln(\lambda_c-1)]^2(\lambda_c-1)}{4} = \frac{\lambda_c-1}{4}.$$

Over the continuum, $S(q,\omega)$ approaches the HF structure. The energy-weighted sum, supported only by the continuum, is correct up to a factor $\frac{m^*}{m}$:

$$\lim_{F_0\to 0}S_1(q) \approx \hbar^2\int_0^1 S(q,\omega)\omega d\omega = \frac{\hbar^2q^2}{2m^*} \tag{2.12a}$$

At the other extreme, both λ_c and F_0 approach infinity. $\frac{1}{F_0}$ and ζ_1 can then be expanded in $\frac{1}{\lambda_c}$, where some care is warranted because of the cancellations of terms of leading orders. The result is

$$\frac{1}{F_0} = \frac{\lambda_c}{2}\ln(1+\frac{2}{\lambda_c-1})-1 \approx \frac{1}{3\lambda_c^2}+\cdots \quad ; \quad \zeta_1 \approx \frac{4}{3\lambda_c^3}+\cdots$$

The contribution of the single particle-hole pair to $S_1(q)$ clearly falls as $\frac{1}{F_0^2}$, leaving the collective mode to exhaust the sum :

$$\lim_{F_0\to\infty} S_1(q) \approx \hbar\omega_c S_c \approx \frac{1}{\rho}\left(\frac{k_F}{\pi}\right)^2 \frac{q}{12\lambda_c}\cdot\hbar\omega_c = \frac{\hbar^2 q^2}{2m^*} \qquad (2.12b)$$

To summarize, the collective excitation starts out in the strong-coupling limit as a totally dominating mode far from the threshold $\lambda_c=1$. As the interaction decreases in magnitude, it slides down the energy axis, its strength being channeled into the continuum at the same time. This draining is completed at $F_0=0$ where the resonance disappears. The EWSR, which the full RPA satisfies exactly, is an obvious limitation of this model when m^* is significantly different from m. In these cases either the scale of $S(q,\omega)$ or its distribution over the spectrum will be off substantially.

We may also note an interesting phenomenon in the continuum when F_0 is positive and small. For any small F_0 a λ can be found to make $1-F_0\chi_1(\lambda)=0$, leading to a peak at that point. As $\chi_1\to\infty$ when $\lambda\to 1$, the peak is drawn closer to 1 as the collective mode λ_c approaches from the other side. This is analogous to the low-energy resonance in elastic scattering when a bound state is nearby [Ba69]. In a sense, the collective mode is a particle-hole pair in a bound state.

As F_0 draws closer to -1, a structure resembling a damped resonance peak becomes perceptible. The F_0-dependence of the derivative at $\lambda=0$, $\frac{\partial S(q,\omega)}{\partial \omega}|_{\omega=0} \sim \frac{1}{1+F_0}$, indicates that this peak shifts downwards in energy until it reaches zero at the onset of instability. In fact, it has been interpreted as a collective mode embedded and thus damped -- Landau-damped is the jargon -- by the particle-hole continuum.

2.3. A Smoothing Procedure for the Continuum

By its nature, the quadrature approximation described in Section 2.1 displays its eigenvalues as a set of discrete points. Over what should be a continuum, then, the 'measure' of the smooth part of the dynamic form factor is drawn into artificial poles as typified by (2.3). This feature is of course a general symptom of solving integral equations by discretization. What is called for, then, is a suitable measure-redistributing procedure to recover the continuum of $S(q,\omega)$. This is largely a theoretical exercise for the hypothetical nuclear matter but is relevant experimentally for liquid ^{3}He and the electron gas.

In principle, all smoothing recipes give the same result when a sufficiently fine mesh is used. Nevertheless, as we shall see, the computer processing time goes up as the cube of the mesh size, while $S(q,\omega)$ as given in (2.3) converges only at a rate roughly proportional to the square root of the same. It is thus not practical to pepper the integration region heavily with quadrature nodes. An efficient procedure should accelerate the convergence, i.e., provide a reliable approximation to the RPA-$S(q,\omega)$ with a relatively coarse mesh. The compromise between reliability and computing time may have to be reached empirically in each case. A description of the smoothing procedure employed here follows.

First one must be able to identify genuinely discrete eigenvalues, if any exist. The analysis in the previous section is helpful here. Accessible through perturbation with the correction terms of $O(A^{-1})$, the continuous spectrum is identical to the HF particle-hole spectrum. It turns out that, for the potentials we consider, the single particle energy $\varepsilon_{\vec{k}}$ is a monotonically increasing function of k. For each $\vec{q}$, therefore, the upper end of the continuum is equal to $\Delta\varepsilon_q(k_F,0)\equiv\hbar\omega_b$. Any eigenvalue lying beyond this point belongs to the discrete set. Owing to its collective nature, the coherent eigenvalue enjoys relatively rapid convergence with respect to mesh size. Depending on its exact position, a coarse mesh (e.g. 16 points) is usually sufficient to demonstrate its presence separated from of the continuum.

For each spurious pole created by discretization, we substitute a Lorentzian for the delta function :

$$\delta(\omega-\omega_n) \rightarrow \frac{1}{\pi}\cdot\frac{\Gamma}{(\omega-\omega_n)^2+\Gamma^2}$$

This is equivalent to replacing $i\eta$ by a finite imaginary part $i\Gamma$ in the denominators of $\Pi^R(q,\omega)$ and had been used by [Be75] in the finite-nuclear RPA problem. Before discussing the choice of Γ, we note that Lorentzian smoothing alone is not adequate in the case of nuclear matter. The examples of the ideal gas and the local-kernel show that $S(q,\omega)$ may drop to zero rather abruptly at the upper branch point. Decaying slowly, the Lorentzian will very likely allow too much strength to be taken away from the continuum. To satisfy the boundary conditions explicitly, we superimpose a triangle with vertices at (0,0), $(\omega_n,1)$ and $(\omega_b,0)$. Thus

$$S(q,\omega) = \sum_n S_n g_n \frac{\Gamma}{(\omega-\omega_n)^2+\Gamma^2}\begin{cases}\dfrac{\omega}{\omega_n} & 0<\omega<\omega_n \\ \dfrac{\omega_b-\omega}{\omega_b-\omega_n} & \omega_n<\omega<\omega_b\end{cases} \qquad (2.13)$$

S_n is the residue at each pole, and the normalizing factor g_n ensures that the integral over each term equals S_n. It is given by

$$\frac{1}{g_n} = \tan^{-1}\left(\frac{\omega_n}{\Gamma}\right)+\tan^{-1}\left(\frac{\omega_b-\omega_n}{\Gamma}\right)-\frac{\Gamma}{2\omega_n}\ln\left[1+\left(\frac{\omega_n}{\Gamma}\right)^2\right]-\frac{\Gamma}{2(\omega_b-\omega_n)}\ln\left[1+\left(\frac{\omega_b-\omega_n}{\Gamma}\right)^2\right]$$

Usually too flat, the triangle alone is very poor at reproducing sharper features.

With the help of the solvable example of the free Fermi gas, we next illustrate (and justisfy) the procedures described above. k_F and q are set at the realistic values of 1.4 fm^{-1} and $0.1k_F$ respectively. The mesh has 8 k-points and 2,6,10,12,12,14,16,24 α-points corresponding to them respectively. In Figure 4, the solid curve with a kink is the exact $S(q,\omega)$ according to (0.6), and (2.13) gives the other solid line with $\hbar\Gamma$=0.8 Mev. We may compare this reconstructed $S(q,\omega)$ with two simpler variants. The dotted line represents Lorentzian smoothing without the triangle, while the dashed line, at the other extreme, is obtained without the Lorentzian. Their inadequacy, for reasons mentioned above, is amply demonstrated.

We now turn to the question of determining Γ given a certain mesh size. It is shown in the last section that $\Delta\varepsilon_q(\vec{k})$ is proportional to k_z for small q. At least for our purpose here, this proportionality is crudely upheld to much larger q. Suppose the mesh points were uniformly distributed in a square region in (k_ρ,k_z)- space. The measure in each artificial singularity should then be spread, on either side, over an interval proportional to the distance between the corresponding quadrature node and its neighbor in the k_z-direction. In the case of nonuniform distribution in an irregular region, the same formula may still be used on the average :

$$\frac{\hbar\Gamma}{\Delta\varepsilon_q(k_F,0)} = \left[\frac{a}{N}\right]^{1/2}\left[\frac{\hbar^2}{2m}(2k_Fq+q^2)\right]^{-1} \qquad (2.14)$$

where N is the number of quadrature points and a, the area of the region, is given by

$$a = k_F^2 [\sin^{-1}x + x\sqrt{1-x^2}] \quad , \quad x \equiv \frac{q}{2k_F}.$$

one can take Γ^{-1} to be a measure of the accuracy of the discretized version of $S(q,\omega)$. In this sense the earlier estimate that the convergence of the mesh goes as $N^{-\frac{1}{2}}$ is implied by (2.14). It should be quite safe to extend this argument to any other smoothing procedures involving a damping width. Figure 6 displays the same $S(q,\omega)$ in the above example with $\dot{\Gamma}$ prescribed by (2.14). (From now on, the width calculated this way will be denoted by Γ_0.) This considerably smaller width results in fluctuations and, at the same time, better agreement with the exact function on the average. Also shown is a very satisfactory curve obtained with $\hbar\Gamma_0$=2.93 Mev for $q=0.5k_F$ (Figure 7). We may conclude that the region containing the excitable orbitals for $q=.1k_F$ is too irregular for the 'averageness' of (2.14) to hold. Nevertheless, rather than overworking this point, we will continue to use Γ_0 or a larger Γ, keeping their limitations in mind.

2.4 Spin and Isospin

The inclusion of the spin (and isospin) degrees of freedom causes a 4(16)-fold expansion of the particle-hole basis. Fortunately, many effective hamiltonians currently in use are scalars or simple tensors under rotations in these subspaces. More block diagonalizations are thus expected to occur. The quantum numbers of the excitations for a general v6 force (defined below) will be explicitly extracted. In the process, we can define a particle-hole force, useful in understanding the qualitative behavior of $S(q,\omega)$, in terms of the given potential in the *particle-particle* channels. Called the Pandya relations, this result is

well-known for a spin-isospin-scalar or v4 hamiltonian, a special case of v6.

We begin with notational matters in the particle-particle channel. S,T,m_S,T_3 denote, respectively, the total spin and isospin, and the z-components of these vectors. σ_p,σ_h are spin directions of individual particles. P_σ^S,P_τ^T stand for projection operators with the numbers 0, 1 in the place of S, T; and $P^{ST}\equiv P_\sigma^S P_\tau^T$. $\hat{S}_{12}\equiv 3(\vec{\sigma}_1\cdot\hat{r})(\vec{\sigma}_2\cdot\hat{r})-\vec{\sigma}_1\cdot\vec{\sigma}_2$ is the familiar tensor operator. Where appropriate, the corresponding quantities in the particle-hole channel are denoted by the same symbols with tildes. In this notation, a v6 force has the general form :

$$V(12) = V^{1-}(r)P^{00}+V^{1+}(r)P^{01}+V^{3+}(r)P^{10}+V^{3-}(r)P^{11}+V_T^+(r)P_\tau^0\hat{S}_{12}+V_T^-(r)P_\tau^1\hat{S}_{12}$$

Without the terms involving $\hat{S}_{12}$, $V(12)$ is said to be of the v4 form. For the spin and isospin algebra, we follow the phase convention of [Ed60]. Where there is no risk of ambiguity, we omit the label for the total spin (isospin) : 'spin σ_k' and 'spin $\tilde{m}_S$' mean 'spin $(\frac{1}{2},\sigma_k)$' and 'spin $(\tilde{S},\tilde{m}_S)$' respectively.

In the ground state of free nuclear matter, each momentum orbital below the Fermi level is fourfold degenerate to allow for the possible orientations in spin and isospin spaces, all of which are filled. Under the v4 force, these orbitals form an orthonormal basis diagonalizing the HF hamiltonian (1.4a). Thus with the degeneracy preserved by this force, the free fermion state is still the best static HF state for our purposes. The same holds for a v6 force, as the tensor terms do not contribute to the HF equation (1.4) by spin conservation. To see this we note that our candidate for $|\Phi_0\rangle$ has $\tilde{S}=\tilde{T}=0$, and while $\hat{S}_{12}$ is a rank-2 tensor, $a_p^\dagger a_h|\Phi_0\rangle$ is a superposition of states with $\tilde{S}=1$ and $\tilde{S}=0$. The matrix element thus vanishes by the Wigner-Eckart theorem.

We now work through the part of RPA-response theory involving the spin of the orbitals. The momentum and isospin labels are suppressed for the moment.

In our convention, $a^\dagger_{\sigma_p}$, $(-1)^{\frac{1}{2}-\sigma_p} a_{-\sigma_p}$ are tensor operators of spin σ_p, while $a^\dagger_{\sigma_h}$, $(-1)^{\frac{1}{2}+\sigma_h} a_{-\sigma_h}$ have spin σ_h [see, e.g., Fe71]. With these, we can construct tensor particle-hole operators, of rank 0 and 1, through Clebsch-Gordan coefficients[†] :

$$\xi^\dagger_{\tilde{S}\tilde{m}_S} = \sum_{\sigma_p \sigma_h} <\sigma_p \sigma_h \,|\, \tilde{S}\tilde{m}_S> a^\dagger_{\sigma_p} a_{-\sigma_h} (-1)^{\frac{1}{2}+\sigma_h}$$

$\xi^\dagger_{\tilde{S}\tilde{m}_S}$ and $(-1)^{\tilde{S}-\tilde{m}_S} \xi_{\tilde{S}\,-\tilde{m}_S}$, both of spin $\tilde{m}_S$, creates and annihilates respectively a particle-hole pair when acting to the right. The Slater determinant can then be written as

$$|\Phi> = \exp\Big(\sum_{\tilde{S}\tilde{m}_S} C_{\tilde{S}\tilde{m}_S}(t) \xi^\dagger_{\tilde{S}\tilde{m}_S}\Big) |\Phi_0>$$

where $C_{\tilde{S}\tilde{m}_S} \equiv \sum_{\sigma_p \sigma_h} (-1)^{\frac{1}{2}+\sigma_h} <\tilde{S}\tilde{m}_S \,|\, \sigma_p \sigma_h> C_{\sigma_p \sigma_h}$.

Easily checked is $<\Phi_0 | \xi_{\tilde{S}'\tilde{m}_S'} \xi^\dagger_{\tilde{S}\tilde{m}_S} | \Phi_0> = \delta_{\tilde{S}\tilde{S}'} \delta_{\tilde{m}_S \tilde{m}_S'}$, which allows us to formally transcribe the derivation in Chapter 1 in terms of $C_{\tilde{S}\tilde{m}_S}$. For simplicity, $\hat{P}$ is taken to be a tensor of spin, say $(\tilde{S}_P, \tilde{m}_P)$. To allow for its possible non-hermiticity, we must take $C_{\tilde{S}\tilde{m}_S}$ and $C^*_{\tilde{S}\tilde{m}_S}$ to be independent and make use of both equations in (1.3)[*]. The relevant terms in $\hat{P}$ are, by the Wigner-Eckart theorem

$$\hat{P} = P_{\tilde{S}_P}[\xi^\dagger_{\tilde{S}_P \tilde{m}_P} P_{ph} + (-1)^{\tilde{S}_P} \xi_{\tilde{S}_P\,-\tilde{m}_P} (-1)^{\tilde{S}_P - \tilde{m}_P} P_{hp}] + \cdots \qquad (2.16)$$

[†] The j-label : $\frac{1}{2}$ is also omitted from the Clebsch-Gordan coefficients.

[*] Or we may use two entirely different functions. L being not necessarily real, the two equations in (1.3) are not equivalent.

where $P_{\tilde{S}_P} \equiv \frac{<\frac{1}{2}\|\tilde{S}_P\|\frac{1}{2}>}{\sqrt{2\tilde{S}_P+1}}$.

P_{ph} represents the parts dependent on momentum and isospin. The analog of (1.14) is

$$\tilde{\lambda}(\omega)P_{\tilde{S}_P}\delta_{\tilde{S}_P\tilde{S}}\begin{pmatrix} P_{ph}\delta_{\tilde{m}_P\tilde{m}_S} \\ (-1)^{\tilde{S}_P}P_{hp}\delta_{-\tilde{m}_P\tilde{m}_S}\end{pmatrix} = \begin{pmatrix} A-\hbar\omega-i\eta & \bar{B} \\ B^* & \bar{A}^*+\hbar\omega+i\eta\end{pmatrix}\begin{pmatrix} \tilde{C}_{\tilde{S}\tilde{m}_S}(\omega) \\ (-1)^{\tilde{S}+\tilde{m}_S}\tilde{C}^*_{\tilde{S}\tilde{m}_S}(-\omega)\end{pmatrix}$$

where $A_{\tilde{S}\tilde{m}_S,\tilde{S}'\tilde{m}_{S'}} \equiv <\Phi_0|\xi_{\tilde{S}\tilde{m}_S}\hat{H}\xi^\dagger_{\tilde{S}'\tilde{m}_{S'}}|\Phi_0> - <\Phi_0|\hat{H}|\Phi_0>\delta_{\tilde{S}\tilde{S}'}\delta_{\tilde{m}_S\tilde{m}_{S'}}$,

$$B_{\tilde{S}\tilde{m}_S\tilde{S}'\tilde{m}_{S'}} \equiv <\Phi_0|\xi_{\tilde{S}'\tilde{m}_{S'}}\xi_{\tilde{S}\tilde{m}_S}(-1)^{\tilde{S}+\tilde{m}_S}\hat{H}|\Phi_0>,$$

$$\bar{A}_{\tilde{S}\tilde{m}_S,\tilde{S}'\tilde{m}_{S'}} \equiv (-1)^{\tilde{S}+\tilde{m}_S+\tilde{S}'+\tilde{m}_{S'}}A_{\tilde{S}\tilde{m}_S,\tilde{S}'\tilde{m}_{S'}},$$

$$\bar{B}_{\tilde{S}\tilde{m}_S,\tilde{S}'\tilde{m}_{S'}} \equiv (-1)^{\tilde{S}+\tilde{m}_S+\tilde{S}'+\tilde{m}_{S'}}B_{\tilde{S}\tilde{m}_S,\tilde{S}'\tilde{m}_{S'}}.$$

The linear response manifested by $\hat{Q}^\dagger$ ($\hat{Q}$ having spin $(\tilde{S}_Q,\tilde{m}_Q)$) becomes

$$\frac{\tilde{\delta}_\omega<\hat{Q}^\dagger,\hat{P}>}{\tilde{\lambda}(\omega)} = Q_{\tilde{S}_Q}\sum_{ph}[\tilde{C}_{\tilde{S}_Q\tilde{m}_Q}(\omega)Q^\dagger_{hp} + (-1)^{\tilde{S}_Q}\tilde{C}_{\tilde{S}_Q-\tilde{m}_Q}(-\omega)(-1)^{\tilde{S}_Q-\tilde{m}_Q}Q^\dagger_{ph}]$$

$$= Q_{\tilde{S}_Q}P_{\tilde{S}_P}[\,Q^\dagger_{hp}\;\;(-1)^{\tilde{S}_Q}Q^\dagger_{ph}\,]\begin{pmatrix} A-\hbar\omega-i\eta & \bar{B} \\ B^* & \bar{A}^*+\hbar\omega+i\eta\end{pmatrix}^{-1}\begin{pmatrix} P_{ph} \\ (-1)^{\tilde{S}_P}P_{hp}\end{pmatrix}.$$

The above matrix does not satisfy the generic symmetries of the RPA matrix which lead to the representation (1.16). Rather than tackling yet another RPA-type problem, we specialize to cases where $\hat{H}$ has simple symmetries. With a v4-force, $\hat{H}$ is a scalar in spin space, and we can see immediately from the definitions of A and B that they are diagonal with $\tilde{S}=\tilde{S}'$, $\tilde{m}_s=\tilde{m}_s'$ for A and $\tilde{S}=\tilde{S}'$ $\tilde{m}_s=-\tilde{m}_s'$ for B. Independent of the sign of $\tilde{m}_s$ by the WE theorem, the matrix

reduces back to the form of the ordinary RPA matrix. We can repeat the process for isospin, and, diagonalizing as before, write

$$<\Psi_n|\hat{P}|\Psi_0> = P_{\tilde{S}_P}P_{\tilde{T}_P}\sum_{ph}[X^{n*}_{\tilde{S}_P\tilde{m}_P\tilde{T}_P\tilde{T}_{3P}}P_{ph}+(-1)^{\tilde{S}_P+\tilde{T}_P}Y^{n*}_{\tilde{S}_P-\tilde{m}_P\tilde{T}_P-\tilde{T}_{SP}}P_{hp}] \quad (2.17)$$

Putting $\hat{P}$ to be one of the (spin-isospin) density operations in Section 0.3 and $\hat{Q}=\hat{P}$, we can construct the RPA approximant to the particle-hole propagation and dynamic form factor in each channel. The reduced matrix elements in this case are easily concluded: $<\frac{1}{2}\|\frac{\sigma}{2}\|\frac{1}{2}>=\sqrt{\frac{3}{2}}$, $<\frac{1}{2}\|1\|\frac{1}{2}>=\sqrt{2}$. The expressions are finally the same as (1.19) and (1.20) except for a coefficient $\rho_{\tilde{S}\tilde{T}}$ and a factor $(-1)^{\tilde{S}+\tilde{T}}$ in front of Y^{n*}_{ph}. Thus

$$S_{\tilde{S}\tilde{m}_3\tilde{T}\tilde{T}_3}(q,\omega) = \frac{\rho_{\tilde{S}\tilde{T}}}{\hbar A}\sum_{\omega_n>0}[\sum_{\vec{h}}(X^{n*}+(-1)^{\tilde{S}+\tilde{T}}Y^{n*})]^2\delta(\omega-\omega_n) \quad (2.18)$$

where

$(\tilde{S},\tilde{T})$	(0,0)	(0,1)	(1,0)	(1,1)
$\rho_{\tilde{S}\tilde{T}}$	4	1	1	$\frac{1}{4}$

The reader is referred to (1.20) and (2.17) for the omitted subscripts on X and Y.

As in Section 2.1, the single-particle part is separated from A. The ingredients of the matrix can be phrased in terms of a single-particle potential and particle-hole potentials in r-space:

$$\Delta\varepsilon(\vec{p},\vec{h}) = \frac{\hbar^2}{2m}(q^2+2\vec{q}\cdot\vec{h})+\sum_{j<k_F}<\vec{h}\vec{j}\,|\,V_{sp}\,|\,\vec{j}\vec{h}>-<\vec{p}\vec{j}\,|\,V_{sp}\,|\,\vec{j}\vec{p}> \quad (2.19)$$

$$A^{\tilde{S}\tilde{T}}_{\vec{p}\vec{h},\vec{p}'\vec{h}'} = <\vec{h}'\vec{p}\,|\,V_d^{\tilde{S}\tilde{T}}|\vec{p}'\vec{h}>+<\vec{h}'\vec{p}\,|\,V_e^{\tilde{S}\tilde{T}}|\vec{h}\vec{p}'>$$

$$B^{\tilde{S}\tilde{T}}_{\vec{p}\vec{h};\vec{p}'\vec{h}'} = (-1)^{\tilde{S}+\tilde{T}}[<\vec{p}\vec{p}'|V^{\tilde{S}\tilde{T}}_d|\vec{h}\vec{h}'>+<\vec{p}\vec{p}'|V^{\tilde{S}\tilde{T}}_e|\vec{h}'\vec{h}>]$$

where

$$V_{sp}(r) = \frac{9}{4}V^{1-} - \frac{3}{4}V^{1+} - \frac{3}{4}V^{3-} + V^{3-}$$

$$V^{\tilde{S}\tilde{T}}_d = \sum_{ST}(-1)^{1-S-T}C(\tilde{S},\tilde{T};S,T)V(r)P^{ST}$$

$$V^{\tilde{S}\tilde{T}}_e(r) = \sum_{ST}C(\tilde{S},\tilde{T};S,T)V(r)P^{ST}$$

$$C(\tilde{S},\tilde{T};S,T) = -(2S+1)(2T+1)\begin{Bmatrix} \frac{1}{2} & \frac{1}{2} & \tilde{S} \\ \frac{1}{2} & \frac{1}{2} & S \end{Bmatrix}\begin{Bmatrix} \frac{1}{2} & \frac{1}{2} & \tilde{T} \\ \frac{1}{2} & \frac{1}{2} & T \end{Bmatrix}.$$

The relevant numerical values of $C(\tilde{S},\tilde{T};S,T)$, the so-called Pandya coefficients [Pa56], are included in Table 2.1 . The factor $(-1)^{1-S-T}$ in front of the direct term ensures overall antisymmetry of the kernel. As probably expected, the matrix, and thus the results, is degenerate in $\tilde{m}_S$, $\tilde{T}_3$. Repeating the coefficient space analysis in Section 2.1 amounts to substituting these particle-hole potentials into (2.2):

$$A^{\tilde{S}\tilde{T}}_{qm}(k,\alpha,k',\alpha') = \frac{1}{\pi}[\delta_{m0}V^{\tilde{S}\tilde{T}}_d(q)+\sum_l(2l+1)\frac{(l-m)!}{(l+m)!}P^m_l(\alpha)P^m_l(\alpha')V^{\tilde{S}\tilde{T}}_e(k,k')] \qquad (2.20)$$

$$B^{\tilde{S}\tilde{T}}_{qm}(k,\alpha,k',\alpha') = \frac{(-1)^{\tilde{S}+\tilde{T}}}{\pi}[\delta_{m0}V^{\tilde{S}\tilde{T}}_d(q)+\sum_l(2l+1)\frac{(l-m)!}{(l+m)!}P^m_l(\alpha)P^m_l(-\alpha'_p)V^{\tilde{S}\tilde{T}}_{el}(k,p')]$$

The overlap of these potentials with various spherical Bessel functions are most relevant in determining the behavior of the spectrum and $S^{\tilde{S}\tilde{T}}(q,w)$.

The tensor operator $\hat{S}_{12}$ is the scalar product of two second rank tensors, one in configuration space and the other in spin space : $\hat{S}_{12}=(\frac{24\pi}{5})^{\frac{1}{2}}\sum_{m_T}(-1)^{m_T}Y_{2m_T}(\vartheta,\varphi)\bar{S}_{2\,-m_T}$ where

m_T	$\bar{S}_{2m_T}$
2	S_+^2
1	$-(S_+S_z+S_zS_+)$
0	$\sqrt{\frac{2}{3}}(3S_z^2-S^2)$
-1	$S_-S_z+S_zS_-$
-2	S_-^2

Thus although it eliminates m and $\tilde{m}_S$ from the class of good quantum numbers, it still honors their sum, the z-component of the total angular momentum, $M=m+\tilde{m}_S$. $(-1)^{\tilde{m}_s}$ is replaced by $(-1)^M$ in the definition of $\bar{A}$ making $\bar{A}=A$. The triangle rule of spin addition -- $\begin{pmatrix}\tilde{S} & 2 & \tilde{S}'\\ \tilde{m}_s & m_T & -\tilde{m}_s'\end{pmatrix} \neq 0$ only when $\tilde{S}=\tilde{S}'=1$ -- keeps the spin channels decoupled with the tensor force contributing only in the $\tilde{S}=1$ channel. When averaged over the Fermi sea, the tensor term vanishes and therefore has no effect on the energy, and $\Delta\varepsilon(p,h)$. The isospin analysis stays intact. So for $\tilde{S}=1$, the v4 terms of the matrix elements are as given in the last paragraph. The tensor terms read: $(m=M-\tilde{m}_s)$

$$A^{\tilde{S}=1\ \tilde{T}Mq}_{\tilde{m}_s k\alpha;\tilde{m}_s k'\alpha'} = A^{\tilde{S}=1\ \tilde{T}Mq}_{\tilde{m}_s' k'\alpha';\tilde{m}_s k\alpha} = A^{\tilde{S}=1\ \tilde{T}Mq}_{\tilde{m}_s k\ -\alpha;\tilde{m}_s' k\ -\alpha'} \tag{2.21}$$

$$=\sum_T C_T(\tilde{S}=1,\tilde{T}=1;S=1,T)(-1)^{\tilde{m}_s}\begin{pmatrix}1 & 2 & 1\\ -\tilde{m}_s & \tilde{m}_s-\tilde{m}_s' & \tilde{m}_s'\end{pmatrix}$$

$$\cdot\langle h'p\mid V_T(r)Y(2,\tilde{m}_s-\tilde{m}_s')P_\tau^T\mid p'h\rangle_\alpha\cdot\left(\frac{24\pi}{5}\right)^{\frac{1}{2}}$$

$$=\sum_T C_T(\tilde{T},T)\begin{pmatrix}1 & 2 & 1\\ -\tilde{m}_s & \tilde{m}_s-\tilde{m}_s' & \tilde{m}_s'\end{pmatrix}\cdot\frac{1}{\pi}[\delta_{m0}\delta_{m'0}\delta_{\tilde{m}_s\tilde{m}_s'}(-1)^{\tilde{m}_s-T}V_2^T(q)+$$

$$(-1)^M\sum_{ll'}(-1)^{\frac{l-l'}{2}+1}(2l+1)(2l'+1)\left[\frac{(l-m)!(l'-m')!}{(l+m)!(l'+m')!}\right]^{\frac{1}{2}}$$

$$\cdot \begin{pmatrix} l & 2 & l' \\ 0 & 0 & 0 \end{pmatrix} \begin{pmatrix} l & 2 & l' \\ m & m'-m & -m' \end{pmatrix} P_l^m(\alpha) P_{l'}^{m'}(\alpha') V_{ll'}^T(k,k')]$$

where

$$V_2^T(q) = \int_0^\infty dr\ r^2 j_2(qr) V^T(r)$$

$$V_{ll'}^T(k,k') = \int_0^\infty dr\ r^2 j_l(kr) j_{l'}(k'l) V^T(r)$$

and

$$V^1(r) \equiv V_T^+(r)$$

$$V^3(r) \equiv V_T^-(r)$$

$$C_T(\tilde{S}=1,\tilde{T},S=1,T) = (2\tilde{S}+1)(2S+1)\langle 1||\bar{S}_2||1\rangle \begin{Bmatrix} \frac{1}{2} & \frac{1}{2} & 1 \\ \frac{1}{2} & \frac{1}{2} & 1 \\ 1 & 1 & 2 \end{Bmatrix} (2T+1) \begin{Bmatrix} \frac{1}{2} & \frac{1}{2} & \tilde{T} \\ \frac{1}{2} & \frac{1}{2} & T \end{Bmatrix}.$$

The numerical values of this C_T are given in Table 2.2. The elements in matrix B are the same as the corresponding ones in matrix A with k' replaced by p', and α' replaced by α_p'. Here a factor $(-1)^m$ has been absorbed into y_m: $y(-\alpha,\varphi)=\sum_m (-1)^m y_m(-\alpha) e^{im\varphi}$. Since $\tilde{m}_s$ ranges from -1 to 1, the size of the matrix must be tripled to obtain the same accuracy as the v4 case. The discretization process described earlier can still be used here.

In this chapter, we have fully utilized the available symmetries of the system to reduce the number of independent variables to only two, namely k and α. For a v4 potential, the excitations are explicitly classified by the momentum, the total spin and total isospin and their respective z-components, and the orbital magnetic quantum number. The z-components of the spin and the orbital angular momentum are not individually conserved by a v6 force, but their sum is. A numerical scheme has been described to solve the resulting integral equations, obtaining the dynamic form factor for each particle-hole channel. The analytic conclusions will be shown to hold also for CRPA in Chapter 4. The results of applying this method to schematic (weak) potentials are presented in the next chapter.

Chapter 3

The method of solution of the RPA and the DDRPA equations described in the last two chapters are illustrated here with model potentials. As an example for each of the categories : v4, density-dependent v4, and v6, we choose, respectively, Molinari double square-well, Gogny d1-potential, and Brown 1π-1ρ exchange force. A hypothetical spinless, isospinless (ν=1) fermion system is used to contrast the exact solution with that coming from the local-kernel approximation (Section 2.2).

Physically, the resulting $S(q,\omega)$'s are to be interpreted as exhibiting collective motion, or Landau-damped collective motion, of the system as discussed in Section 2.2 within the Landau limit. The range and strength of the particle-hole potential in each channel, compared to $\Delta\varepsilon$, determine what type of behavior to expect. As q increases, the kernel diminishes ($\tilde{V}(q)$ decreases and the average of $\tilde{V}(k-k')$ does not change much) while the integration region is bounded by the volume of the Fermi sea. The diagonal term, with the kinetic contribution q^2, will eventually dominate, and all results will approach the free-particle values.

In this chapter and the next, q is quoted in units of k_F. Just the ordered pair $(\tilde{S},\tilde{T})$ is used in the place of the phrase 'the $(\tilde{S},\tilde{T})$ channel', and $S_L(q,\omega)$ denotes the $S(q,\omega)$ gotten in the local-kernel approximation. Finally, the symbols for the different meshes used are explained in Table 3.1.

3.1. The Molinari Square-Well

In Green function language, Molinari *et al* [Al78] did an exercise in the RPA-response theory of nuclear matter in the local-kernel (ring) approximation. The v4-potential they used consists of a channel-independent, finite square-core and a square-well in the spatially even channels (dashed curve in Figure 8) :

$$V(r) = U_0 \qquad 0<r<c$$

$$\begin{cases} V^{1+}(r) = V^{3+}(r) = -V_0 \\ V^{1-}(r) = V^{3-}(r) = 0 \end{cases} \qquad c<r<r_0$$

$$V(r) = 0 \qquad r>r_0$$

The following set of parameters :

U_0 = 2565 Mev $\quad c$ = 0.5 fm
V_0 = 85 Mev $\quad r_0$ = 2.0 fm

lead to saturation at reasonable density and compressibility :

B/A = 16.0 Mev $\quad \rho_0 = 0.185\ \text{fm}^{-3}$ $(k_F = 1.4\text{fm}^{-1})$
κ = 177.3 Mev

The single-particle potential is entirely positive :

$$V_s(r) = U_0 \qquad 0<r<c$$

$$= \frac{3}{2} V_0 \qquad c<r<r_0$$

which (cf. (2.2)) guarantees an increase of particle-hole energy from the ideal-gas value. Indeed, the effective mass at the Fermi surface is $\frac{m^*}{m} = 0.44$. (0,1),(1,0), and (1,1) share a common set of particle-hole potentials (hereafter we only refer to (1,1)) :

$$V_d^{11}(r) = \frac{1}{2} V_0 \qquad c<r<r_0$$

$$= 0 \qquad \text{elsewhere}$$

$$V_e^{11}(r) = -U_0 \qquad 0<r<c$$

$$= \frac{1}{2} V_0 \qquad c < r < r_0$$

$$= 0 \qquad r > r_0$$

while that in (0,0) is

$$V_d^{00}(r) = 4 U_0 \qquad 0 < r < c$$

$$= -\frac{3}{2} V_0 \qquad c < r < r_0$$

$$= 0 \qquad r > r_0$$

$$V_e^{00}(r) = -U_0 \qquad 0 < r < c$$

$$= -\frac{3}{2} V_0 \qquad c < r < r_0$$

$$= 0 \qquad r > r_0$$

F_0 is taken to be the direct matrix element plus the $l=0$ component of the exchange term. Its numerical values for the two channels, as read from Table 3.2, are $F_0^{00} = -.679$ and $F_0^{11} = 0.353$. The results in Section 2.2 suggest, then, that the uniform phase is stable against fluctuations in all channels, and a collective mode is present in (1,1). Note that if only the direct term is included -- the usual practice in textbook treatments of the ring-diagram approximation [e.g. Fe71] -- the local-kernel approximation will predict collective states in all channels.

We now present numerical results of the exact RPA problem. First the convergence of $S^{\mathcal{ST}}(q,\omega)$ with respect to the mesh size is checked at strategically selected values of q. Here we illustrate the process with $q = 0.1$, where the meshes $2^1, 4^1, 6^1, 8^1$, and 12^1 (Table 3.1) are used. With a VAX/VMS 780 plus a

floating-point accelerator, the amounts of computing time, in ascending order, are 12 secs, 2 mins., 12 mins., 23 mins., and 1 hour. Of these, the bulk is consumed by the diagonalization process : e.g., all but 2 mins. for 12^1. In calculating the matrix elements, (2.2) expresses the exchange term as an expansion in l. Truncation at the values of l listed in Table 3.3 for various potentials limits the error to 10^{-5}. As explained in the case of the free fermions, the choice of the smoothing width is not beyond ambiguity. We again adopt the rule that the smallest Γ (Γ_s) producing a smooth curve be picked. Figure 9 displays the curves obtained by Γ_0, given by (2.14), Γ_s, and some intermediate values of Γ in (0,0) with the 8^1 mesh. The error involved can be roughly extrapolated from the free-fermion results. In Tables 3.4 and 3.5 are listed the Γ_0 and Γ_s of the different meshes with some salient features of the resulting $S(q,\omega)$. The columns under S_0 and S_1 come from the delta-function representation (2.3). They clearly converge to within 1% at the level of 4^1. Normalized by the values of S_0, the smoothed curves introduce errors in S_1, headed by $\frac{\Delta S_1}{S_1}$ in the tables, which can also be a measure of convergence. The pointedness of the Landau-damped peak in (0,0) may be the cause of the higher $\frac{\Delta S_1}{S_1}$ in this channel, although the curves in (1,1) generally require a larger Γ_s. In fact the position of this peak, ω_p, and the value of $S(q,\omega_p)$, are the least ready to converge. In contrast, the collective quantities in (1,1), $\hbar\omega_c, S_c, r_0$, remain practically the same beyond 4^1. Figure 10 shows that, with this mesh, convergence is already quite good outside the peak region in (0,0) and even better in (1,1). The disagreements, though, are beyond the range of uncertainty of the smoothing procedure, as can be seen by a comparison with Figure 9. Finally it is likely that the result will not be rid of the few percent error in S_1 until impractically large meshes are used.

Next the surface $S^{\tilde{S}\tilde{T}}(q,\omega)$ is constructed to the accuracy of 8^1. Sections parallel to the ω-axis at four values of q : 0.05, 0.1, 0.25, 0.5 are shown in Figures

11 and 12 for the two channels. In the latter, the spikes are drawn with a height of $10\frac{S_c}{\pi\omega_c}$ to favor comparison of the diagrams. More detailed q-dependence is highlighted by the quantities in Tables 3.6 and 3.7. One of our main concerns is to delineate the region where $S(q,\omega)$ can be regarded linear in q. As shown in Table 3.6, a cancellation of nonlinear effects from the kinetic part and the potential part of the particle-hole energy leaves the range of the continuum remarkably linear in q. Indeed, while the free-particle branch point, $\Delta\varepsilon_f(k_F)$, at $q=.5$ is 24% above the linear value, its HF counterpart, $\Delta\varepsilon(k_F)$, is off by only 4%. Drawn close to the branch point by a relatively weak interaction, the collective frequency in (1,1) should not deviate much from linearity either. The column under v_c in Table 3.7 bears out this expectation. $\frac{S_0}{q}$ shifts upwards at around $q=.3$, but the first sign of nonlinearity appears between $q=.1$ and .15 where r_0 starts to drop significantly. Supporting this estimate, one may note that Figures 11 and 12 are scaled in such a way that the plotted curves should be identical over the linear region, and clearly those for $q=.05$ and .1 agree rather well. At low q, the collective mode runs at $.69c$ and exhausts 40% of S_0. The weight of the single-pair excitations rises with q up to a point slightly above .25 where the collective mode merges into the continuum. As the damping threshold draws near (Figure 12c), we can see the enhancement analogous to low-energy scattering resonance near a bound state, mentioned in Section 2.2. We leave the curve as it is because further smoothing aimed at the ripples will reduce the peak, a real structure, into the background. An elaboration on our smoothing procedure is needed here. In (0,0) there is a steady decline in both $\frac{S_0}{q}$ and $S(q,\omega_p)$ starting at $q=.1$.

κ_0 and κ compare S_0 and S_1 with the free-particle values : $\frac{\nu S_0(q)}{\rho^{\mathfrak{SF}}}=(1+\kappa_0)S_F(q)$ where $\rho^{\mathfrak{SF}}$ is given by (2.18) and κ is explained in Sections

0.3 and 2.4. κ=1.59 is too high compared to the accepted experimental estimate : 0.8<κ<1. [Zi78]. The κ_0's are mostly below the free-particle value which is also the HF and Tamm-Dancoff values in infinite matter [Ro70] : the difference is caused by the B-matrix. Following Feenberg [Fe69] we may look at S_0 as the virtual (spin-isospin) density fluctuations present in the ground state in either of the two half-spaces ($\vec{q}\cdot\vec{k}>0$ and $\vec{q}\cdot\vec{k}<0$). In the equation-of-motion framework, our results imply that these fluctuations are in most cases suppressed by built-in particle-hole correlations. In Green-function language, allowing the particle-hole pair to propagate backward in time destroys a part of the fluctuations created by the forward-going parts of the propagator.

The local-kernel approximation is now evaluated through comparison with the 'exact' result at q=0.05, which is well within the linear regime. In Figure 5, the dotted curve is given by (2.11) while the dashed curve is the RPA $S^{00}(q,\omega)$. Most striking is the excessive damping of the peak to the advantage of the high-energy single-pair excitations in the local-kernel curve. As a result, while S_0 is off by 40%, S_1 is 2.27 (which is $\frac{m}{m^*}$, as explained in Section 2.2) times the exact value (Table 3.6). κ_0=0.543 is also obtrusively high. Noting that a stronger (more negative) F_0 may gather the excitation strength back under the peak, we plot $S_L(q,\omega)$ for several values of F_0 throughout the range (-1,0) (solid curves). It is evident from these curves that the functional form (2.11) cannot reasonably fit the exact form factor by adjustment of the values of F_0 and m^*. The higher-l components of the exchange term are important qualitatively. The approximation fares no better in (1,1) where both $\lambda_c \equiv \frac{\hbar\omega_c}{\Delta\varepsilon(k_F)}$ and the coherent share of the total strength are far below the exact values (Table 3.7). The proximity of the approximate collective frequency also draws a 'resonance' near the branch point in $S_L(q,\omega)$ which is absent in the exact curve. The Bethe-Levinson enhancement factor to the E1 sum rule, due to the motion of neutrons against

protons, $(1+\kappa(0)=2.59$, Section 2.4) happens to be close to the erroneous enhancement in the local-kernel value (=2.27), bringing the two values of S_1 to within 13% of each other.

3.2. The Gogny D1

In the last decade, Gogny *et al* [Go75, Go77, De80, Gi82] have developed a density-dependent, finite-range potential to correlate through Hartree-Fock-Bogoliubov calculations the ground-state properties of selected nuclei spread over the periodic table as well as nuclear matter. Channelwise, it is a v4 plus a spin-dependent part. A first-rank tensor in spin space, the latter does not contribute to the single-particle energy and is neglected in the kernel. The relevant component in each particle-particle channel is a sum of two Gaussians and a zero-range density-dependent term :

$$V^{1-}(r) = -775.04e^{-(\frac{r}{0.7})^2} + 96.55e^{-(\frac{r}{1.2})^2}$$

$$V^{1+}(r) = 170.24e^{-(\frac{r}{0.7})^2} - 115.61e^{-(\frac{r}{1.2})^2}$$

$$V^{3+}(r) = -1022.16e^{-(\frac{r}{0.7})^2} - 64.61e^{-(\frac{r}{1.2})^2} + 2700\rho^{\frac{1}{3}}\delta(\vec{r})$$

$$V^{3-}(r) = 17.36e^{-(\frac{r}{0.7})^2} - 1.53e^{-(\frac{r}{1.2})^2}$$

The novel feature here is, of course, the density-dependent delta-function term which will receive particular attention in the following discussions. In the HF ground state, it simulates the short-range repulsive core and accommodates effects due to the change in density at the nuclear surface. As pointed out in [De80], the interplay between this repulsive core and the strongly attractive well in the triplet-even channel is the basic mechanism for saturation of nuclear matter with this force. The saturation parameters are k_F = 1.355 fm^{-1}, B/A =

16.32 Mev, and κ = 228 Mev. The equilibrium density is 0.168 fm^{-1}, making the strength of the density-dependent core 1490. Mev. An important fact is that any matrix element of this term is a constant : k-independent. One consequence is the cancellation of its contribution to $\Delta\varepsilon(k_F)$, leaving a relatively weak single-pair potential :

$$V_s = 484.24e^{-(\frac{r}{0.7})^2} + 155.86e^{-(\frac{r}{1.2})^2}$$

In Figure 15, it is compared with and shown to be considerably shorter-ranged and weaker than the Molinari square-well, which accounts for the linearity of the potential contribution to $\Delta\varepsilon(k_F)$ ($\frac{\Delta u(k_F)}{\hbar cq}$ in Table 3.8) up to q=0.5 and a much bigger effective mass : $\frac{m^*}{m}$=0.668 . For the kernel, the particle-hole potential is given by

$$V_d^{\tilde{S}\tilde{T}}(r) = C_{d1}^{\tilde{S}\tilde{T}}\, e^{-(\frac{r}{0.7})^2} + C_{d2}^{\tilde{S}\tilde{T}}\, e^{-(\frac{r}{1.2})^2} + \frac{1}{4\pi} C_{\rho}^{\tilde{S}\tilde{T}}\, \delta(\vec{r})$$

$$V_e^{\tilde{S}\tilde{T}} = C_{e1}^{\tilde{S}\tilde{T}}\, e^{-(\frac{r}{0.7})^2} + C_{e2}^{\tilde{S}\tilde{T}}\, e^{-(\frac{r}{1.2})^2}$$

where the coefficients in the various channels are listed here :

$(\tilde{S}\tilde{T})$	(0,0)	(0,1)	(1,0)	(1,1)
$C_{d1}^{\tilde{S}\tilde{T}}$	-793.6	1016.0	-176.4	23.6
$C_{d2}^{\tilde{S}\tilde{T}}$	-114.5	- 5.7	45.3	68.8
$C_{e1}^{\tilde{S}\tilde{T}}$	-484.2	602.4	-590.0	402.4
$C_{e2}^{\tilde{S}\tilde{T}}$	-155.9	44.8	95.8	21.3
$C_{\rho}^{\tilde{S}\tilde{T}}$	276.7	-177.9	59.3	-59.3

Note that $C_{\rho}^{\tilde{S}\tilde{T}}$ is the sum of the direct and exchange coefficients of the density-dependent term. From the table of Pandya coefficients, these contributions to

(0,0) and (0,1) should be of equal magnitude and opposite signs. The extra strength in (0,0), of course, comes from the rearrangement terms, which is crucial for the stability of the uniform phase against fluctuations in this channel. Table 3.2 gives the following values for the F_0's : F_0^{00}= -0.307 ; F_0^{01}=0.621 ; F_0^{10}=0.470 ; F_0^{11}=0.599 . F_0^{00} can be broken down into 'normal' and rearrangement contributions, which are, respectively, -1.68 and 1.37 : without the latter, the D1 force would predict instability against density fluctuations. The finite-range parts of $V_d^{\tilde{S}\tilde{T}}$ and $V_e^{\tilde{S}\tilde{T}}$, plotted in Figures 13 and 14 respectively, have relative strengths roughly in accord with the F_0's. The mesh 6^2(N=78) is used for low values of q (<0.3) and 8^2 for the rest. The computing time is roughly equally divided between matrix construction (14 mins.) and diagonalization (11 mins.). Figures 16-19 and Tables 3.8-3.10 contain the results of diagonalization as functions of q, while Figures 20 and 21 and Table 3.11 compare certain low-q results with local-kernel values. (Note the different scales in some of the graphs.) The numerical quality is comparable to that of the square-well. Except in (0,0), linearity in q is again maintained in S_0, $\frac{S_1}{q}$, $\hbar\omega_c$ up to q=0.3 or higher. Being the major component in V_d^{01} and V_e^{01}, the strong triplet-even force pushes 0.57 of the total excitation strength into the collective isospin mode. Although this mode is much stronger than its counterpart supported by the square-well, they are damped at more or less the same q, which is attributable to the faster non-linear growth of the single-pair spectrum : the deviation from linearity at q=0.3 is 10% here compared to 4% for the square-well. The low value of λ_c -- a few percent above 1 -- makes the damping threshold very sensitive to this upswing of the branch point, so much so that the spin mode is damped at the remarkably low q of 0.05! The local-kernel r_0's are below the exact values in all channels. Even the largest error, 50% in (0,1), though, is considerably smaller than that of the square-well : 83% . The explanation lies again in the longer range of $V_e^{\tilde{S}\tilde{T}}$, and

therefore greater importance of terms of higher-l, in the latter case. In the three spin-isospin channels, the effects of the B-matrix measured by κ are stronger here. Gogny and Padjen [Go77] solved the Landau transport equation (2.5) exactly with this force, and their results agree with ours at low q.

To summarize, at the HF level, the density-dependent term brings the ground-state saturation properties to consistency with a high effective mass, or, in the words of [De80], a compressed particle-hole spectrum. The rearrangement terms stabilize the uniform phase against density fluctuations. It may also be mentioned that the finite-range part, allowed to be weaker, gives a more realistic value of the E1 enhancement factor κ=0.78. The longer range of the square well delays the damping of the collective mode in (0,1) while causing more serious inaccuracy in the local-kernel approximation.

At the early stage of the project, we looked at a hypothetical spinless (ν=1) Fermi system interacting with only the finite core of the Molinari potential. It is thus not self-bound, but is supposed to be kept by some other force at k_F=1.4 fm^{-1}. The effective mass is 0.935 and F_0=0.201, predicting zero sound. In order to obtain a collective mode at the relatively low q=0.1, we switched to the v4 potential. Recently we returned to this system and discovered some unexpected behavior of $S(q,\omega)$ which calls for theoretical explanation. The system is unstable at very low q. As q grows, so does the magnitude of the imaginary eigenvalue. Between q=0.003 to q=0.005, the imaginary eigenvalue goes to infinity and returns along the real axis (as a collective mode)! As q increases further, $\hbar\omega$ and r_0 continue to fall, the mode disappearing at $q\sim$0.05.

3.3. The Brown 1π-1ρ

In the past few years, Brown et. al. [e.g. Br77, An77] have considered the effects in (1,1) of the finite-range tensor force coming from 1π-1ρ exchange. Specifically they have in mind the magnetic resonances and the possibility of pion condensation at near-saturation densities. In our notation the force is

$$V(\vec{r}) = g(r)[V_\pi(\vec{r}) + V_\rho(\vec{r})]$$

where

$$V_\pi(\vec{r}) = f_\pi^2 m_\pi \frac{e^{-m_\pi r}}{m_\pi r}\left[3P^{11} - P^{13} - P^{31} + \frac{1}{3}P^{33} + \left(\frac{1}{3} + \frac{1}{m_\pi r} + \frac{1}{(m_\pi r)^2}\right)(P_T^3 - 3P_\tau^1)S_{12}\right]$$

$$V_\rho(\vec{r}) = f_\rho^2 m_\rho \frac{e^{-m_\rho r}}{m_\rho r}\left[6P^{11} - 2P^{13} - 2P^{31} + \frac{2}{3}P^{33} + \left(\frac{1}{3} + \frac{1}{m_\rho r} + \frac{1}{(m_\rho r)^2}\right)(3P_\tau^1 - P_T^3)S_{12}\right]$$

$$g(r) = 1 - j_0(q_c r)$$

m_π ($\frac{m_\pi}{\hbar c}$ when multiplied to r) =138 MeV and m_ρ =770 MeV are the masses of the pion and the ρ-meson respectively. The pion coupling parameter f_π^2 equals 0.08. The value of f_ρ^2 varies between 1.86 and 4.86 according to different meson-exchange theories [Br77]. $g(r)$ is a cutoff function to mimic the repulsion caused by the exchange of the ω-meson, to the mass of which we set q_c (=3.93 fm^{-1}; for the legitimacy of this approximation, see the end of Section 4.1). Missing some important pieces for saturation, this force does not bind HF nuclear matter at the right density and energy. It is assumed, however, that the system is in equilibrium at 1.4 fm^{-1} and the effect of the tensor terms is studied more in the spirit of Landau theory than of self-consistent HF/RPA. This invalidates results in all channels other than (1,1). We only use the force here to illustrate the procedure set down in Chapter 2 and consider its bearing on instability

leading to pion condensation. For this purpose a relatively coarse mesh is chosen: 4^2 with N= 40. The computing time needed for the triple matrix (N=120) is 58 mins.

Looking only at M=0, we note from the definition of the tensor force, Section 2.4 and Table 2.2, that the contributions of the pion to the matrix elements are negative while those from the ρ-meson are positive. The j_2's in the radial integrals also favor the longer-ranged π. For the v4 part, the positive direct term is four times the negative exchange contribution for both mesons. Thus the best chance of obtaining a pion condensation is when f_ρ^2 assumes the minimum value: 1.86. We display in Figures 22-25 and Table 3.12 the results of choosing both extremes of f_ρ^2 at q=0.1 and 0.5. The solid (dashed) curves are $S(q,\omega)$ projected into $\tilde{m}_s$=0(1). Clearly the pion interaction is not strong enough to cause an instability, although the (spin-isospin) zero sound for the smaller f_ρ^2 is weaker. Actually both modes are unusually prominent (r_0=0.74, 0.63, $\lambda_c(q=.1)$=1.07, 1.03) because the tensor force does not contribute to the damping single-pair excitations. The strength is to be found, however, totally in the $\tilde{m}_s$=0 space. Also worth considering is the channel M=1, $\tilde{m}_s$=1 where the direct contribution from ρ is negative. Since the ρ is much heavier than the pion, one may hope to find ρ-induced instability at high density. Nevertheless, now that we are convinced about the adequacy of our method in treating the tensor force, we will wait for the Jastrow calculation with realistic tensor force, such as Reid-soft-core, to make any physically meaningful conclusion about this issue.

Chapter 4

The dynamical properties of nuclear matter at long but finite wavelengths have been investigated with weak two-body forces. The more fundamental problem of relating these properties to the realistic, strong nucleon-nucleon potential will be tackled in this chapter. For this purpose, we formally arrived at an RPA in a correlated particle-hole basis $F(1\cdots A)a_p^\dagger a_h|\Phi_0>$ etc. in Chapter 1. Though having the same structure as ordinary RPA, this equation has kernels made up of A-body matrix elements. With the Jastrow ansatz $F(1\cdots A)=\prod_{i<j}^{A} f(r_{ij})$, these matrix elements are to be cluster-expanded and the series evaluated to two levels of accuracy: (i) two-body cluster-order and (ii) Fermi-hypernetted-chain (FHNC) resummation. For the former, since any correlation involving more than two-body is omitted, an effective energy-dependent potential can be extracted. The metric matrix M can also be expressed as plane-wave matrix elements of a function in r-space. With slight modifications, then, all the analyses in Chapter 2 apply here. A further approximation achieves the same for FHNC. We will only sketch the general theory of FHNC collecting the results relevant to CRPA, and leave the details to the references. [Kr79b], [Kr80], [Sa82] have direct bearing on CRPA, and [Cl79a] may be consulted for a general review of the FHNC method.

Let us first, from general considerations, simplify as much as possible the matrix elements in (1.13) [Kr79b]. $\hat{N}_{ph,0}$ vanishes by momentum conservation and $\hat{N}_{ph,ph}=1$. As will be seen, to $O(A^{-1})$, the p-dependent part and h-dependent part of the diagonal energy term $\hat{H}_{ph,ph}-\hat{H}_{00}$ can be separated ($=\varepsilon(p)-\varepsilon(h)$, say)† and also $z_{ph,p'h'}=z_{ph}z_{p'h'}$. Fermi statistics excludes the diagonal terms in the B-matrix. A similarity transformation passes the common factor $z_{ph}z_{p'h'}$ to

†In this sense the particle-hole picture is still valid

the eigenvectors which become $\begin{pmatrix} z_{ph} X_{ph} \\ z_{ph} Y_{ph} \end{pmatrix}$. The remaining components then assume a more familiar form:

$$A_{ph,p'h'} = [\varepsilon(p)-\varepsilon(h)]\delta_{pp'}\delta_{hh'} + \hat{H}_{ph,p'h'} - \hat{H}_{00}\hat{N}_{ph,p'h'} \tag{4.1}$$

$$B_{ph,p'h'} = \hat{H}_{php'h',0} - \hat{H}_{00}\hat{N}_{php'h',0}$$

$$M_{ph,p'h'} = \delta_{pp'}\delta_{hh'} + \hat{N}_{ph,p'h'} \ ;$$

$(p,h)\neq(p',h')$ in all matrix elements of $\hat{H}$ and $\hat{N}$ in (4.1). The diagonal terms may be expressed, and calculated, very economically if we define the following extension of ξ_{ph}:

$$\xi_{ph}(\beta) \equiv \langle\Phi_{ph}|F^{\dagger}e^{\beta\hat{H}}F|\Phi_{ph}\rangle \tag{4.2}$$

$$\ln z_{ph} = \frac{1}{2}\left[\ln\left(\frac{\xi_{ph}}{\xi_0}\right)\right]_{\beta=0}$$

$$\varepsilon(p)-\varepsilon(h) = \left[\frac{\partial}{\partial\beta}\ln\left(\frac{\xi_{ph}}{\xi_0}\right)\right]_{\beta=0}$$

All non-diagonal factors are of the general form $\langle\Phi_m|F^{\dagger}\hat{O}F|\Phi_n\rangle$ where the sets of occupied orbitals $\{m\}$ and $\{n\}$ differ in exactly two orbitals and one of them may be $\{o\}$ -- the free ground state. We may similarly define

$$\hat{N}_{mn}(\beta) = [\xi_m(\beta)\xi_n(\beta)]^{-\frac{1}{2}}\langle\Phi_m|F^{\dagger}e^{\beta\hat{H}}F|\Phi_n\rangle$$

which gives on differentiation,

$$\hat{Y}_{mn} \equiv \left[\frac{\partial}{\partial\beta}\hat{N}_{mn}(\beta)\right]_{\beta=0}$$

$$= \hat{H}_{mn} - \frac{1}{2}(\hat{H}_{mm}+\hat{H}_{nn})\hat{N}_{mn} \ .$$

Writing

$$\hat{H}_{mn}-\hat{H}_{00}\hat{N}_{mn} = \hat{Y}_{mn}+[\frac{1}{2}\hat{H}_{mm}+\frac{1}{2}\hat{H}_{nn}-\hat{H}_{00}]\hat{N}_{mn} \tag{4.3}$$

$$= \hat{Y}_{mn}+\frac{1}{2}[\varepsilon(p)-\varepsilon(h)+\varepsilon(p')-\varepsilon(h')]\hat{N}_{mn}$$

we have formally reduced the problem to the calculation of $\xi_{ph}(\beta)$, $\hat{N}_{mn}(\beta)$ and their β-derivatives. The decomposition into independently dressed particle-hole pairs in the second line of (4.3) will be seen to also apply to $\hat{H}_{php'h';php'h'}-\hat{H}_{00}$

4.1. Cluster Expansion, Diagrammatics, and the Fermi-Hypernetted Chain (FHNC)

This section reviews the method to compute the generic quantities arrived at in the last paragraph with a given $F=\prod_{i<j}^{A} f(r_{ij})$. We will first state the rules to write down the graphical expansion of our generator

$$\ln \xi_0 = \int d\vec{r}_1 \cdots d\vec{r}_A \, |\Phi_0|^2 \prod_{i<j}^{A} [\eta(r_{ij})+1] \tag{4.4}$$

The expansion of the radial distribution function

$$g(r) = \frac{\rho^2}{\xi_0 A(A-1)} \int d\vec{r}_3 \cdots d\vec{r}_A \, |\Phi_0|^2 F^2$$

is then formally extracted and the derivation of the FHNC equations for various graphical elements related to $g(r)$ is sketched. The kinetic energy $\sum_i \nabla_i^2$ introduces three-body graphical elements into the analogous expansion for the (variational upper bound of the) ground state energy. We will discuss two ways to regroup terms into these elements. Next comes the modification of the expansion for $\ln \xi_{ph}(\beta)$, $\hat{N}_{mn}$ and their β-derivatives. Throughout these developments

we will limit our attention to two-body graphical elements. Merely technical extensions of the pattern, the three-body elements will be skipped.

The definitions of the graphical elements go as follows :

(i) an open circle (external point) represents an independent coordinate, such as $\vec{r}_1$ and $\vec{r}_2$ in $g(|\vec{r}_1-\vec{r}_2|)$;

(ii) a closed dot (internal point) represents a dummy variable, or the operator $\rho\int_\Omega d\vec{r}$;

(iii) a dashed line (dynamical correlation) represents $\eta(r_{12})=f^2(r_{12})-1$;

(iv) a solid line (exchange) with an arrow pointing from point 1 to point 2 represents $-\frac{1}{\nu}l(k_F r)$ where $l(x)=\frac{3j_1(x)}{x}$.

It has been proved [Fa75, Kr75] that $\ln \xi_0$ are represented by the sum of all possible biconnected (i.e., any point can reach any other point via more than one path; the logarithmic combination cancels all the non-biconnected elements) graphs with closed dots subject to the following constraints:

(i) solid lines may appear only in non-overlapping closed loops;

(ii) each point must be touched by at least one dashed line;

(iii) no more than one dashed line may exist between any pair of points.

Rule (iii) is obvious as only one factor $\eta(r_{ij})$ appears for each pair (ij) in the integral (4.4). Rules (i) and (ii) may be understood by a closer look at the function $|\Phi_0(\vec{r}_1\cdots\vec{r}_A)|^2$. It is clear that any term different from 1 involves a permutation of the assignment of orbitals in Φ_0 relative to that in Φ_0^*, and any permutation can be decomposed into non-overlapping (no common point) cycles. A typical term is $\frac{1}{\Omega^3}e^{i\vec{k}_1\cdot\vec{r}_{12}}e^{i\vec{k}_2\cdot\vec{r}_{23}}e^{i\vec{k}_3\cdot\vec{r}_{31}}$ in which the momenta can range through all occupied orbitals except that $\vec{k}_1\neq\vec{k}_2\neq\vec{k}_3\neq\vec{k}_1$. If no η factor is touching point 3 say, we will have the factor $e^{i(\vec{k}_2-\vec{k}_3)\cdot\vec{r}_3}$ which vanishes when the integral over $\vec{r}_3$ is

taken; hence rule (ii). Summing over $\vec{k}$ gives the statistical factor $\sum_{k}^{k_F} = \frac{A}{\nu} l(k_F r)$. A minus sign is attached to each transposition. Suppose n particles are correlated in a particular diagram. Trivial integration can then be performed on $\frac{A!}{n!}$ permutations of labels of particles which cancels with the normalizing factor $\frac{1}{A!}$ to give $\frac{1}{n!}$. A factor of topological symmetry t for each graph also arises from the arbitrariness of labelling the points. A factor $-\nu$ is regained when an exchange loop returns to the starting dot. With these we have the final rule of assigning numerical weights:

(iv) each n-body graph is multiplied by a factor $(-\nu)^m \frac{t}{n!}$ where t is the number of topologically distinct ways to label the graph (as an example, $t=12$ for the graph shown in Figure 26a) and m is the number of closed loops.

The factor ρ^n should now be obvious. η and $l(k_F r)$ being local functions, each term in the series is $O(\Omega)$ or $O(A)$.

If $\hat{H}$ in $\ln \xi_0(\beta)$ is replaced by any two-body operator $\hat{O} \equiv \prod_{i<j}^{A} O_{ij}$ such that the O_{ij}'s are c-number functions , the generator can be written as

$$\ln \xi_0(\beta) = \ln \langle \Phi_0 | \prod_{i<j}^{A} [f^2(r_{ij}) e^{\beta O_{ij}}] | \Phi_0 \rangle \ .$$

Then exactly the same expansion as that of $\ln \xi_0$ can be used with the dashed line representing $\eta(\beta; r_{ij}) = f^2 e^{\beta O_{ij}} - 1$. If $O_{ij} = \delta(\vec{r}_1 - \vec{r}_i)\delta(\vec{r}_2 - \vec{r}_j) + \delta(\vec{r}_1 - \vec{r}_j)\delta(\vec{r}_2 - \vec{r}_i)$, the β-derivative at $\beta=0$ is $g(r_{12})$. The expansion for $\hat{g}(r) \equiv \frac{g(r)}{f^2(r)}$ is obtained by 'graphical differentiation': remove each dashed line in turn and turn the dot at each end of the removed line into an open circle and multiply by 2. The biconnectedness of $\ln \xi_0$ is translated to the absence of articulation point -- a point at which if the graph is cut, a subdiagram not containing the external points is

separated from the rest of the graph† (point x in Figure 26b). Such points are allowed, though, to exist between the external points, in which case they are called nodes. Also, an external point does not need to be touched by dashed lines.

The construction of the FHNC equations is now described. In this brief account, we only seek to explain how the correspondence between topological characters of graph linkage and analytical operations is exploited. The consistency of assigning numerical weights under these operations will not concern us here. The basic ideas are best illustrated without the exchange lines at first, i.e., in classical or Bose fluids. From the basic element of a dashed line, form a set of nodal diagrams $N(r_{12})$ (containing at least one node) by repeated series connection*. Then form all parallel compositions of the graphs belonging to $N(r_{12})$ to get a non-nodal set $X(r_{12})$ (Figure 26c). This is used, in turn, as a basic element for the chaining to provide for a correction to $N(r_{12})$, and the process is repeated indefinitely. Each chaining changes an open circle to a dot and thus represents an integration. Structurally similar to the RPA ring-diagrams, this series connection can be summarised by an integral equation. A parallel connection is simply the multiplication of two functions of r_{12}. The combinatorics turn out to produce numerical weights of an exponential series. In short, the sets of diagrams are related by the following equations :

$$N(r_{12}) = \rho \int d\vec{r}_3 [X(r_{13}) + N(r_{13})] X(r_{32}) \tag{4.5}$$

or $$\tilde{N}(k) = \frac{\rho[\tilde{X}(k)]^2}{1-\rho\tilde{X}(k)}$$

†Irreducibility here is effected by the cancellation of articulated graphs from the numerator with those from the denominator.

*The same symbol will be used to denote the set of diagrams and the analytical quantity it represents.

and $X(r_{12}) = [1+\eta(r_{12})]e^{N(r_{12})}-N(r_{12})-1$

An approximation to the correlation function $\Gamma(r_{12})=g(r_{12})-1$ can then be made through

$$\Gamma(r_{12}) = X(r_{12})+N(r_{12})$$

Actually this relation will be exact if the remaining class of diagrams is included in the parallel composition of $X(r_{12})$:

$$X(r_{12}) = [1+\eta(r_{12})]e^{N(r_{12})+E(r_{12})}-N(r_{12})-1 \qquad (4.6)$$

(4.5) and (4.6) are the HNC equations in classical statistical mechanics [e.g. Hu63]. The graphs $E(r_{12})$ are called elementary: they are non-nodal and cannot be factorized into a product of simpler functions of r_{12}. Given an approximation of $E(r_{12})$, $\Gamma(r_{12})$ can be obtained by solving (4.5) and (4.6). The simplest elementary diagram is shown in Figure 26d. If we replace the dashed line in the proper ij-subdiagram $(i,j\neq1,2)$ by more complicated elements of $g(r_{ij})$, the resulting graph is again elementary. in fact, counting all elementary diagrams of this form amounts to replacing $\eta(r_{ij})$ by $\Gamma(r_{ij})$ which can then be regarded as a 'dressed' correlation line. The simplest representation of such a subset of $E(r_{12})$, as the one in Figure 26d, is called a basic diagram. It renders an infinite number of graphs tractable by collecting them into (4.6). The level of approximation to $\Gamma(r_{ij})$ is labelled by HNC/n where the basic diagrams $B(r_{12})$ included contain at most n particles. The first two are HNC/0 and HNC/4 where B is set to 0 and the diagram in Figure 26d respectively.

In the extension to Fermi statistics, it is profitable to define four exchange types for each graphical element. *dd* means no exchange lines are linked to the external points; *de* means one of the two external points has a pair of exchange

lines hooked to it; *ee* means each external point is touched by a pair of exchange lines; *cc* means the graph includes an incomplete exchange loop entering at one external point and exiting at the other. The restrictions on exchange loops place severe constraints on the possible ways these elements are linked. For example, a *cc* graph can only be linked to another *cc* graph or the exchange line. $\Gamma_{dd}(r_{12})$ can still be considered as the dressed version $\eta(r_{12})$. Fantoni and Rosati [Fa74] gave the following Fermi generalization of (4.5) and (4.6):

$$N_{dd}(r_{12}) = \rho\int d\vec{r}_3[X_{dd}(r_{13})+N_{dd}(r_{13})]P(r_{32}) \tag{4.7}$$

$$N_{cc}(r_{12}) = \rho\int d\vec{r}_3[-\frac{1}{\nu}l(k_F r_{13})+X_{cc}(r_{13})+N_{cc}(r_{13})]X_{cc}(r_{32})$$

where $P(r_{ij}) = X_{dd}(r_{ij})+2X_{de}(r_{ij})+\rho\int d\vec{r}_k[X_{dd}(r_{ik})X_{ee}(r_{kj})-X_{de}(r_{ik})X_{de}(r_{kj})]$

and

$$X_{dd}(r) = f^2(r)e^{N_{dd}(r)+E_{dd}(r)}-1-N_{dd}(r) \tag{4.8}$$

$$X_{cc}(r) = \Gamma_{dd}(r)[N_{cc}(r)-\frac{1}{\nu}l(k_F r)]+E_{dd}(r)[1+\Gamma_{dd}(r)]$$

X_{cc} and N_{cc} can only depend linearly on other *cc* quantities but can have the entire Γ_{dd} of direct graphs. X_{de} and X_{ee} may be approximated successively by low-order diagrams or obtained by solving additional FHNC equations which are collected in the Appendix. The results of solving these equations for the ground-state problem to various approximations are reviewed in [Cl79a]. The version that generates our inputs, the FHNC/C is briefly described in the Appendix.

We now consider the only nontrivial operator, namely the kinetic energy. While only the ground-state expression $\sum_i <\Phi_0|F\nabla_i^2 F|\Phi_0>$ is considered, the end

result can be extended to other occupation sets by simply replacing $|\Phi_0^2|$ with $\Phi_m^* \Phi_n$. Integrations by parts can attach the gradient operator to different combinations of F and Φ_0 which might have different merits and drawbacks. In constructing these various forms of expansion, the Jackson-Feenberg [Ja61] identity is useful as an intermediate step:

$$F\Phi^* \nabla_i^2 (F\Phi) + \text{c.c.} = F^2 \Phi^* \nabla_i^2 \Phi + \text{c.c.} + 2\left[\nabla_i \cdot (|\Phi|^2 F \nabla_i F) - |\Phi|^2 (\nabla_i F)^2\right]$$

After integration and summation over i, the first two terms give the free kinetic energy $T_F = \frac{3}{5} \cdot \frac{\hbar^2 k_F^2}{2m}$. There are numerous ways to manipulate the last two terms. The surface term is numerically zero and the Clark-Westhaus form (CW) is most straightforward :

$$-\frac{\hbar^2}{2m} \sum_i \langle \Phi_0 | F \nabla_i^2 F | \Phi_0 \rangle_{CW} = T_F + \frac{\hbar^2}{2m} \sum_i \int d\vec{r}_1 \cdots d\vec{r}_A \, |\Phi|^2 (\nabla_i F)^2$$

Alternatively, we may choose to write half of the surface term as

$$\begin{aligned} \nabla_i \cdot (|\Phi|^2 F \nabla_i F) &= |\Phi|^2 (\nabla_i F)^2 + |\Phi|^2 F \nabla_i^2 F + \nabla_i |\Phi|^2 \cdot F \nabla_i F \\ &= |\Phi|^2 (\nabla_i F)^2 + |\Phi|^2 F \nabla_i^2 F - \frac{1}{2} F^2 \nabla_i^2 |\Phi|^2 + \nabla_i \cdot (\nabla_i |\Phi|^2 F^2) \end{aligned}$$

Discarding the last surface term we have the Jackson-Feenberg form (JF):

$$-\frac{\hbar^2}{2m} \sum_i \langle \Phi_0 | F \nabla_i^2 F | \Phi_0 \rangle_{JF} = T_F - \frac{1}{4} \frac{\hbar^2}{2m} \sum_i \int F^2 \nabla_i^2 |\Phi|^2 + \frac{1}{2} \sum_i \int |\Phi|^2 \left[(\nabla_i F)^2 - F \nabla_i^2 F\right]$$

The explicit expressions for a Jastrow correlation factor are

$$\sum_i (\nabla_i F)^2 = F^2 \left[\sum_{ij} (\nabla_i \ln f(r_{ij}))^2 + \sum_{i,j \neq k} \nabla_i \ln f(r_{ij}) \cdot \nabla_i \ln f(r_{ik})\right]$$

$$\sum_i (\nabla_i F)^2 - F \nabla_i^2 F = \frac{1}{2} F^2 \sum_{ij} \nabla_i^2 \ln f(r_{ij})$$

We can group the two-body terms with the potential to form an effective two-body potential:

$$V_{CW}(r) = V(r) + \frac{\hbar^2}{m}[\nabla \ln f(r)]^2$$

$$V_{JF} = V(r) - \frac{\hbar^2}{4m}\nabla^2 \ln f^2(r)$$

One approximation for the cluster expansion of the energy can be produced by the recipe $:\eta(\beta;r)=f^2 e^{\beta V_{CW}}-1$. There are still some two-body contributions from $\nabla_i^2|\Phi|^2$ in JF which complicates the expansion at the two-body level. Its advantage is the numerical insignificance of the three-body element which involves only derivatives of $l(k_F r)$. The upper bound property of the variational wavefunction is also shown to be best upheld using JF in ^{4}He [Ja79]. The CW form has been used in the two-body calculation here, while the FHNC inputs to our program are computed with JF.

We are now ready to generalize the cluster expansion and resummation procedure to cases where the Slater determinant is $a_p^\dagger a_h|\Phi_0>$ or $a_p^\dagger a_h a_p^\dagger a_h|\Phi_0>$. Assuming in RPA we are concerned with the difference between matrix elements involving slightly different sets of occupied orbitals. Let us first look at $\ln \xi_{ph}$. The only difference from $\ln \xi_0$ is in terms in $|\Phi_{ph}|^2$ containing exchange factors $e^{i\vec{k}\cdot\vec{r}_{12}}$ where $\vec{k}$, instead of ranging through the ground-state set, leaves out $\vec{h}$ and adds $\vec{p}$. All elements, including equivalent diagrams, stay the same formally if the exchange factor for the solid line changes from $l(k_F r)$ to

$$l_{ph}(r_{12}) = l(k_F r) + \frac{1}{A}e^{i\vec{p}\cdot\vec{r}_{12}} - \frac{1}{A}e^{i\vec{h}\cdot\vec{r}_{12}}$$

Expanding the series around $\ln \xi_0$ we have, to $O(A^0)$,

$$\ln \xi_{ph} - \ln \xi_0 = \delta\xi(p) - \delta\xi(h) + O(A^{-1})$$

where $\delta\xi(p)$ is formed by replacing each solid line in each group of $\ln \xi_0$ in turn by the factor $\frac{1}{A}e^{i\vec{p}\cdot\vec{r}_{12}}$, or formally

$$\delta\xi(p) = \rho\int[\frac{\delta \ln\xi_0}{\delta l(k_F r_{12})}]e^{i\vec{p}\cdot\vec{r}_{12}}d\vec{r}_{12} \ .$$

It is the Fourier transform of a graph with two external points of the cc-type. The two-body term is clearly

$$-\sum_{j}<\vec{jp}\,|\eta|\,\vec{pj}>$$

[Kr79b] showed that the non-nodal contribution to this graph is exactly $X_{cc}(r_{12})$, and that the numerical weights after collecting equivalent diagrams of the chaining of these $X_{cc}(r_{12})$ are those of a logarithmic series:

$$\delta\xi(p) = -\ln\,[1-\rho\widetilde{X}_{cc}(p)]$$

or
$$z_{ph} = \left[\frac{\xi_{ph}}{\xi_0}\right]^{\frac{1}{2}} = \left[\frac{1-\rho\widetilde{X}_{cc}(h)}{1-\rho\widetilde{X}_{cc}(p)}\right]^{\frac{1}{2}}$$

In like manner, it is easy to see

$$\ln\,\xi_{php'h'} - \ln\,\xi_0 = \delta\xi(p)-\delta\xi(h)+\delta\xi(p')-\delta\xi(h')+O(A^{-1})$$

or
$$z_{ph,p'h'} = z_{ph}\,z_{p'h'}+O(A^{-1})$$

as promised before.

The non-diagonal quantities of interest to us are those in which the bra and the ket differ by exactly two orbitals. We denote these orbitals by m_1,m_2,n_1,n_2. The formal considerations on generalized cluster expansions of such quantities as $\hat{N}_{mn}$ can be found in [Cl79b]. We will take it for granted and rely on the intuitive notions gained in the foregoing discussions of diagonal quantities. Let us

first distinguish three types of contributions to $\hat{N}_{mn}$ from one another: (i) The same two particles are occupying $(m_1 m_2)$ and $(n_1 n_2)$; (ii) one particle is common to the two sets; (iii) the sets $(m_1 m_2)$ and $(n_1 n_2)$ are occupied by completely different pairs. If we formally extract the pairs:

$$\hat{N}_{mn} = <m_1 m_2 | \hat{N}(1,2,1',2') | n_1 n_2>_a$$

the effective operators corresponding to the three types above can be expressed by graphs with 2,3,4 external points respectively. Type (i) diagrams are local and must be of dd type since no exchange loops are extending to the pair of external points. Similar considerations show that types (ii) and (iii) are non-local and contain part of one and two exchange loops respectively. Denoted by $\hat{N}_{dd}(12)$, $\hat{N}_{dcc}(12;12')$ and $\hat{N}_{cc,cc}(12;1'2')$, the simplest diagram for each of them is depicted in Figure 27a. In our case, $(m_1 m_2)$ and $(n_1 n_2)$ are the only possible orbitals not belonging to the ground-state set. Thus we may expect $\hat{N}_{dd}(12)$ to be $\Gamma_{dd}(12)$ to $O(A^0)$. The study [Kr79b] showed the validity of this expectation. In a first approximation we may just neglect the non-local terms. Again it is shown in [Kr79b] that a series of graphs in $\hat{N}_{dcc}$ and $\hat{N}_{cc,cc}$ are factorizable into single-particle quantities. The simplest example is the first graph of $\hat{N}_{dcc}$ (in Figure 27a) which is

$$<m_1 m_2 | \eta(r_{12}) | n_1 n_2>_a \left[\sum_j <j m_1 | \eta(r_{12}) | m_1 j> + \text{same for } m_2, n_1, n_2 \right]$$

Terms like those in the square brackets are consistently separated out and found to be forming a binomial expansion of $[1-\rho\tilde{X}_{cc}(m_1)]^{-\frac{1}{2}}$ etc.. The part to be multiplied by this series is irreducible in this sense. We may then include this in our otherwise local approximation :

$$\hat{N}_{mn} = D^{-1} <m_1 m_2 | \Gamma_{dd}(r) | n_1 n_2>_a \qquad (4.9)$$

$$D = [(1-\rho\tilde{X}_{cc}(m_1))(1-\rho\tilde{X}_{cc}(m_2))(1-\rho\tilde{X}_{cc}(n_1))(1-\rho\tilde{X}_{cc}(n_2))]^{\frac{1}{4}}$$

Even neglecting three-body contributions, one must pay extra attention to the term $\nabla_i^2|\Phi_{ph}|^2$ during graphical differentiation with JF. Again, each $\nabla^2 l(k_F r)$ factor may be replaced by $\nabla^2 l_{ph}(r)$ and to $O(A^0)$

$$\nabla^2 l_{ph}(r) = \nabla^2 l(k_F r) + \frac{1}{A}(p^2 e^{i\vec{p}\cdot\vec{r}} - h^2 e^{i\vec{h}\cdot\vec{r}})$$

Just as $V_{JF}(r)$ is absorbed in the general $\eta(\beta,r)=f^2(r)e^{\beta V_{JF}(r)}-1$, so can $\nabla^2 l(k_F r)$ be safely stored in $l(\beta,r)=\exp[\beta\frac{\hbar^2}{2m}\cdot\frac{\nabla^2 l(k_F r)}{l(k_F r)}]l(k_F r)$ and appear in the β-derivative of $\tilde{X}_{cc}(k)$. This is taken in the first approximation to the diagonal energy:

$$\hat{H}_{ph,ph} - \hat{H}_{00} = \frac{\hbar^2}{2m}(p^2-h^2) + u(p) - u(h) \qquad (4.10)$$

$$u(k) = \frac{\tilde{X}'_{cc}(k)}{1-\rho\tilde{X}_{cc}(k)}$$

where the prime denotes graphical differentiation. The two-body term is just the HF single-particle matrix element of the β-derivative of $\eta(\beta;r)$, or $f^2 V_{C\prime\prime}$. To $O(A^0)$, in contributions involving $k^2 e^{i\vec{k}\cdot\vec{r}}$, the latter just takes the place of $e^{i\vec{k}\cdot\vec{r}}$ in the earlier analysis of $\ln \xi_{ph}$ and we expect a term of the form

$$\frac{\hbar^2 k^2}{2m}\ln\left[\frac{1}{1-\rho\tilde{X}_{cc}(k)}\right]$$

In our example below, $\rho\tilde{X}_{cc}(k)$ is ~0.08 around $k\sim k_F$ and this term amounts to about 1% of (4.10) and is neglected for convenience sake. Taking the β-derivative of $\tilde{N}_{cc}$ in (4.7) and X_{cc} in (4.8) gives the FHNC' equation :

$$\tilde{N}'_{cc}(k) = \left[\frac{1-\nu^{-1}\tilde{l}(k)}{[1-\rho\tilde{X}_{cc}(k)]^2}-1\right]\rho\tilde{X}'_{cc}(k) \qquad (4.11)$$

$$X'_{cc}(r)=-\frac{1}{\nu}[(l(k_F r)-\nu N_{cc}+\nu E_{cc})\Gamma'_{dd}+(1+\Gamma_{dd})E'_{cc}]+\Gamma_{dd}[N'_{cc}-\frac{\hbar^2}{4m}\nabla^2 l(k_F r)]$$

Differentiating $\widetilde{N}_{dd}(k)$ in (4.7) and $X_{dd}(r)$ in (4.8) gives the FHNC' equation for Γ'_{dd} :

$$X'_{dd}(r) = [1+\Gamma_{dd}(r)][V_{JF}(r)+E'_{dd}(r)]+\Gamma_{dd}(r)N'_{dd}(r) \tag{4.12}$$

$$\widetilde{N}'_{dd}(k) = [S_d^2(k)-1]\widetilde{X}'_{dd}(k)+2\widetilde{\Gamma}_{dd}(k)S_d(k)\widetilde{X}'_{de}(k)+\widetilde{\Gamma}^2_{dd}(k)\widetilde{X}'_{ee}(k)$$

where

$$S_d(k) = \frac{1 + [1+\widetilde{X}_{ee}(k)]\widetilde{\Gamma}_{dd}(k)}{1 - \widetilde{X}_{de}(k)}$$

This is a linear integral equation for $\widetilde{N}'_{dd}(k)$. The additional equations for $\widetilde{X}'_{de}$, $\widetilde{N}'_{de}$, etc. are given in [Kr81b]. Note that Γ'_{dd} is the sum of all diagrams in which exactly one $\eta(r_{12})$ line is replaced by V_{JF}. If we write the potential in the form

$$V(12) = V^{(1)}(r) + V^{(2)}(r)\vec{\sigma}_1\cdot\vec{\sigma}_2 + V^{(3)}(r)\vec{\tau}_1\cdot\vec{\tau}_2 + V^{(4)}(r)\vec{\sigma}_1\cdot\vec{\sigma}_2\vec{\tau}_1\cdot\vec{\tau}_2$$

only $V^{(1)}$ may appear in the internal subdiagrams of Γ'_{dd} since Tr $\vec{\sigma}$=0. The non-radial parts can only be present connecting the external points. We may then leave them out when solving the FHNC' equation and include them at the end in the form

$$\Gamma'_{dd}(r) + (1+\Gamma_{dd}(r))(V^{(2)}\vec{\sigma}_1\cdot\vec{\sigma}_2+V^{(3)}\vec{\tau}_1\cdot\vec{\tau}_2+V^{(4)}\vec{\sigma}_1\cdot\vec{\sigma}_2\vec{\tau}_1\cdot\vec{\tau}_2) \tag{4.13}$$

In the presence of the incomplete exchange loop, the spin (isospin) at the external points of $X'_{cc}(r)$ add up after the fashion of the exchange term of the HF single-particle energy. In other words, $\Gamma'_{dd}(r)$ in (4.11) is to be replaced by

$$\Gamma'_{dd}(r) + (1+\Gamma_{dd}(r))[3V^{(2)}(r)+3V^{(3)}(r)+9V^{(4)}(r)] \ . \tag{4.14}$$

For the β-derivative of $\hat{N}_{mn}$, we again have extra terms involving $\frac{1}{A}\nabla^2 e^{i\vec{p}\cdot\vec{r}}$. In this case, however, we may shift the Laplacian to the Γ_{dd} through two integrations by parts. Finally we have

$$\hat{Y}_{mn} = D^{-1}[\langle m_1 m_2 | V_h(r) | n_1 n_2 \rangle_a \tag{4.15}$$

$$+\frac{1}{2}[u(m_1)+u(m_2)+u(n_1)+u(n_2)]\langle m_1 m_2 | \Gamma_{dd} | n_1 n_2 \rangle_a]$$

$$V_h(r) = \Gamma'_{dd}(r) + (1+\Gamma_{dd}(r))[(V^{(2)}\vec{\sigma}_1\cdot\vec{\sigma}_2 + V^{(3)}\vec{\tau}_1\cdot\vec{\tau}_2 + V^{(4)}\vec{\sigma}_1\cdot\vec{\sigma}_2\vec{\tau}_1\cdot\vec{\tau}_2)] + \frac{\hbar^2}{4m}\nabla^2\Gamma_{dd}$$

The corresponding two-body effective interaction is

$$V_2(r) = \frac{\hbar^2}{m}[\nabla \mathrm{f}]^2 + \mathrm{f}^2 V(r)$$

It may be noted that the u's in (4.15) and those in the remainder of (4.3) cancel in such a way that a term $[u(p)+u(p')]\langle ph' | \Gamma_{dd} | hp' \rangle$ will remain. Divergence problems at low q will arise later in cases where Γ_{dd} is long-ranged : $\Gamma_{dd} \sim 1+r^{-2}$ as $r \to \infty$. This difficulty implies that contributions from more diagrams have to be brought in. An estimate of these contributions have been introduced and is collected in the Appendix. At the 2-body level, we just discard the term as giving unrealistic contributions at low q.

To summarize, given an $\mathrm{f}(r)$, one first solves the FHNC equations (4.7) and (4.8) to get the correlation functions Γ_{dd}, X_{cc} etc.. With these as inputs, the primed equations (4.11) and (4.12) are solved to give Γ'_{dd} and $\tilde{X}'_{cc}$. (4.10) then gives the single-pair energy, while the elements of A,B and M of the CRPA matrix are spelled out by (4.15) with (4.9).

It is worth noting that all effects of non-orthogonality disappear at the Landau limit. We recall that the kernel is finite and the integration region is $O(q)$.

$\hbar\omega$ assumed proportional to q, the non-diagonal part of M contributes only to $O(q^2)$. The same is true for the energy-dependent part of A and B. With $z_{ph}=1+O(q)$, the equation reduces to the normal collisionless Landau equation (2.5), the F_l's claculated with V_h.

Taking the two-body CW form of the kinetic energy, one can easily expand the ground-state expectation value of the Hamiltonian to two-body order:

$$<\hat{H}> = T_F+\frac{\partial}{\partial\beta}[\ln<\Phi_0|Fe^{\beta V_{CW}}F|\Phi_0>]_{\beta=0}$$

By the rule of graphical differentiation, the only slot for dynamical bond between the two points is filled by V_{CW}. In other words, without a third point representing the medium, the result is a HF energy with the effective potential $V_2(r)$. In view of the point in the last paragraph, two-body CRPA, at least at the limit of extremely long wavelength, is formally equivalent to a self-consistent HF/RPA procedure with $V_2(r)$. The inclusion of the term generated by the defect of the wave-function: $\frac{\hbar^2}{m}|\nabla f|^2$ is of course an improvement over the naive cutting off of the bare potential by the radial distribution function $g(r)$ or $f^2(r)$. This analogy can be extended to a certain degree to FHNC by including only terms in Γ'_{dd} which have V_{JF} linking the external points: $(1+\Gamma_{dd})V_{JF}$. Under this approximation, $V_h(r)$ again reduces to a cut-off bare potential plus a 'defect-generated' repulsive term:

$$V_h^{HF}(r) = \frac{\hbar^2}{4m}[\nabla^2\Gamma_{dd}-(1+\Gamma_{dd})\nabla^2\ln f^2]+(1+\Gamma_{dd})V(r). \qquad (4.16)$$

In the final analysis, it is merely a more elaborately dressed version of $V_2(r)$. (Note that $V_h(r)\rightarrow V_2(r)$ when $\Gamma_{dd}\rightarrow\eta$). Allowing two exchange lines between the external points, the distribution function $1+\Gamma_{dd}$ is appropriate between HF orbitals. Using $V_h^{HF}(r)$, in a self-consistent way, in static HF calculations amounts to

substituting $1+\Gamma_{dd}(r)$ for the full radial distribution function $g(r)$. The quantity

$$V_h(r) - V_h^{HF} = \Gamma'_{dd}(r) - [1+\Gamma_{dd}(r)]V_{JF}(r) \tag{4.17}$$

represents, strictly speaking, the first step beyond the HF/RPA framework. It is made up of diagrams (Figure 27b) which have V_{JF} between internal points. In the variational ground state, when we express the energy as

$$<\hat{H}> = T_F + \frac{1}{2}\rho\int g(r)V_{JF}(r)d\vec{r} + \cdots$$

we can always choose these points to be the external points of $g(r)$. Focusing our attention on the set $\{p,h\}$ destroys symmetry among these orbitals. Vaguely expressed, (4.17) comes from the change in the medium when a particle-hole pair is excited. This notion may remind one of the rearrangement terms in DDRPA. While they may serve the same function in some cases (section 4.3), their connection is hard to demonstrate. Moreover, an extension of CRPA to allow dependence of f(r) on local density fluctuations will generate its own rearrangement terms (see suggestions in Chapter 5). The next higher step in the hierrachy involves further entwining with the medium, leading to non-local potentials -- from N_{dcc} and $N_{cc,cc}$. Although the three-body elements are avoided in our review, their small contributions are included in the actual computations of V_h.

4.2. Symmetries of CRPA Excitations

The last section essentially achieves the transfer of dynamical correlations from the Jastrow wave-function to an effective local operator. Most imporant are the involved ways in which the 'defective' wave function can generate extra kinetic energy. In place of (4.1) we now have antisymmetrized matrix elements of a local potential dependent on energy and momentum. To take advantage of

the symmetry analysis in Chapter 2, we project the effective potential into particle-particle spin-isospin channels. Recall that only the purely radial part of the bare nucleon-nucleon potential is involved in Γ'_{dd}. Thus from (4.15), we have

$$V_h(r) = W(r) + [1+\Gamma_{dd}(r)]V(r) \tag{4.18}$$

where

$$W(r) = \Gamma'_{dd}(r) - [1+\Gamma_{dd}(r)][V^{1-}(r)+3V^{1+}(r)+3V^{3+}(r)+9V^{3-}(r)] + \frac{\hbar^2}{4m}\nabla^2\Gamma_{dd}(r).$$

and $V(r)$ denotes the free-space v4-potential. $\Gamma_{dd}(r)$ being central, the symmetry arguments in Chapter 2 are trivially extended to take the M-matrix into account. The counterpart of (2.20) in M is

$$M(k,\alpha,k',\alpha') = \frac{1}{\pi}[4\delta_{\tilde{S}0}\delta_{\tilde{T}0}\delta m_0\Gamma_{dd}(q) - \sum_l \frac{(l-m)!}{(l+m)!}(2l+1)\Gamma_{ddl}(k,k')P_l^m(\alpha)P_l^m(\alpha')$$

where

$$\Gamma_{dd}(q) = \int dr\ r^2 j_0(q)\Gamma(r) \quad ; \quad \Gamma_{ddl}(k,k') = \int dr\ r^2 j_l(kr) j_l k'r)\Gamma(r)$$

It is written here with the explicit Pandya coefficients characteristic of a spin-isospin-independent component. The excitations are therefore classified again by $\tilde{S}$, $\tilde{m}_S$, $\tilde{T}$, $\tilde{T}_3$, m and q.

The ground-state expectation value of the double commutator (1.28) can also be evaluated to two-body and FHNC accuracy and, for the Jastrow correlation function, should be equal to S_1 through (1.28). The HF calculation is applicable at the two-body level, and is carried out in our example below. Involving constructions of radial distribution functions in different channels

$$g^{ST} = \frac{\rho^2}{\xi_0 A(A-1)} \int d\vec{r}_1 \cdots d\vec{r}_A\ \Psi^* P^{ST} \Psi$$

the FHNC values will be calculated in the near future.

4.3. The OMY Potential

The illustrative example we choose has a long history in Jastrow Variational calculations. Constructed by Ohmura et.al. [Oh56], it consists of a hard core of radius c=0.6 fm and an attractive exponential tail in each spatially even channel (solid in Figure 8):

$$V^{1+}(r) = -397.31e^{-2.627(r-c)} \qquad r>c$$

$$V^{3+}(r) = -947.02e^{-3.677(r-c)}$$

$$V^{1-}(r) = V^{3-}(r) = 0$$

It fits the singlet and triplet scattering lengths and effective ranges reasonably well. Bäckman *et al.* [Ba72] used this potential to demonstrate the discrepancy between the energy calculated by the lowest-order Brückner-Bethe method and the Jastrow variational bound to three-body order. Throughout the last decade, it has served as a test model for various numerical schemes [e.g. Ca76].

To date, we only have FHNC results for one to two values of q for each channel. Still we will present the results as a comparison between two-body cluster-order and FHNC. The following correlation function has been used to generate the FHNC inputs:

$$f_h(r) = 0 \qquad r<c$$

$$= (1-e^{-\mu_1(r-c)})(1+re^{-\mu_2(r-c)}) \qquad r>c$$

These parameters are set at each density to minimize the two-body-order energy. The FHNC energy reaches a minimum at k_F=1.4 fm^{-1}, μ_1=2.460 fm^{-1},

μ_2=2.080 fm^{-1}, γ=1.012 and B/A =15.69 MeV. In the two-body calculations, only the first factor is used, i.e. r=0:

$$f_2(r) = 0 \qquad r<c$$

$$= 1-e^{-\beta(r-c)} \qquad r>c$$

The only quantitative difference of $f_2(r)$ and $f_h(r)$ is the overshooting ($f_h(r)>1$) of the latter. The 'saturation' parameters are k_F=1.4 fm^{-1}, β=5.5 fm^{-1}, and B/A =15.8 MeV. It has been shown [Ca76] that to FHNC accuracy, the two functions give the same result for binding energy. As 'distribution functions' cutting off the bare potential, $f_2(r)$ (dashed) and $1+\Gamma_{dd}(r)$ (solid) generated by $f_h(r)$ are plotted in Figure 28. Our focus of interest is at $W(r)$ of (4.18). At the two-body level it reduces to $\frac{\hbar^2}{m}\beta^2 e^{-2\beta(r-c)}$. These two 'defect generated' terms are shown in Figure 30. The functions are virtually identical within 0.2 fm of the core. We shall see that the long-range positive tail of the FHNC-$W(r)$ is crucial for the stability of the uniform phase. In Figure 29 $W(r)$ is broken down into its major components, from which the significance of $V_h - V_h^{HF}$ in the intermediate range (dotted) is evident. Figures 31-34 contain the particle-hole potentials in each channel. (Again dashed for two-body and solid for FHNC). Contributing to V_d only in (0,0), the central $W(r)$ is responsible for making V_h positive there, keeping F_0^{00} away from -1 (cf. Table 3.2). The long-range dip below 0 of FHNC-V_e in all spin (isospin) channels can be traced to the overshooting of $1+\Gamma_{dd}(r)$. As a result the F_0's for these channels assume lower values than the two-body ones (Table 3.2). The strong triplet-even component again leads to the usual ordering of the F_0's according their algebraic values.

The additional diagonalization (of M) adds a considerable amount of time to that taken for the construction of the matrix. A typical two-body run takes

roughly 70 min. for this purpose and 11 min. for diagonalization for N=76. The FHNC inputs are given numerically as pieces of potentials in r-space and so actually involve simpler algebra than in the two-body case, reducing the construction cost to 18 min. for N=76. The results are summarized in Figures 35-37 and Tables 4.1 and 4.2. The most striking contrast is certainly the instability in (0,0) in the two-body results, as indicated by the F_0's. The persistence to the relatively high q=0.3 is helped by the negative energy-dependent term the magnitude of which grows initially with q. At low q, the direct contribution to F_0 can be estimated by $\frac{q}{k_F}\cdot\frac{4k_F^3}{\pi^2}\frac{m^*}{m}\int d\vec{r}\ \eta(r)$ which can reach ~ -0.25 at q=0.3. The corresponding contribution from Γ_{dd} in FHNC is positive but with magnitude of only about a quarter of the above. As mentioned in Section 4.1, the role of $V_h - V_h^{HF}$ here may be compared to the rearrangement term in DDRPA, but the physical connection, if any exists, is not clear. As the F_0's indicate, the two-body truncation makes the system over-collective in the three spin (isospin) channels as measured by r_0. It also raises the effective mass from 0.496 to 0.572. Both values are lower than the accepted value ~0.7 if V_h (V_2) was treated as a HF/RPA potential.

Chapter V

5.1. Outlook

While V_h has still to be analysed, we would like to conclude this report at this point when we have reasonable confidence in the code and understanding of the results. In this short chapter, we summarize the loose ends and survey the possible extensions and applications of this work. After V_h is considered understood for OMY, the Hamada-Johnston, the Reid soft-core, the Lennard-Jones for ^{3}He and the Coulomb electron gas will be next in line. As a first application one can follow the macroscopic approach to giant resonances by imposing boundary conditions on the travelling collective mode and projecting $S(q,\omega)$ into angular momentum components. Aside from the frequency, it is hoped that the transition density [Bl80]

$$\delta n(\vec{r}) \equiv <\Psi_n | \sum_i \delta(\vec{r}-\vec{r}_i) | \Psi_0>$$

in the nuclear interior depends predominantly on the bulk properties. Although $S(q,\omega)$ and $S_L(q,\omega)$ can be compared in this way, it is not clear whether the difference between them is of experimental significance under all the uncertainties of the method. Still it is interesting to calculate these obscurable quantities, even in terms of $S_L(q,\omega)$, from the realistic free-space potentials through CRPA. While the enhancement factors $\kappa(q)$ of photonuclear and other sum rules are certainly important, they can be computed without resort to $S(q,\omega)$. The smoothing procedure will be further developed when we apply the method to real laboratory infinite systems: ^{3}He and the electron gas.

In its discretized form (2.3) $S(q,\omega)$ is much more important in an indirect way. The Landau theory of elementary excitations adapted to finite nuclear system [Mi67, An77] provides a simple phenomenological framework to discuss

intermediate-energy nuclear physics. Various giant nuclear and nucleonic [Sp81] resonances and signature of pion-condensation in scattering are some of the outstanding topics. The $S(q,\omega)$ of nuclear matter is basic to the calculation of the 'polarization' contributions of the theory's essential parameters: the effective mass $\frac{m^*}{m}$ and Landau parameters F_l's. The local kernel approximation and schematic potentials has been traditionally employed [Bl82, also Fe71]. The inadequacy of $S_L(q,\omega)$ shown in Chapter 3 undoubtedly urges a new round of computations based on the full RPA propagator†. Recently the formalism of CRPA has been extended to cover these aspects [Kr82, Sa82]. The relevance of the same calculations to the low-temperature dynamical and thermodynamical properties of ^{3}He, the electron gas and the neutron star hardly needs emphasis [e.g. Pi66].

What is suggested above is an integration of essentially $\Pi^{RPA}(q,\omega)V^2(q)$ over the first quadrant of the (q,ω) space. Faced with such stupendous demand of numerical efforts, one would certainly welcome analytical approximations which nevertheless gives results superior to $S_L(q,\omega)$. Phrased differently, our brute-force method of solution will probably serve eventually as an exact model against which approximation methods are evaluated. The search for improved approximations is promising in view of the relative lack of variance of the shapes of $S(q,\omega)$. For example, including the $l=1$ term in the Landau limit is known to allow analytical solution and should be pursued††.

A further line of research should be directed towards the inclusion of time-dependence in f(r). In Chapter 1, we evaded the issue under the premise that

†(1.19) implies that $S(q,\omega)$ contains all information to determine Π^{RPA} [Fe71].

††With separable kernel $\sum_l F_l P_l(\alpha)P_l(\alpha')$, the exact Landau equation is well-suited to treatment by Padé approximants [Ba81]. It is suggested that in more complicated cases this method may help uncover separability.

using the ground-state f(r) is justified when the wavelength q^{-1} is long compared to the healing distance of f. In DDRPA, however, we have seen an example where local density fluctuations generate through $V(r;p)$ crucial contributions at any q. The equilibrium f(r) -- which minimizes the energy -- clearly depends on the local density. Following DDRPA then, we can allow time-dependence in f through the density fluctuations. A prototype 'rearrangement' term to be expected in correlated TDHF is

$$\sum_{kl}\rho_{kl}<\Phi\,|\,F^{\dagger}Fa_k^{\dagger}a_l\,a_p^{\dagger}a_h\,|\,\Phi><\Phi\,|\,F^{\dagger}\sum_{ij}\frac{\delta \ln f(r_{ij})}{\delta\rho}F\,|\,\Phi>.$$

The non-orthogonality leads to a proliferation of terms. Nevertheless there is no apparent reason to assume that these terms are any more negligible than the rearrangement terms in DDRPA. In a fit of ambition, one may even confront the time-dependent variational problem (1.1) over a product of the space of Slater determinants and that of the correlation functions.

Appendix

The other two pairs of equations needed to calculate X_{de} and X_{ee} are

$$X_{de}(r) = f^2(r)[N_{de}(r)+E_{de}(r)]\exp[N_{dd}(r)+E_{dd}(r)]-N_{de}(r)$$

$$X_{ee}(r) = f^2(r)Q_{ee}(r)\exp[N_{dd}(r)+E_{dd}(r)]-N_{ee}(r)$$

$$Q_{ee}(r) = -\frac{1}{\nu}l^2(k_F r)+N_{ee}(r)+E_{ee}(r)+[N_{de}(r)+E_{de}(r)]^2 -$$

$$\nu[N_{cc}(r)+E_{cc}(r)]^2+2l(k_F r)[N_{cc}(r)+E_{cc}(r)]$$

$$N_{de}(r) = \rho\int d\vec{r}_3[X_{dd}(r_{13})X_{de}(r_{32})-X_{de}(r_{13})X_{de}(r_{32})]+[X_{de}(r_{13})+N_{de}(r_{13})]P(r_{32})$$

$$N_{ee}(r_{12}) = \rho\int d\vec{r}_3[X_{de}(r_{13})X_{de}(r_{32})-X_{dd}(r_{13})X_{ee}(r_{32})]+[X_{ee}(r_{13})+N_{ee}(r_{13})]P(r_{32})$$

The $X_{de}(r)$ and $X_{ee}(r)$ calculated this way do not explicitly satisfy order by order an low-q requirement from general considerations [Kr79a]

$$\tilde{X}_{de}(q) \sim O(q)$$

$$\tilde{X}_{ee}(q) \sim \frac{1}{\rho}[1+S_F(q)]$$

To keep the computation effort at the level of FHNC/0, [Kr79a] estimated the contribution of additional diagrams and wrote

$$X_{de}(r) = X^0_{de}(r)+X^E_{de}(r)$$

$$X_{ee}(r) = X^0_{ee}(r)+X^E_{ee}(r)$$

$$\tilde{X}^E_{de}(q) \approx (S_F(q)-1)\tilde{X}^0_{de}(q)$$

$$\tilde{X}^E_{ee}(q) \approx (S^2_F(q)-1)(\tilde{X}^0_{ee}(q)-\frac{S_F(q)-1}{\rho})$$

where $X^0_{de}(r)$ is the FHNC/0 $X_{de}(r)$ etc. . The version using these $\widetilde{X}$'s in the calculations is called FHNC/C.

The problem with the 'dangerous' term $[u(p)+u(p')]\langle ph'|\Gamma_{dd}|hp'\rangle$ is in a sense similar. [Kr81b] approximated the additional contributions by the recipe :

(i) Multiply every matrix element $\langle ph'|\Gamma_{dd}|hp'\rangle$ by $[1+\widetilde{E}(p,h)][1+\widetilde{E}(p',h']$;

(ii) Multiply the energy $u(p)+u(h)$ by $\frac{1}{2}S_F(q)[1+\widetilde{E}(p,h)]^{-1}$

where

$$\widetilde{E}(p,h) \approx \frac{1}{2}[S_F(q)-1][\widetilde{X}_{cc}(p)+\widetilde{X}_{cc}(h)]$$

This is adopted in our work here.

References

An77 (1977) Anastasio, M. R. and Brown, G. E., Nucl. Phys., **A285**, 516.

Al78 (1978) Alberico, W. M., Cenni, R. and Molinari, A., Riv. Nuovo Cimento, **1**, 1.

Ba69 (1969) Baym, G., *Lectures on Quantum Mechanics*; Benjamin, Reading.

Ba72 (1972) Bäckman, S.-O., Clark, J. W., Ter Louw, W. J., Chakkalakal, D. A. and Ristig, M. L., Phys. Lett., **41B**, 247.

Ba81 (1981) Baker, G. A. and Graves-Morris, P., *Padé Approximants*, Part II; Addison-Wesley, Reading.

Be71 (1971) Bethe, H. A., Ann. Rev. Nucl. Phys., **21**, 93.

Be75 (1975) Bertsch, G. F. and Tsai, S. F., Phys. Rep., **18**, 125.

Bl80 (1980) Blaizot, J. P., Phys. Rep., **64**, 172.

Bl82 (1982) Blaizot, J. P., to be published.

Bo51 (1951) Bohm, D. and Pines, D., Phys. Rev., **82**, 625.

Br77 (1977) Brown, G. E., Bäckman, S.-O., Oset, E. and Weise, W., Nucl. Phys., **A286**, 191.

Ca76 (1976) Campani, E., Fantoni, S. and Rosati, S., Lett. Nuovo Cimento, **12**, 217.

Ch82 (1982) Chen, J., Clark, J. W. and Sandler, D. G., Z. Physik, **A305**, 223.

Cl79a (1979) Clark, J. W., in *Progress in Particle* and *Nuclear Physics*, Vol. 2, ed. Wilkinson, D.; Pergamon, Oxford.

Cl79b (1979) Clark, J. W., Mead, L., Krostcheck, E., Kürten, K. and Ristig, M. L., Nucl. Phys., **A328**, 45.

Cl80 (1980) Clark, J. W., in *Lecture Notes in Physics*, No. 138, ed. Guardiola, R.; Springer, Berlin.

Da81 (1981) Day, B. D., Phys. Rev., **C24**, 1203.

De80 (1980) Decharge, J. and Gogny, D., Phys. Rev., **C21**, 1568.

Ed60 (1960) Edwards, A., *Angular Momentum in Quantum Mechanics*; Princeton U., Princeton.

Fa74 (1974) Fantoni, S. and Rosati, S., Nuovo Cimento, **20A**, 179.

Fa75 (1975) Fantoni, S. and Rosati, S., Nuovo Cimento, **25A**, 593.

Fe69 (1969) Feenberg, E., *Theory of Quantum Liquids*; Academic, New York.

Fe71 (1971) Fetter, A. L. and Walecka, J. D., *Quantum Theory of Many-Particle Systems*; Mcgraw-Hill, New York.

Gi82 (1982) Girod, M. and Reizhard, P.-G., Nucl. Phys., **A384**, 179.

Go75 (1975) Gogny, D., Nucl. Phys., **A237**, 399.

Go77 (1977) Gogny, D. and Padjen, R., Nucl. Phys., **A293**, 365.

Hu63 (1963) Huang, K., *Statistical Mechanics*; Wiley, New York.

Ja61 (1961) Jackson, H. W. and Feenberg, E., Ann. of Phys., **15**, 266.

Ja79 (1979) Jackson, A., Lande, A. and Lantto, L., Nucl. Phys., **A317**, 70.

Ke76 (1976) Kerman, A. and Koonin, S., Ann. Phys., **100**, 332.

Kr75 (1975) Krotscheck, E., Phys. Lett., **54A**, 123.

Kr79a (1979) Krotscheck, E., Nucl. Phys. **A317**, 149.

Kr79b (1979) Krotscheck, E. and Clark, J. W., Nucl. Phys., **A328**, 73.

Kr81a (1981) Krotscheck, E. and Smith, R., Phys. Lett., **100B**, 1.

Kr81b (1981) Krotscheck, E., Smith, R., Clark, J. W. and Panoff, R., Phys. Rev., **B24**, 6383.

Kr82 (1982) Krotscheck, E. and Smith, R., to be published.

La56 (1956) Landau, L. D., Sov. Phys. JETP, **3**, 920.

La58 (1958) Landau, L. D., Sov. Phys. JETP, **7**, 182.

Le50 (1950) Levinger, J. S. and Bethe, H. A., Phys. Ref.,**78**, 115.

Ma69 (1969) Mathews, J. and Walker, R. L., *Mathematical Methods of Physics*; Benjamin, Reading.

Mi67 (1967) Migdal, A., *Theory of Finite Fermi Systems and Applications to Atomic Nuclei*; Interscience, New York.

Oh56 (1956) Ohmura, T., Morita, M. and Yamada, M., Prog. Theor. Phys., **15**, 222.

Pa56 (1956) Pandya, S., Phys. Rev., **103**, 956.

Pi66 (1966) Pines, D. and Nozières, P., *The Theory of Quantum Liquids*, Vol. I; Benjamin, New York.

Pi81 (1981) Pines, D., in *Lecture Notes in Physics*, No. 142, ed. Zabolitzky, J.; Springer, Berlin.

Ro70 (1970) Rowe, D. J., *Nuclear Collective Motion*; Methuen, London.

Sa80 (1980) Sandler, D. G., Ph.D. Thesis, Washington University, unpublished.

Sa81 (1981) Sandler, D. G., Kwong, N.-H., Clark, J. W. and Krotscheck, E., in *Lecture Notes in Physics*, No. 142, ed. Zabolitzky, J.; Springer, Berlin.

Sa82 (1982) Sandler, D. G., to be published.

Sk76 (1976) Sköld, K., Pelizzari, C., Kleb, R. and Ostrowski, G., Phys. Rev. Lett., **37**, 842.

Sp81 (1981) Speth, J. and van der Wonde, A., Rep. Prog. Phys. **44**, 719.

Th60 (1960) Thouless, D. J., Nucl. Phys., **21**, 225.

Th61 (1961) Thouless, D. J., Nucl. Phys., **22**, 78.

Th72 (1972) Thouless, D. J., *The Quantum Mechanics of Many-Body Systems*, 2nd ed.; Academic, New York.

Zi78 (1978) Ziegler, B., in *Lecture Notes in Physics*, No. 86, ed. Ciofi degli Atti, C.; Springer, Berlin.

Table 2.1

Pandya Coefficients for v4

The Pandya coefficients for a v4 potential are shown. $(\tilde{S},\ \tilde{T})$ $[(S,\tilde{T})]$ denotes particle-hole [particle-particle] channels. The numbers are equal to

$$C(\tilde{S},S,\tilde{T},T) = -(2S+1)(2T+1)\begin{Bmatrix} \frac{1}{2} & \frac{1}{2} & \tilde{S} \\ \frac{1}{2} & \frac{1}{2} & S \end{Bmatrix}\begin{Bmatrix} \frac{1}{2} & \frac{1}{2} & \tilde{T} \\ \frac{1}{2} & \frac{1}{2} & T \end{Bmatrix}.$$

TABLE 2.1

(S,T) \ $(\tilde{S},\tilde{T})$	(0,0)	(0,1)	(1,0)	(1,1)
(0,0)	$-\frac{1}{4}$	$\frac{1}{4}$	$\frac{1}{4}$	$-\frac{1}{4}$
(0,1)	$\frac{3}{4}$	$\frac{1}{4}$	$-\frac{3}{4}$	$-\frac{1}{4}$
(1,0)	$\frac{3}{4}$	$-\frac{3}{4}$	$\frac{1}{4}$	$-\frac{1}{4}$
(1,1)	$-\frac{9}{4}$	$-\frac{3}{4}$	$-\frac{3}{4}$	$-\frac{1}{4}$

Table 2.2

Pandya Coefficients for a Tensor Force

Numerical values of the various parts of the Pandya coefficients for a tensor force are tabulated. The numbers in the table equal

$$(2T+1)\begin{Bmatrix} \frac{1}{2} & \frac{1}{2} & \tilde{T} \\ \frac{1}{2} & \frac{1}{2} & T \end{Bmatrix}.$$

For use in Section 2.4, they are to be multiplied by

$$\langle 1 \| \tilde{S}_2 \| 1 \rangle = \sqrt{20}$$

and

$$\begin{Bmatrix} \frac{1}{2} & \frac{1}{2} & 1 \\ \frac{1}{2} & \frac{1}{2} & 1 \\ 1 & 1 & 2 \end{Bmatrix} = \frac{1}{9}$$

TABLE 2.2

		$\tilde{T}$	
		0	1
T	0	$-\frac{1}{2}$	$\frac{1}{2}$
	1	$\frac{3}{2}$	$\frac{1}{2}$

Table 3.1

The Meshes

The designations of the meshes are explained. η_k is the number of k-points; $\eta_\alpha(k)$ is the number of α-points corresponding to each k-points, starting from the smallest one. N is the dimension of a single matrix.

TABLE 3.1

designations	n_k	$n_a(k)$	N
2^1	2	2,4	6
4^1	4	4,8,12,20	44
4^2	4	2,8,12,18	40
6^1	6	2,8,12,14,16,24	76
6^2	6	2,8,14,14,16,24	78
8^1	8	2,6,10,12,12,14,16,24	96
8^2	8	2,6,8,8,10,12,14,16	76
12^1	12	2,4,6,6,10,10,12,12,14,16,24	128

Table 3.2

F_0 for Local-Kernel Approximations

The effective strength F_0 for each channel and potential are shown together with its direct part, F_0^d, and exchange part, F_0^e. (0,1), (1,0) and (1,1) are degenerate for the square-well and the F_0's are shown under (1,1).

TABLE 3.2

Potentials		Channels (0,0)	(0,1)	(1,0)	(1,1)
	F_0^d	0.880			1.058
Square-well	F_0^e	-1.559			-0.705
	F_0	-0.679			0.353
	F_0^d	0.951	-0.387	0.934	-0.042
Gogny d1	F_0^e	-1.259	1.008	-0.464	0.641
	F_0	-0.307	0.621	0.470	0.599
	F_0^d	0.271	0.876	0.758	0.817
OMY(2-body)	F_0^e	-1.260	-0.120	-0.317	-0.219
	F_0	-0.990	0.756	0.441	0.598
	F_0^d	1.271	0.841	0.699	0.770
OMY(FHNC)	F_0^e	-1.199	-0.098	-0.290	-0.194
	F_0	0.072	0.743	0.408	0.576

Table 3.3

Number of Terms in Exchange Term

This table shows the number l of terms kept in the l-expansion -- (2.20) and (2.21) -- of the exchange term for each potential to limit the error to 10^{-5}.

TABLE 3.3

potentials	l
square-well	8
Gogny d1	8
1π-1ρ	13
OMY 2nd-order	8
OMY fhnc	9

Table 3.4

Convergence in (0,0) for Square-Well

The convergence relative to mesh size (0,0) for the square-well is measured by the numbers shown. S_0 and S_1 are the non-energy-weighted sums respectively. ω_p is the peak frequency. Γ_0 is the smoothing width given by (2.14) while Γ_s is the smallest width that gives a smooth curve. $\Delta\varepsilon(k_F)$ is the extent of the continuum and $\frac{\Delta S_1}{S_1}$ is the relative error in S_1 caused by smoothing with Γ_s.

Table 3.5

Convergence in (0,1) for Square-Well

The convergence of the results relative to mesh size (0,1) is shown here. ω_c is the collective frequency and S_c is the strength of the mode exhausts. $r_0 = \frac{S_c}{S_0}$. Other symbols are defined in Table 3.4.

TABLE 3.4

mesh	S_0	S_1	$\hbar\omega_p$	$S(q,\omega_p)$	Γ_0	Γ_s	$\frac{\Gamma_s}{\Delta\varepsilon(k_F)}$	$\frac{\Delta S_1}{S_1}$
2^1	.0783	.406	3.56	.0103	2.3	4.0	.214	.25
4^1	.0803	.406	5.05	.0114	.85	2.0	.107	.15
6^1	.0804	.406	4.05	.0115	.65	1.5	.080	.11
8^1	.0804	.406	4.35	.0124	.57	1.2	.064	.09
12^1	.0804	.406	4.18	.0132	.50	1.2	.064	.09

TABLE 3.5

mesh	S_0	$\hbar\omega_c$	$S_c^{\dagger}$	τ_0	Γ_0	Γ_s	$\frac{\Gamma_s}{\Delta\varepsilon(k_F)}$	$\frac{\Delta S_1}{S_1}^*$
2^1	.0176	18.92	8.50	.48	2.3	8.0	.427	-.08
4^1	.0176	19.04	6.56	.37	.85	2.5	.134	-.06
6^1	.0176	19.04	6.55	.37	.65	2.0	.107	-.05
8^1	.0176	19.04	6.54	.37	.57	1.8	.096	-.05

*Scaled by 10^3.

†Only the continuum is included in the error when a collective mode is present.

Table 3.6

Features of S(q,ω) in (0,0) for Square-Well

The v's denote speeds assuming a linear dispersion relation with q, and are expressed in units of c. Thus $v_p \equiv \frac{\hbar\omega_p}{\hbar cq}$; $v_F = \frac{\Delta\varepsilon(k_F)}{\hbar cq}$; $v_{Ff} \equiv \frac{\hbar^2}{m}\cdot\frac{k_F}{\hbar c}$. r_0 is the relative difference between S_0 calculated by RPA and the free-particle state structure function S_F: $\kappa_0 \equiv \frac{S_0 - S_F}{S_F}$. The other symbols are explained in the caption of Table 3.4. lk denotes local-kernel approximation.

Table 3.7

Features of S(q,ω) in (0,1) for Square-Well

Here $v_c \equiv \frac{\hbar\omega_c}{\hbar cq}$; κ is the enhancement factor in spin (isospin) modes: $\kappa = \frac{S_1 - S_{1F}}{S_{1F}}$ where $S_{1F} = \rho^{\tilde{S}\tilde{T}}\frac{\hbar^2 q^2}{2m}$ and $\rho^{\tilde{S}\tilde{T}}$ is given by 2.18. Other symbols are explained in connection with Tables 3.5 and 3.6.

TABLE 3.6

$\frac{q}{k_F}$	$\frac{S_0}{q}$	κ_0	$\frac{S_1}{q^2}$	v_p	$S(q,\omega_p)$	v_F	v_{Ff}	$\frac{\Gamma_s}{\Delta\varepsilon(k_F)}$	$\frac{\Delta S_1}{S_1}$
.05	.586	.093	20.7	.156	3.23	.673	.301	.059	.09
.1	.574	.072	20.7	.157	3.10	.678	.309	.064	.09
.2	.534	.001	20.7	.168	2.87	.686	.324	.053	.07
.3	.485	-.088	20.7	.190	2.36	.692	.338	.070	.07
.4	.436	-.175	20.7	.236	2.04	.695	.353	.085	.06
.5	.393	-.250	20.7	.254	1.88	.697	.368	.062	.03
lk	.827	.543	46.9	-	-	.667	.294	-	-

TABLE 3.7

$\frac{q}{k_F}$	$\frac{S_0}{q}$	κ_0	κ_∞	v_c	$\frac{S_c}{\hbar\omega_c}$ †	r_0	$\frac{\Gamma_s}{\Delta\varepsilon(k_F)}$	$\frac{\Delta S_1}{S_1}$ *
.05	.126	-.062	1.60	.689	.363	.39	.097	-.05
.1	.126	-.060	1.59	.689	.344	.37	.096	-.05
.25	.127	-.048	1.57	.691	.209	.22	.042	-.03
.3	.128	-.041	1.56	-	-	-	.070	-.03
.5	.131	-.002	1.50	-	-	-	.058	-.04
lk	.118	-.118	1.27	.668	.062	.07	-	-

Table 3.8

Properties of Single-pair Spectrum of Gogny d1

Properties common to all four channels are displayed here. u_F is the HF potential part of the Fermi speed:

$$u_F = \frac{1}{\hbar c q}[\Delta\varepsilon(f_F) - \frac{\hbar^2}{2m}(q^2 + 2k_f q)].$$

All other symbols are explained in captions of Tables 3.4-3.7.

TABLE 3.8

$\frac{q}{k_F}$	$\Delta\varepsilon(k_F)$	v_F	u_F	v_{Ff}	mesh	Γ_0	$S_F(q)$
.007	.799	.427	.141	.286	6^3	.008	.0052
.01	1.142	.427	.141	.286	6^3	.013	.0075
.03	3.452	.430	.141	.289	6^3	.067	.0225
.05	5.794	.433	.141	.292	6^3	.143	.0375
.1	11.79	.441	.142	.299	6^3	.402	.0749
.2	24.35	.455	.142	.313	6^3	1.12	.1495
.3	37.62	.469	.142	.327	6^3	2.02	.2233
.5	66.11	.494	.138	356	8^2	4.27	.3672

Table 3.9

Features of $S(q,\omega)$ in (0,0) for Gogny d1

See Tables 3.4-3.7 for definitions of symbols.

TABLE 3.9

$\frac{q}{k_F}$	$\frac{S_0}{q}$	κ_0	$\frac{S_1}{q^2}$	v_p	$S(q,\omega_p)$	Γ_s	$\frac{\Gamma_s}{\Delta\varepsilon(k_F)}$	$\frac{\Delta S_1}{S_1}$
.01	.536	-.030	20.7	.196	.0117	.18	.16	.02
.05	.536	-.032	20.7	.182	.0120	.55	.10	.02
.1	.532	-.036	20.7	.198	.0118	1.3	.11	.02
.5	.460	-.149	20.7	.234	.0976	5.5	.08	.01

Table 3.10

Features of $S(q,\omega)$ in Spin Isospin Channels for Gogny d1

See Tables 3.4-3.7 for definitions of symbols.

TABLE 3.10

$(\tilde{S},\tilde{T})$	$\frac{q}{k_F}$	$\frac{S_0}{q}$	κ_0	κ	v_c	$\frac{S_c}{\hbar\omega_c}$ †	r_0	$\frac{\Gamma_s}{\Delta\varepsilon(k_F)}$	$\frac{\Delta S_1}{S_1}$ *
(0,1)	.01	.123	-.11	.78	.455	.784	.57	-	-
	.05	.123	-.11	.78	.456	.773	.57	.14	-.06
	.2	.123	-.11	.78	.461	.590	.44	.05	-.03
	.3	.123	-.10	.77	-	-	-	.07	-.07
	.5	.124	-.09	.75	-	-	-	.06	-.05
(1,0)	.007	.119	-.13	.53	.431	.375	.27	.10	-.06
	.03	.119	-.14	.53	.431	.312	.22	.04	-.03
	.05	.119	-.14	.53	-	-	-	.04	-.04
	.3	.119	-.14	.52	-	-	-	.07	-.04
(1,1)	.05	.120	-.14	.67	.444	.649	.48	.10	-.05
	.1	.120	-.13	.67	.446	.567	.42	.09	-.05
	.3	.120	-.12	.66	-	-	-	.06	-.05
	.5	.121	-.11	.64	-	-	-	.07	-.04

Table 3.11

Evaluation of Local-Kernel Approximation with Gogny d1

The salient features of $S(q,\omega)$ and $S_L(q,\omega)$ are compared in all four channels. 'ex' and 'lk' denote the exact-RPA and local-kernel approximate values respectively. χ_c is a measure of collectivity:

$$\chi_c = \frac{\hbar\omega_c}{\Delta\varepsilon(k_F)}.$$

TABLE 3.11

	(0,0)		(0,1)		(1,0)		(1,1)	
	ex	lk	ex	lk	ex	lk	ex	lk
λ_c^{-1}	-	-	.051	.0115	.0085	.0040	.024	.0103
r_0	-	-	.57	.31	.27	.17	.48	.29
$\frac{S_0}{q}$	.536	.641	.123	.113	.119	.118	.030	.028
$\frac{S_1}{q^2}$	20.7	31.0	9.23	7.81	7.91	7.78	2.16	1.96

Table 3.12

Features of S(q,ω) in (1,1) for Brown $1\pi-1\rho$

The features of $S(q,\omega)$ projected into spin spaces are shown here. f_ρ^2 is the interaction strength of the ρ-meson-exchange. $\tilde{m}_s$ = -1 is degenerate with $\tilde{m}_s$ =1. See Tables 3.4-3.7 for definitions of all other symbols.

TABLE 3.12

$1\pi - 1\rho$

$\tilde{m}_s$	f_ρ^2	$\frac{q}{k_F}$	$\frac{S_0}{q}$	$\frac{S_1}{q^2}$	V_F	V_c	$\frac{S_c}{\hbar\omega_c}$ †	r_0
0	4.86	.1	.094	8.41	.474	.505	.694	.74
1	4.86	.1	.070	3.38	.474	.505	.000	.00
0	1.86	.1	.106	7.55	.398	.411	.818	.63
1	1.86	.1	.071	2.91	.398	.411	.000	.00
0	4.86	.5	.110	8.25	.525	-	-	-
1	4.86	.5	.083	4.17	.525	-	-	-
0	1.86	.5	.138	7.41	.448	-	-	-
1	1.86	.5	.083	3.59	.448	-	-	-

Table 4.1

Features of $S(q,\omega)$ in (0,0) for OMY

Salient features are shown here to both two-body order and FHNC accuracy. V_2 and V_h denote the two-body and FHNC effective interactions respectively and are given by (4.15). 'unst.' means instability of the uniform phase against density fluctuations.

TABLE 4.1

	$\frac{q}{k_F}$	$\frac{S_0}{q}$	κ_0	$\frac{S_1}{q_2}$	v_F	$\frac{\Gamma_s}{\Delta\varepsilon(k_F)}$	$\frac{\Delta S_1}{S_1}$
V_2	.1	-	-	unst.	-	-	-
	.3	-	-	unst.	-	-	-
	.5	.232	.77	5.18	.590	.07	.10
	1.	.103	-.16	5.18	.645	.10	.04
V_h	.05	.103	-.23	5.84	.602	.07	.01

Table 4.2

Features of $S(q,\omega)$ in Spin Isospin Channels for OMY

See Tables 3.4-3.7 and 4.1 for definitions of all symbols.

TABLE 4.2

$(\tilde{S},\tilde{T})$	V	$\frac{q}{k_F}$	$\frac{S_0}{q}$	κ_0	v_c	$\frac{S_c}{\hbar\omega_c}$ †	r_0	$\frac{S_1}{q^2}$
(0,1)	V_2	.01	.109	-.19	.538	.541	.53	9.73
		.05	.109	-.19	.539	.525	.51	9.72
		.1	.110	-.18	.540	.474	.46	9.72
		.3	.111	-.16	-	-	-	9.65
		.5	.111	-.15	-	-	-	9.52
	V_h	.05	1.07	-.20	.613	.408	.46	10.8
(1,0)	V_2	.01	.117	-.13	.523	.345	.30	9.50
		.05	.118	-.12	.525	.264	.23	9.49
		.1	.118	-.12	-	-	-	9.49
		.3	.120	-.10	-	-	-	9.42
	V_h	.05	.116	-.13	-	-	-	10.5
(1,1)	V_2	.01	.113	-.16	.530	.458	.42	9.61
		.05	.113	-.16	.530	.425	.39	9.61
		.1	.113	-.16	.532	.334	.31	9.60
		.3	.115	-.13	-	-	-	9.54
	V_h	.05	.111	-.17	.604	.261	.28	10.7

Figure 1

Excitable Parts of Fermi Sphere

The figure shown is a cross-section of the Fermi sea with $\vec{q}$ pointing upward. Cylindrical symmetry assumed; only the two polar caps are excitable regions.

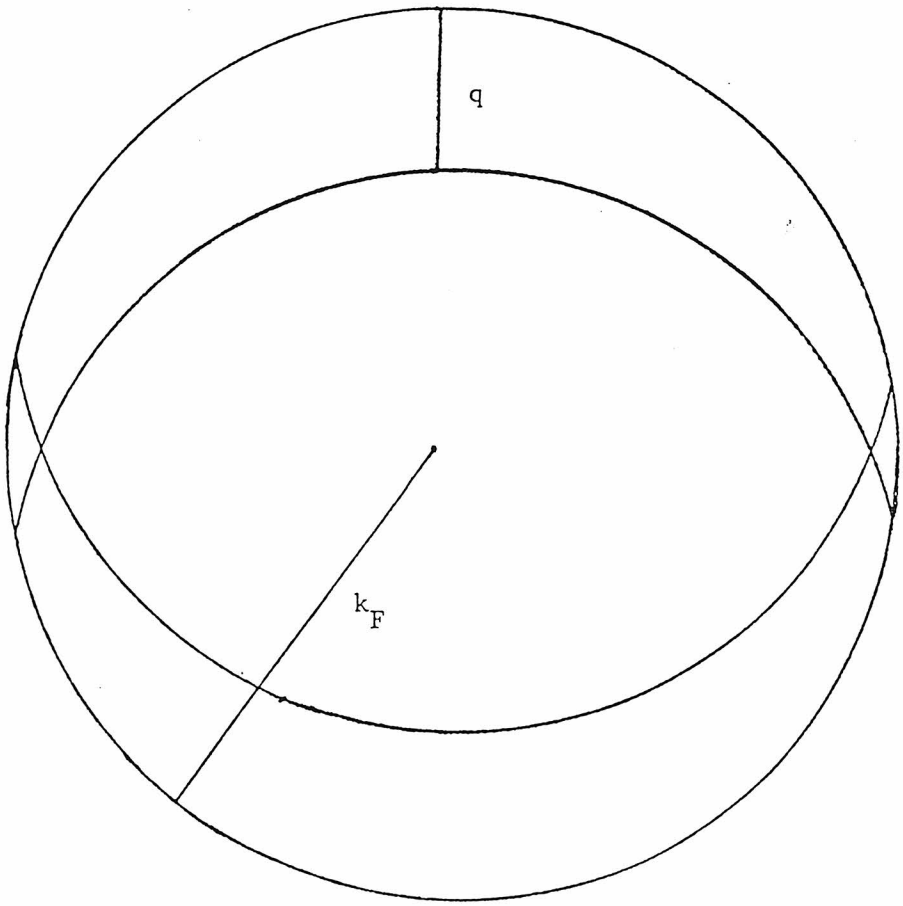

FIGURE 1

Figure 2

Typical Mesh

Called 6^1 in Table 3.1, this is a typical mesh used in the calculations.

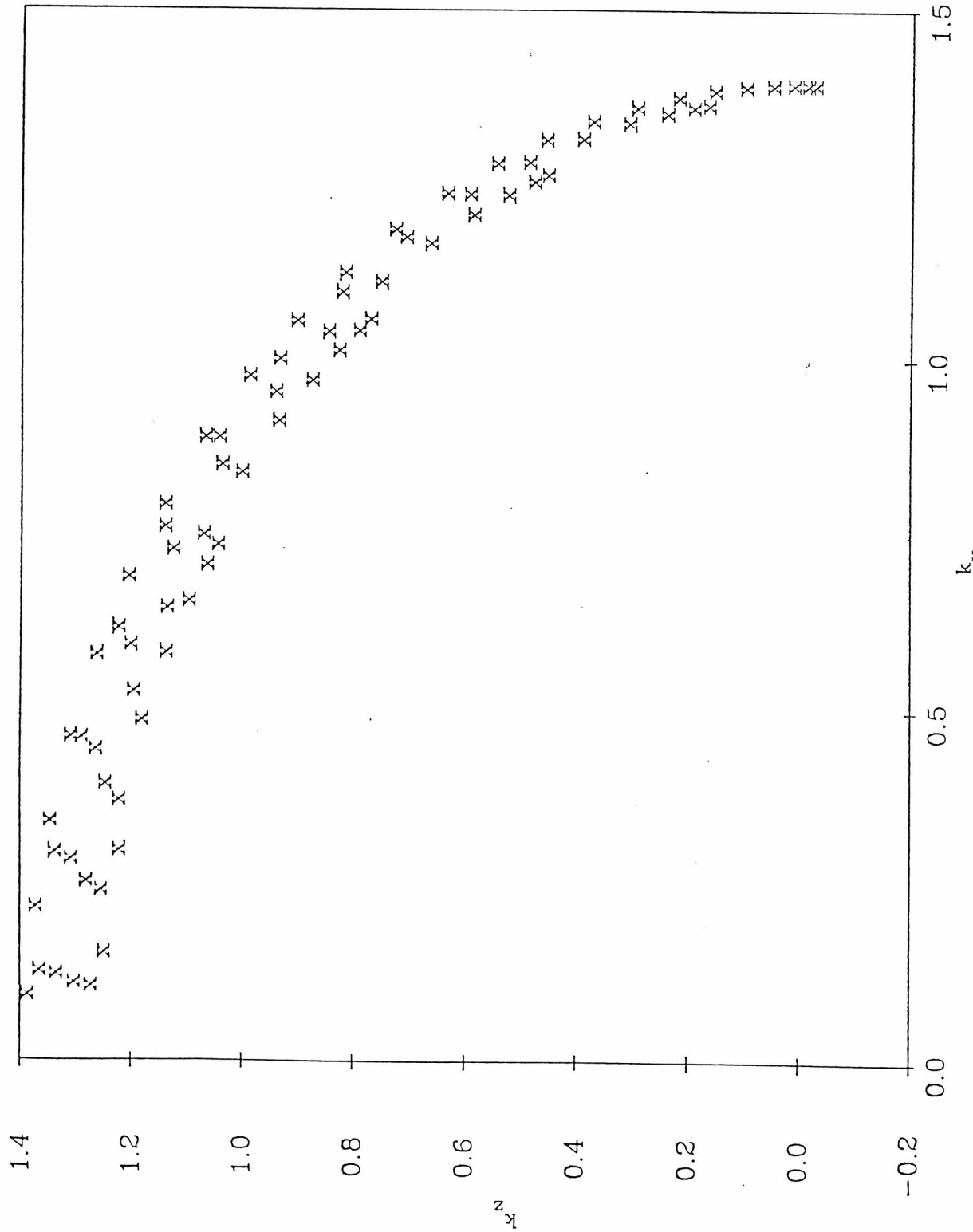

FIGURE 2

Figure 3a

χ_s vs λ

χ_s is the function given in Section 2.2 in the stability analysis (p.41) in the local-kernel approximation.

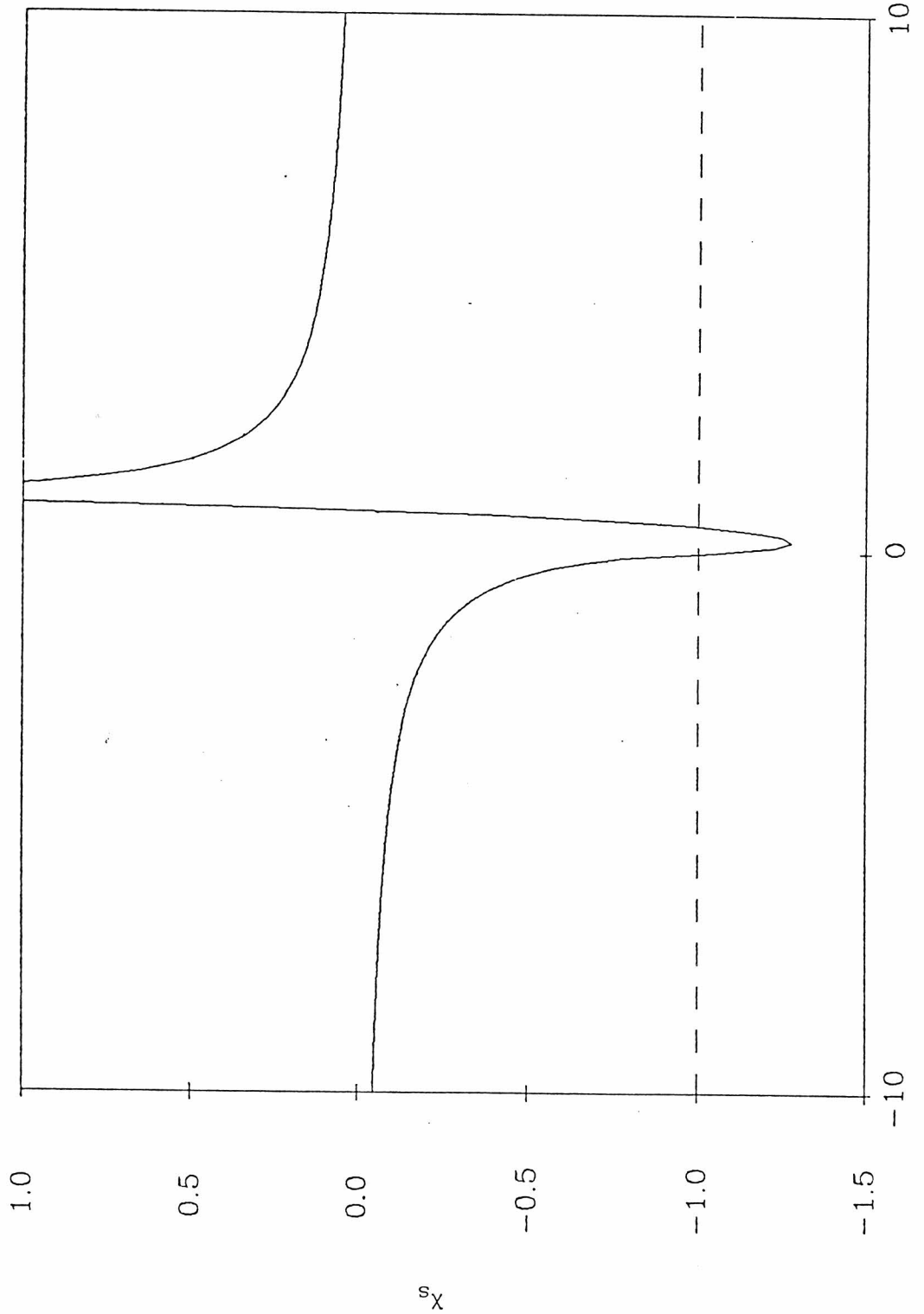

FIGURE 3a

Figure 3b

χ' vs λ

The curves above zero are given by (2.7), defining the collective mode in the local-kernel approximations. The function below is actually $\chi(i\lambda)$ giving imaginary eigenvalues when F_0<-1.

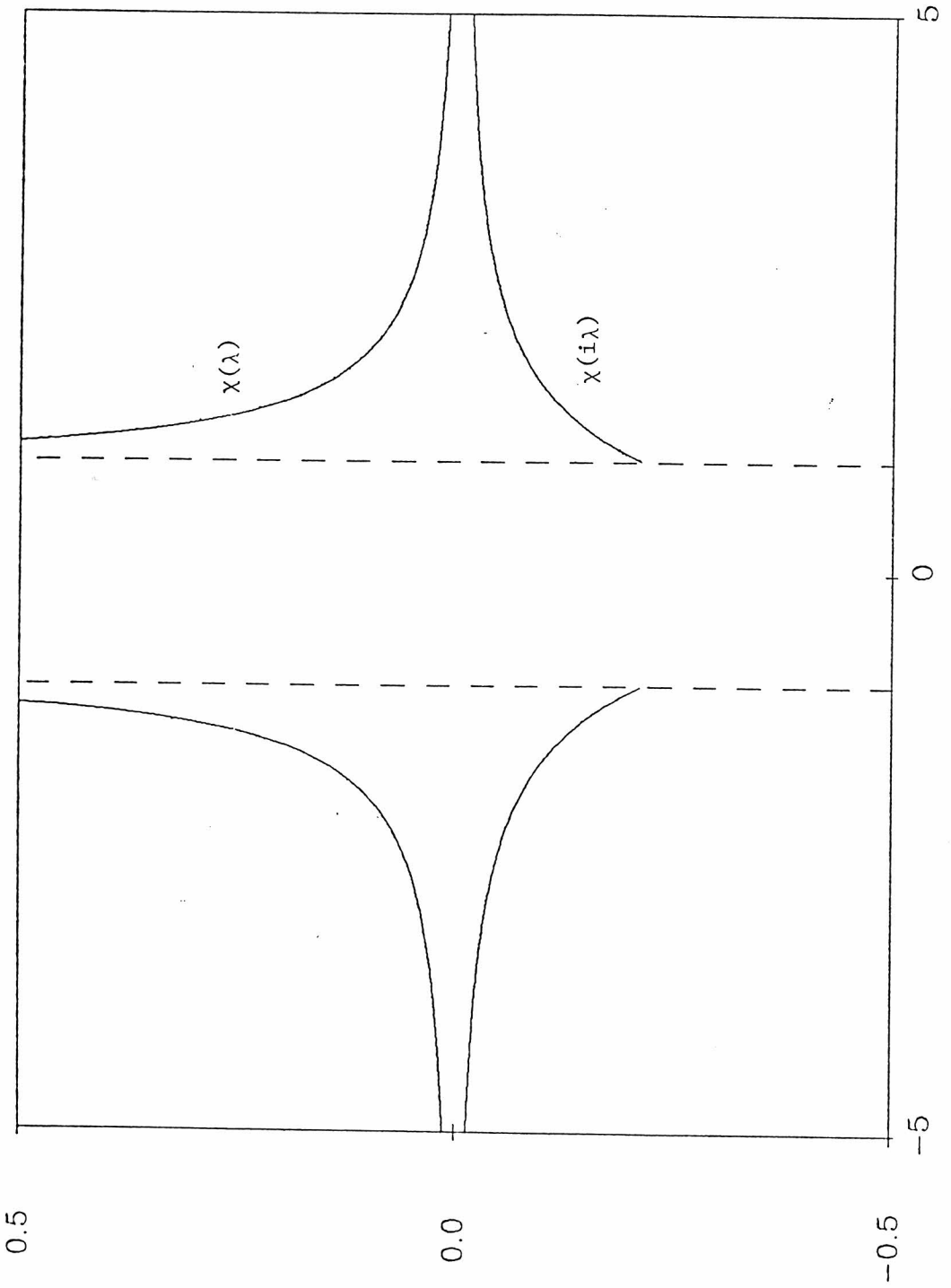

FIGURE 3b

Figure 4

Evaluation of Smoothing Procedure

The curve with the kink is the exact free-particle $S(q,\omega)$. The smooth curve is obtained by the mesh 8^1 (Table 3.1) and $\Gamma_s = .8$ MeV. The dotted curve represents Lorentzian smoothing without the triangle; the dashed curve is obtained without the Lorentzian.

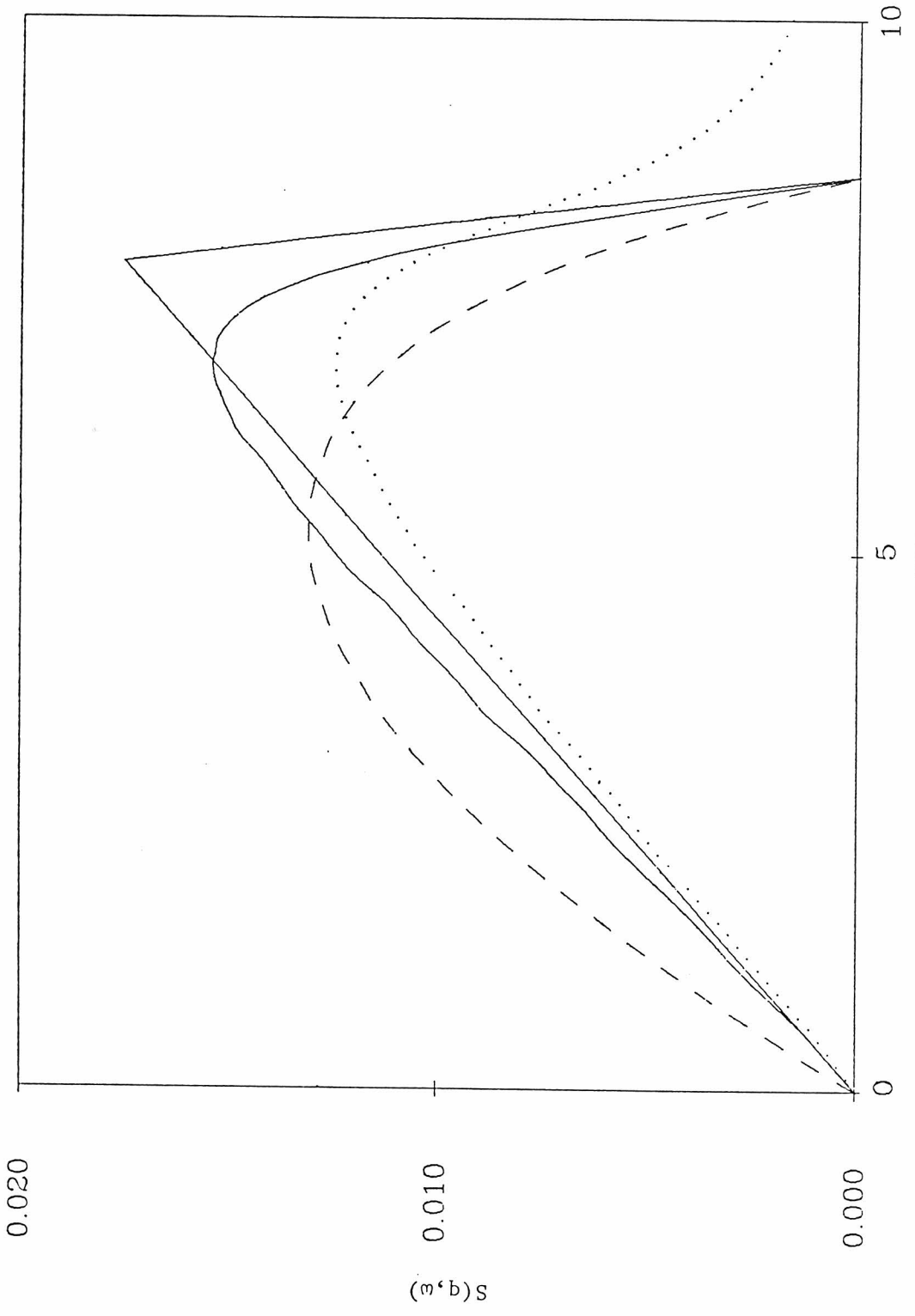

FIGURE 4

Figure 5

Evaluation of Local-Kernel Approximation

These curves are $S(q,\omega)$ at $q = .05\ k_F$ in (0,0). The solid lines and the dotted line are all local-kernel curves while the dashed line is the RPA-$S(q,\omega)$ for the square-well. $F_0 = -.679$.

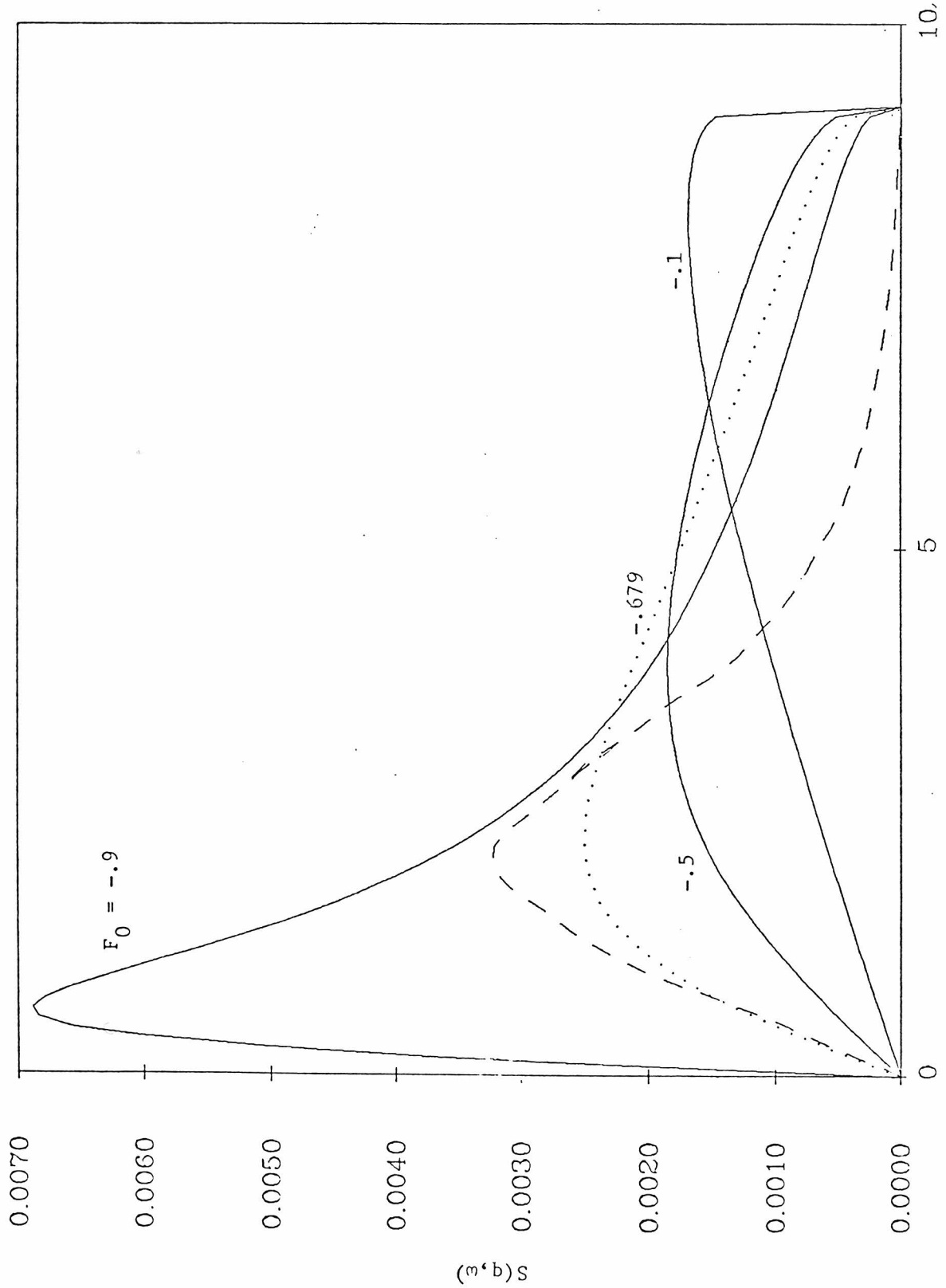
0.0070
0.0060
0.0050
0.0040
0.0030
0.0020
0.0010
0.0000
S(q,ω)
0
5
10.
MEV
F_0 = -.9
-.679
-.5
-.1

FIGURE 5

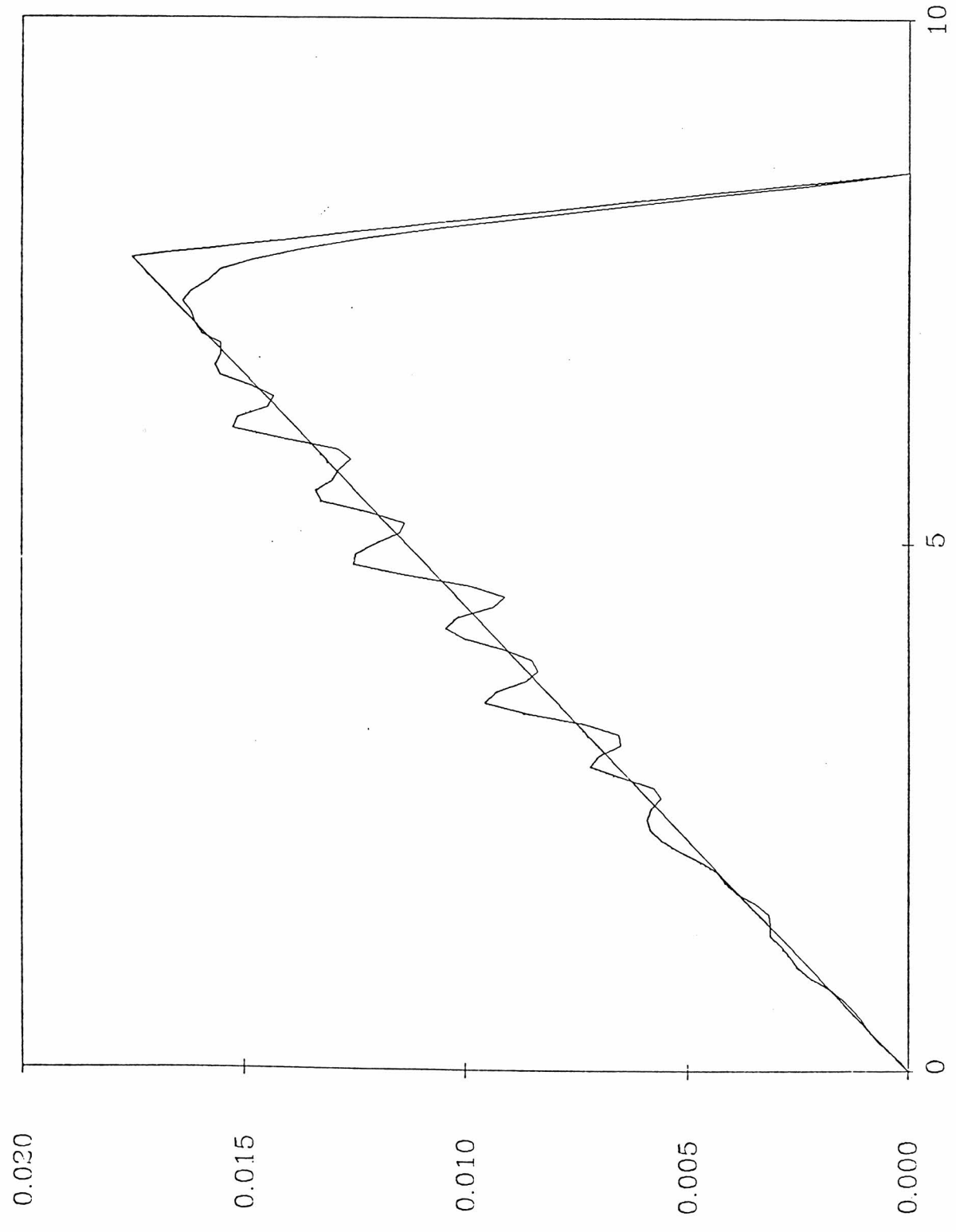

FIGURE 6

Figure 7

Evaluation of Smoothing Procedure

At $q = .5\ k_F$ with δ^1 and $\Gamma = \Gamma_0 = 2.93$, the approximation is better than the low-q case (Figure 6).

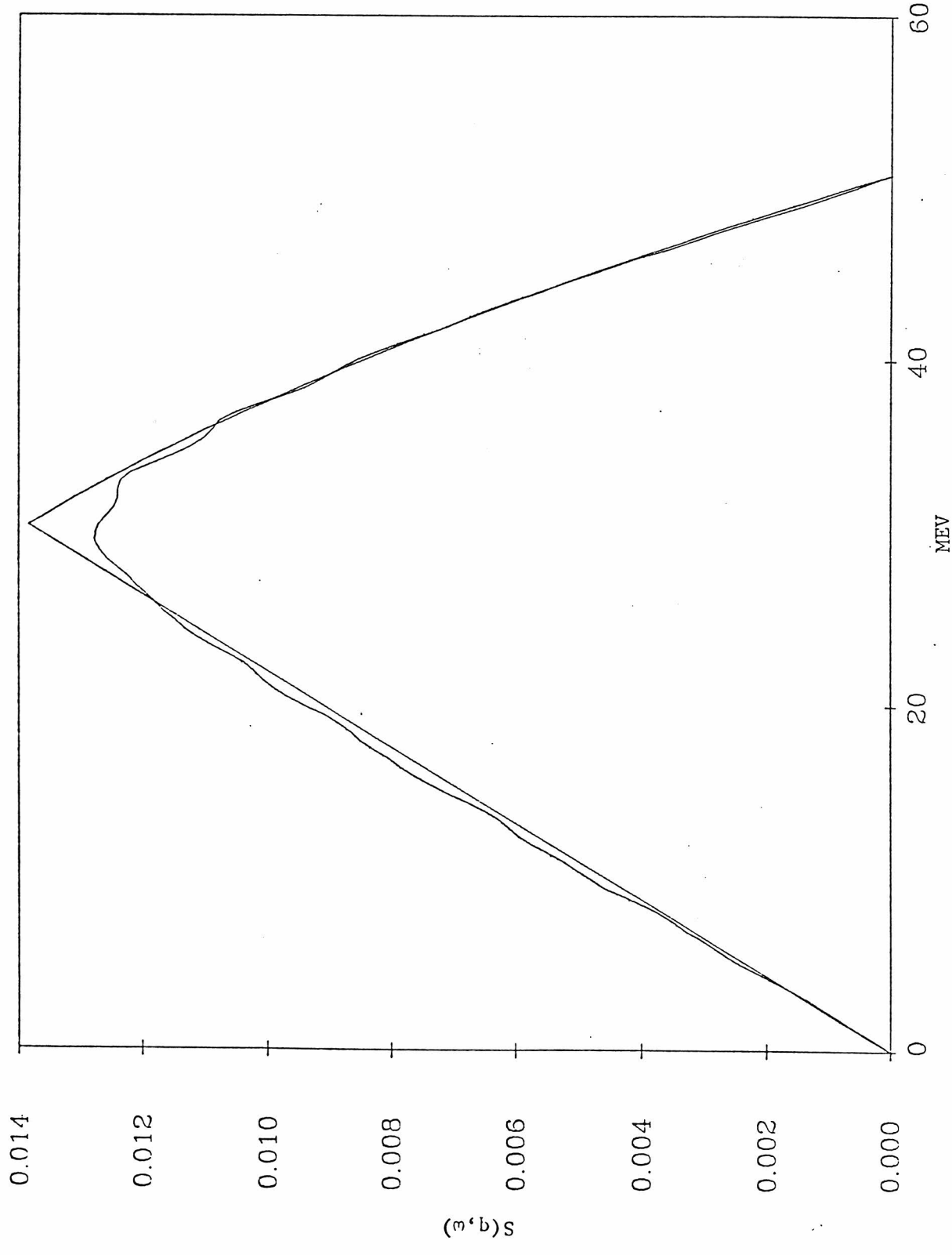

FIGURE 7

Figure 8

Square-Well and OMY

The spatially even components of the Molinari square-well (dashed) and OMY (solid) are shown.

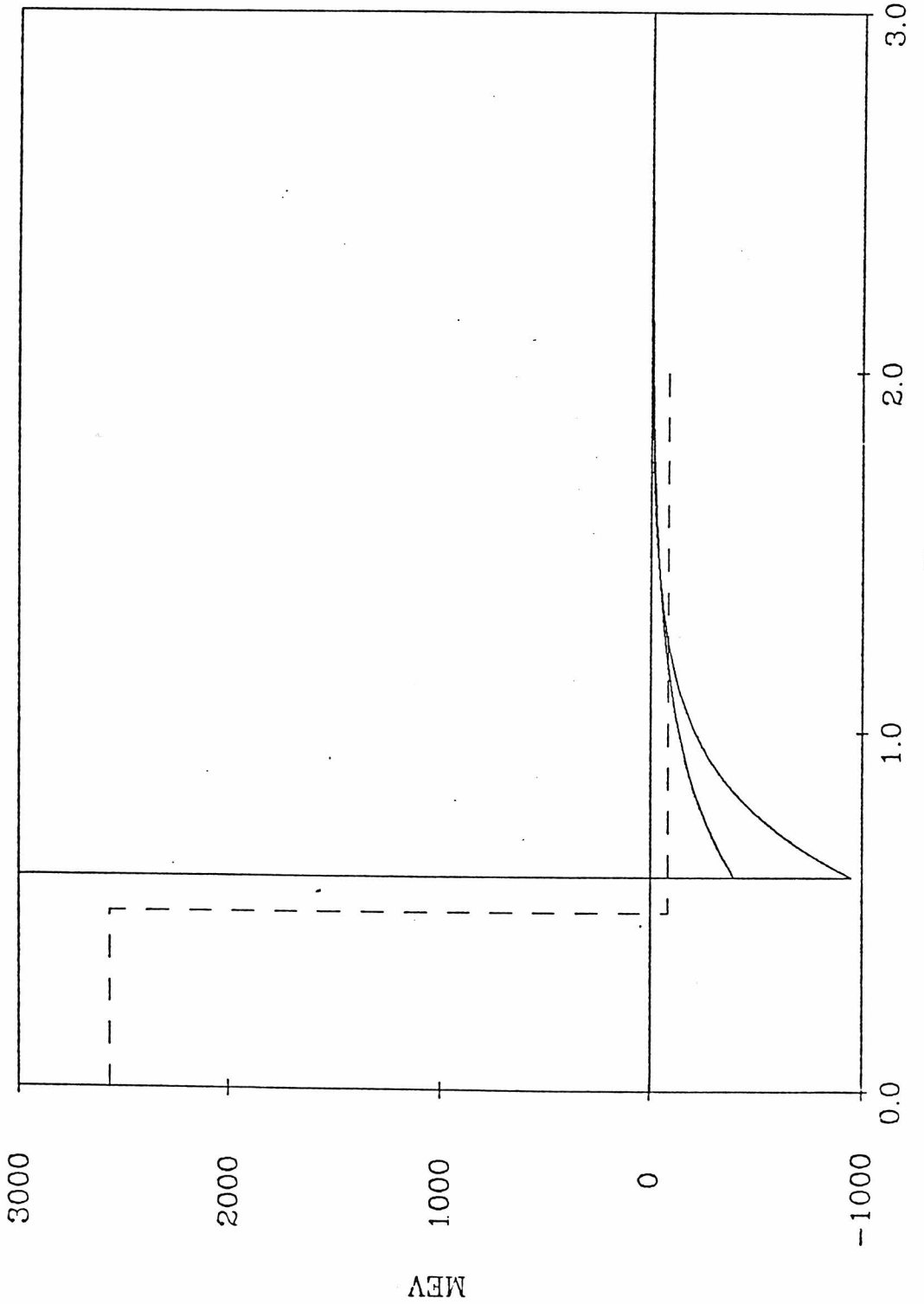

FIGURE 8

Figure 9

Different Smoothing Widths

The curves are produced with the smoothing widths indicated from the discretized version of $S(q,\omega)$ from a 8^1 mesh at $q=.1\ k_F$ in (0,0) for the square-well. $\Gamma=.573$ and $\Gamma_s=1.2$.

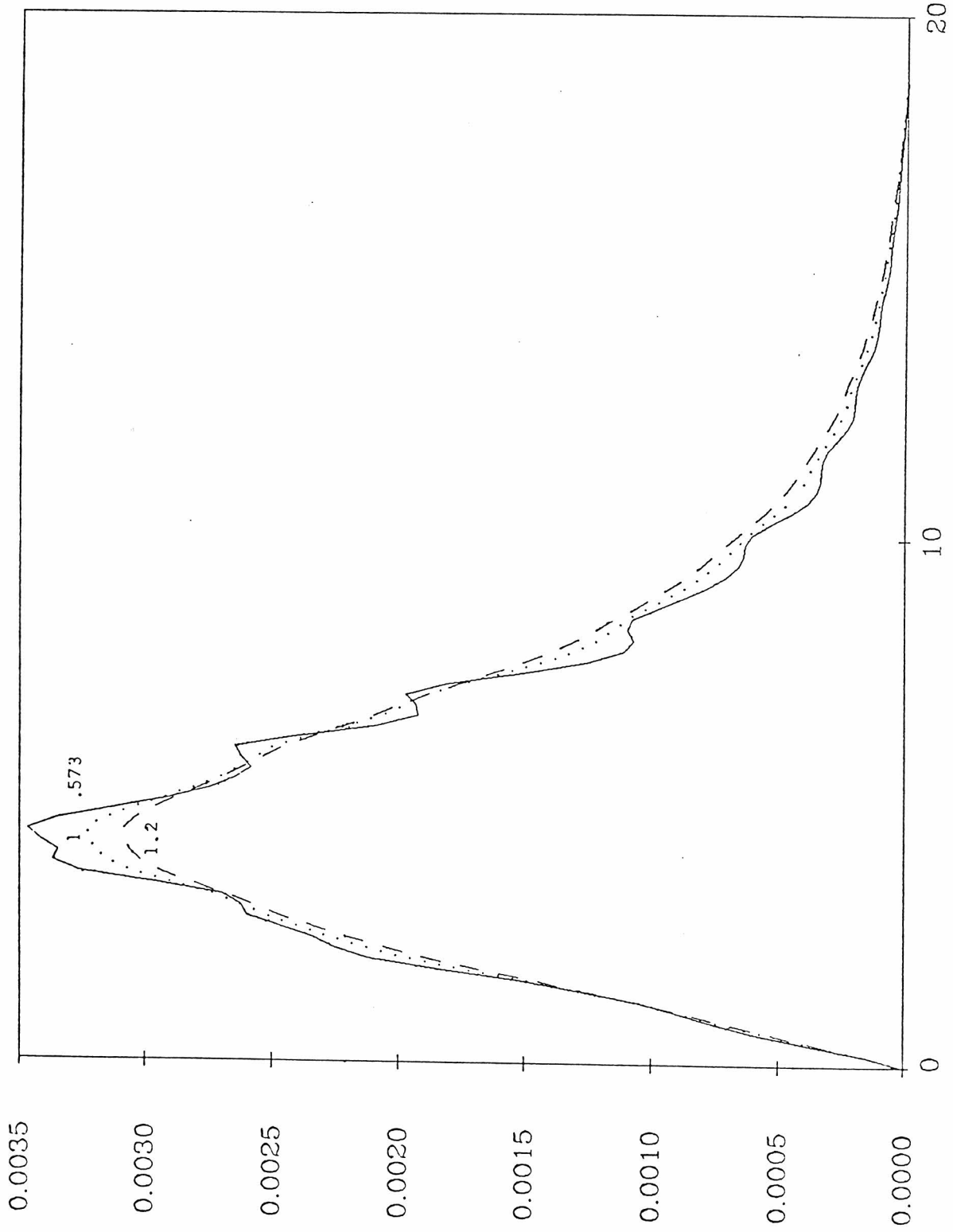
0.0035
0.0030
0.0025
0.0020
0.0015
0.0010
0.0005
0.0000
S(q,ω)
0
10
20
MEV
.573
1
1.2

FIGURE 9

Figure 10

Convergence in (0,0)

Convergence of $S(q,\omega)$ relative to mesh size is depicted here. The four numbers stand for the meshes 2^1, 4^1, 6^1 and 8^1, the association being obvious. The dashed curve, which is barely distinguishable from the 8^1 curve, is produced with 12^1. $q = .1\ k_F$ and (0,0) with the square-well is considered.

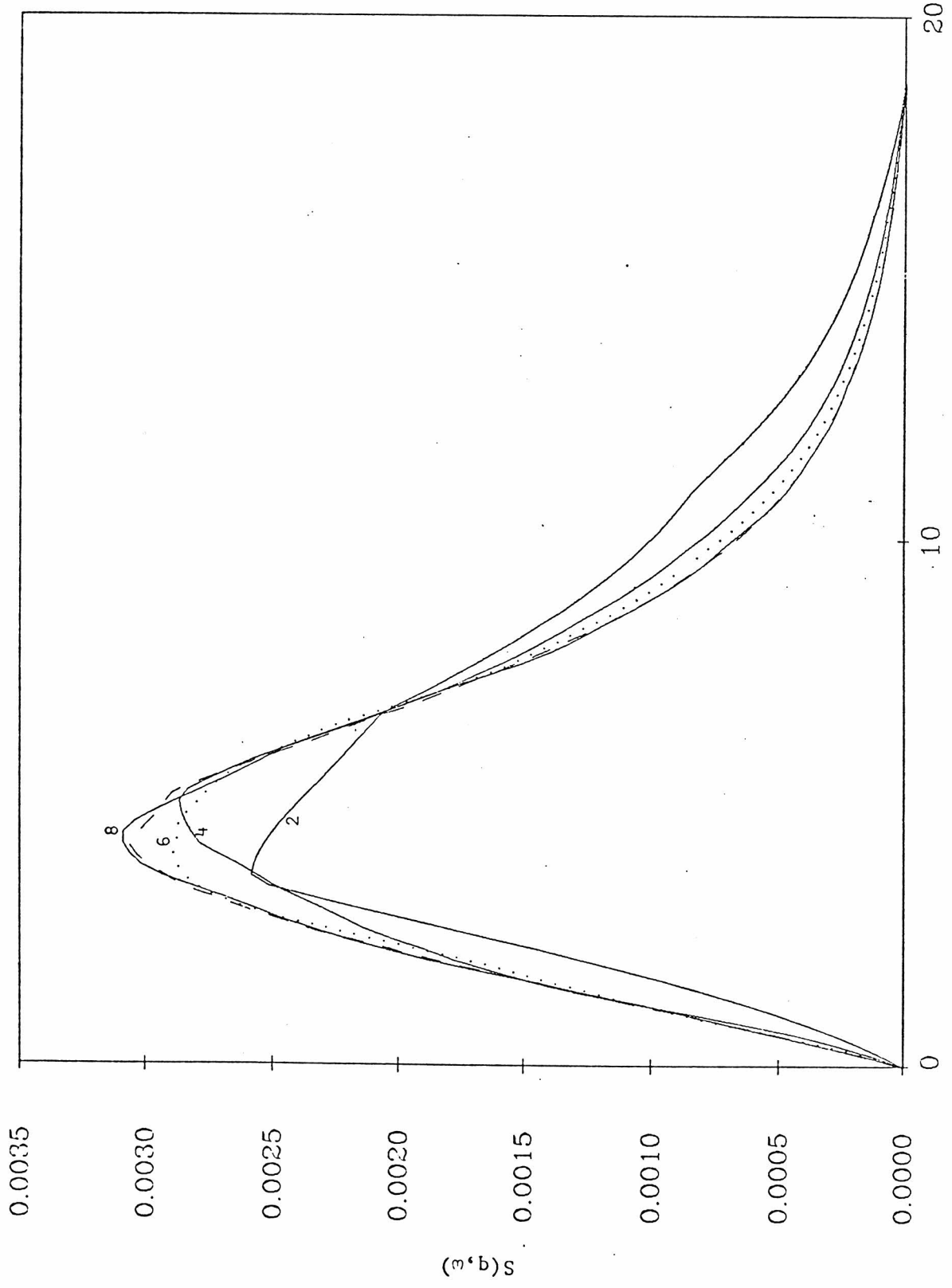
0.0035
0.0030
0.0025
0.0020
0.0015
0.0010
0.0005
0.0000
S(q,ε)
0
10
20
MEV
8
6
4
2

FIGURE 10

Figure 11

Results in (0,0) with Square-Well

In this and all subsequent graphs, $S(q,\omega)$ is scaled by 10^3. (a) $q = .05\ k_F$; (b) $q = .1\ k_F$; (c) $q = .3\ k_F$; (d) $q = .5\ k_F$.

Figure 12

Results in (0,1) with Square-Well

The height of the spike is set at $10\times\frac{S_c}{\hbar\omega_c}$ (scaled by 10^3). (a) $q=.05\ k_F$; (b) $q=.1\ k_F$; (c) $q=.25\ k_F$; (d) $q=.5\ k_F$.

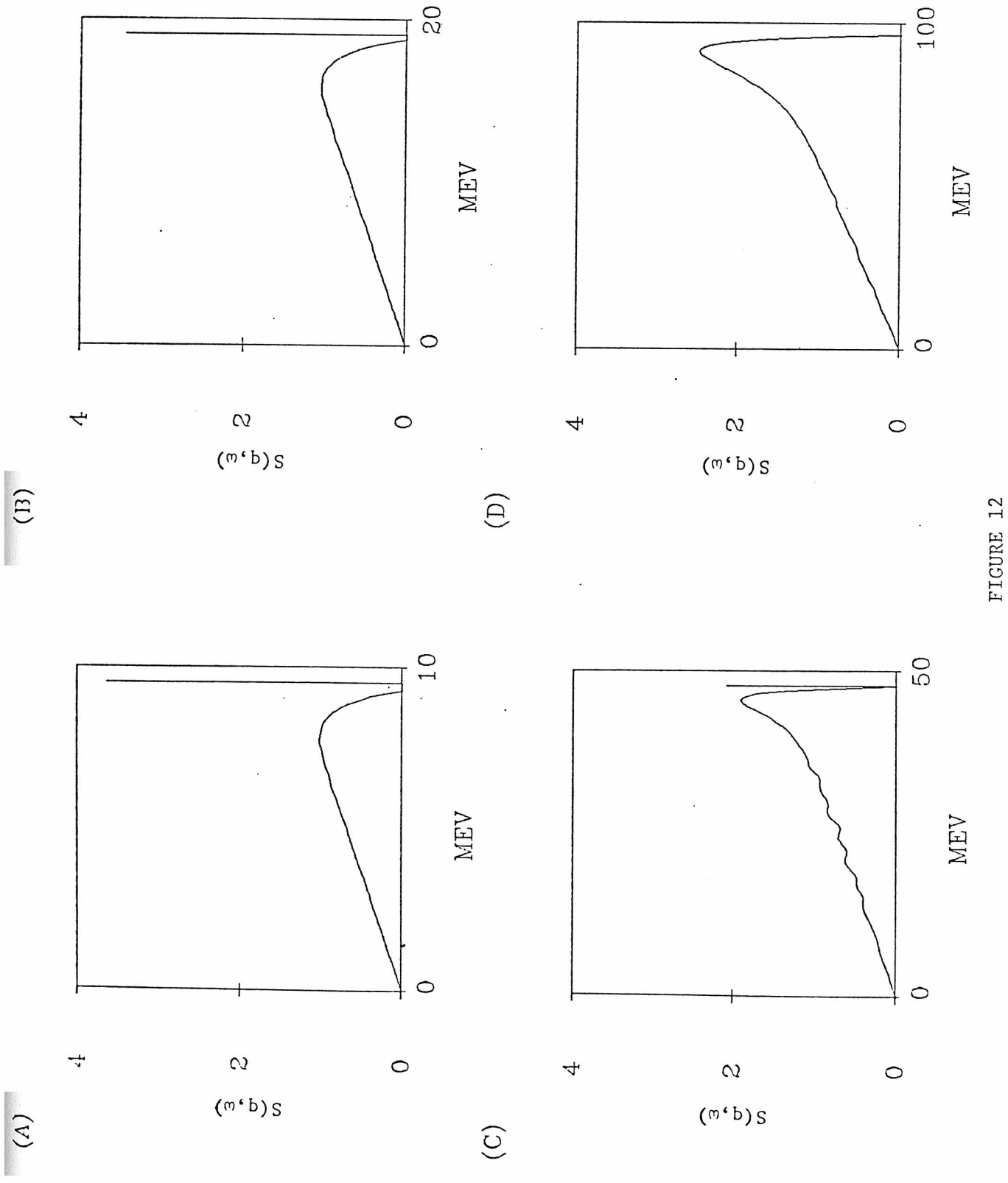
(A)
S(q,ω)
4
2
0
0
10
MEV
(B)
S(q,ω)
4
2
0
0
20
MEV
(C)
S(q,ω)
4
2
0
0
50
MEV
(D)
S(q,ω)
4
2
0
0
100
MEV

FIGURE 12

Figure 13

Direct Particle-Hole Potential (Gogny)

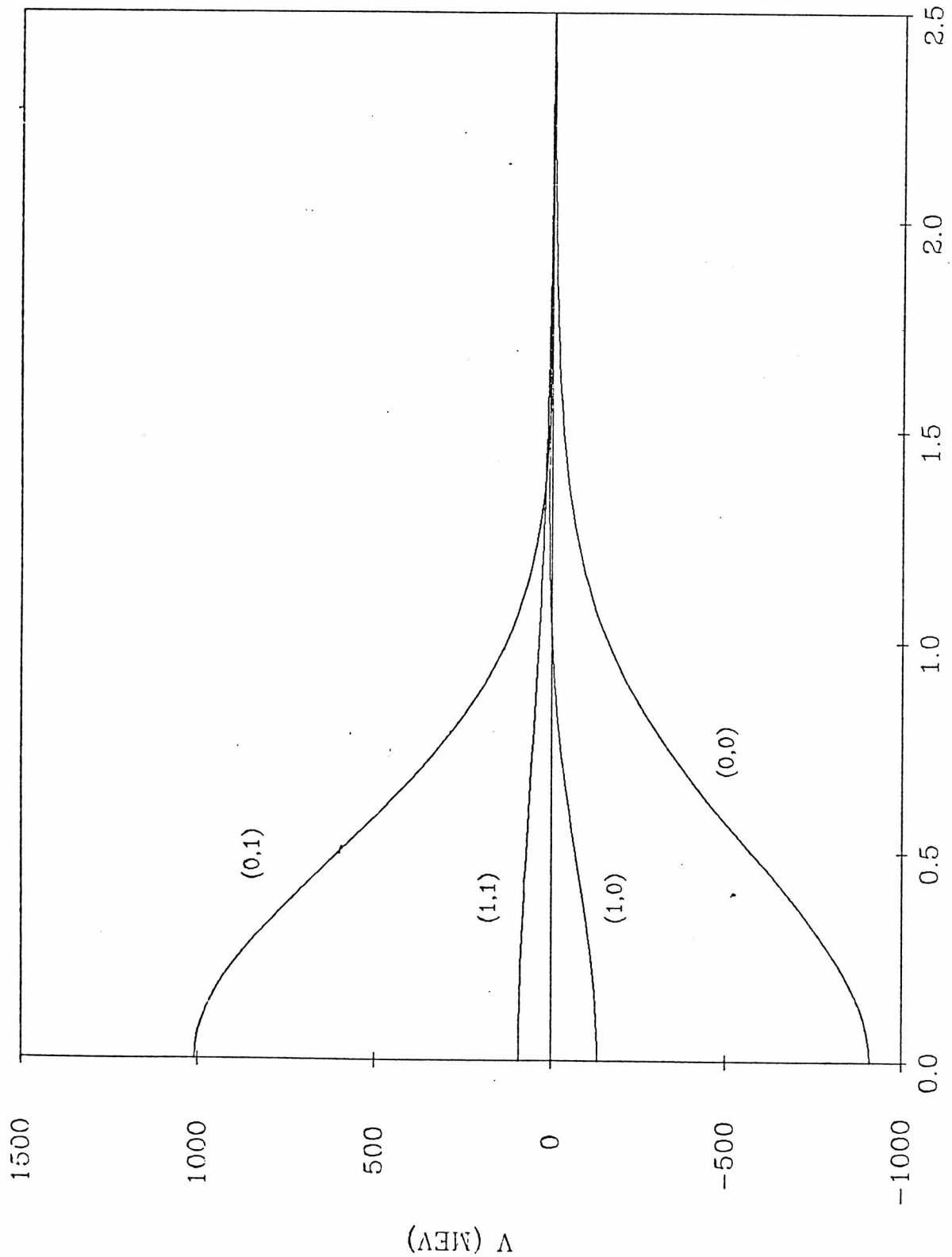

FIGURE 13

Figure 14

Exchange Particle-Hole Potential (Gogny)

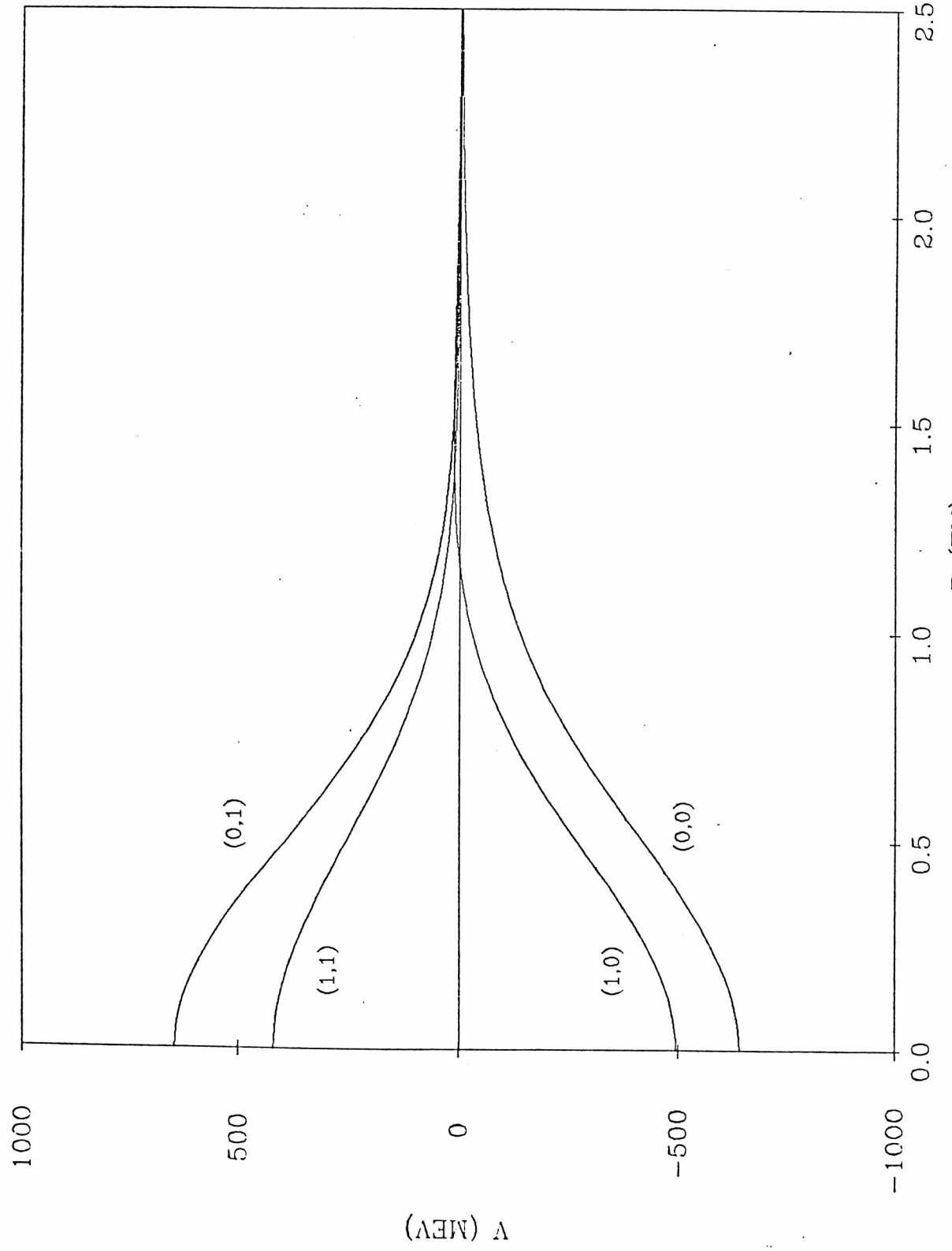

FIGURE 14

Figure 15

Single-Particle Potential from Square-Well and Gogny d1

FIGURE 15

Figure 16

Results in (0,0) with Gogny d1

(a) $q = .01\ k_F$; (b) $q = .05\ k_F$; (c) $q = .1\ k_F$; (d) $q = .5\ k_F$.

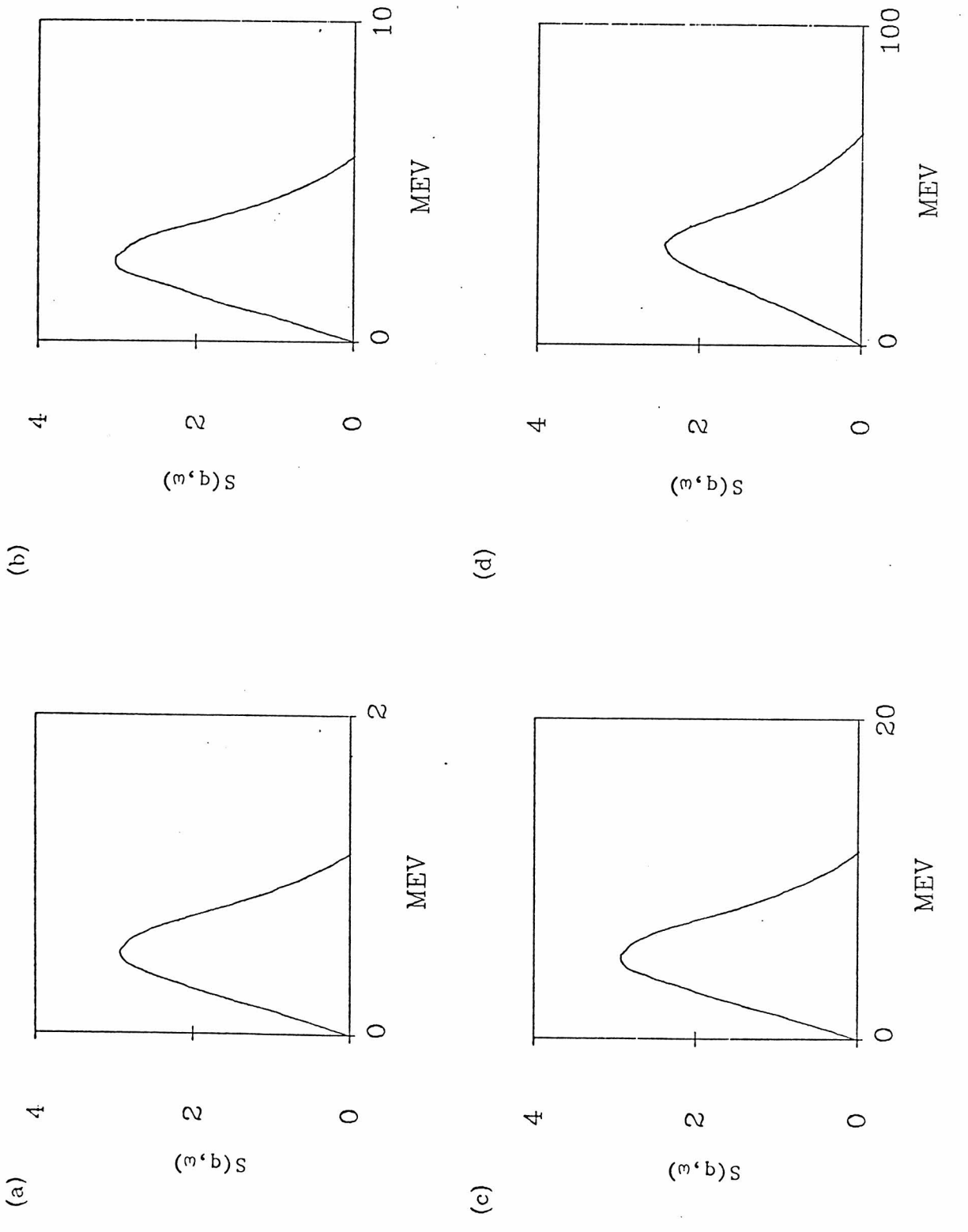
(a)
S(q,ω)
4
2
0
0
2
MEV
(b)
S(q,ω)
4
2
0
0
10
MEV
(c)
S(q,ω)
4
2
0
0
20
MEV
(d)
S(q,ω)
4
2
0
0
100
MEV

FIGURE 16

Figure 17

Results in (0,1) with Gogny d1

The spikes in this and the next two graphs have height = $5\times\frac{S_c}{\hbar\omega_c}$ ($\times 10^3$). (a) $q = .05\ k_F$; (b) $q = .2\ k_F$; (c) $q = .3\ k_F$; (d) $q = .5\ k_F$.

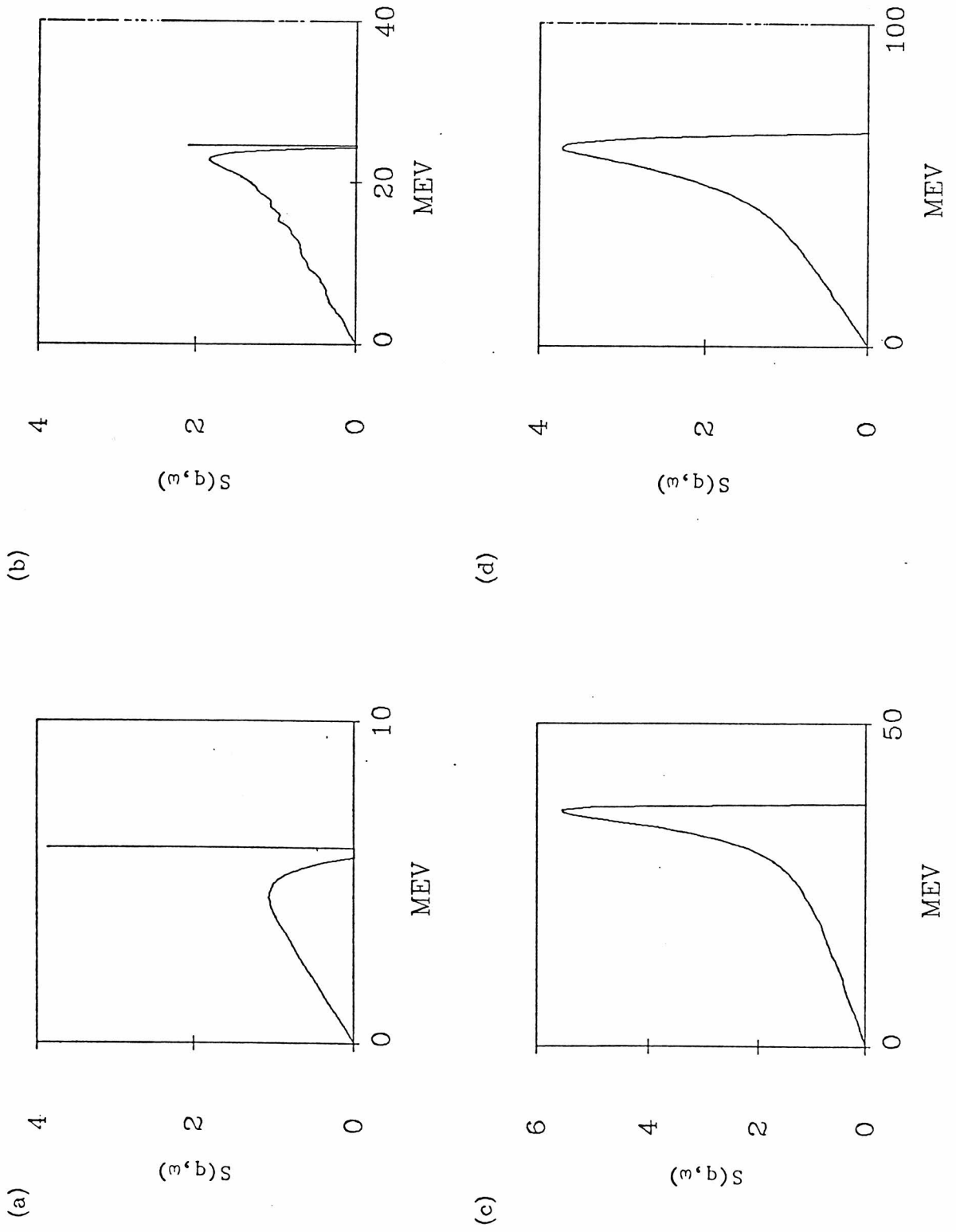
(a)
S(q,ω)
0
2
4
0
10
MEV
(b)
S(q,ω)
0
2
4
0
20
40
MEV
(c)
S(q,ω)
0
2
4
6
0
50
MEV
(d)
S(q,ω)
0
2
4
0
100
MEV

FIGURE 17

Figure 18

Results in (1,0) with Gogny d1

(a) $q = .007\ k_F$; (b) $q = .03\ k_F$; (c) $q = .05\ k_F$; (d) $q = .3\ k_F$.

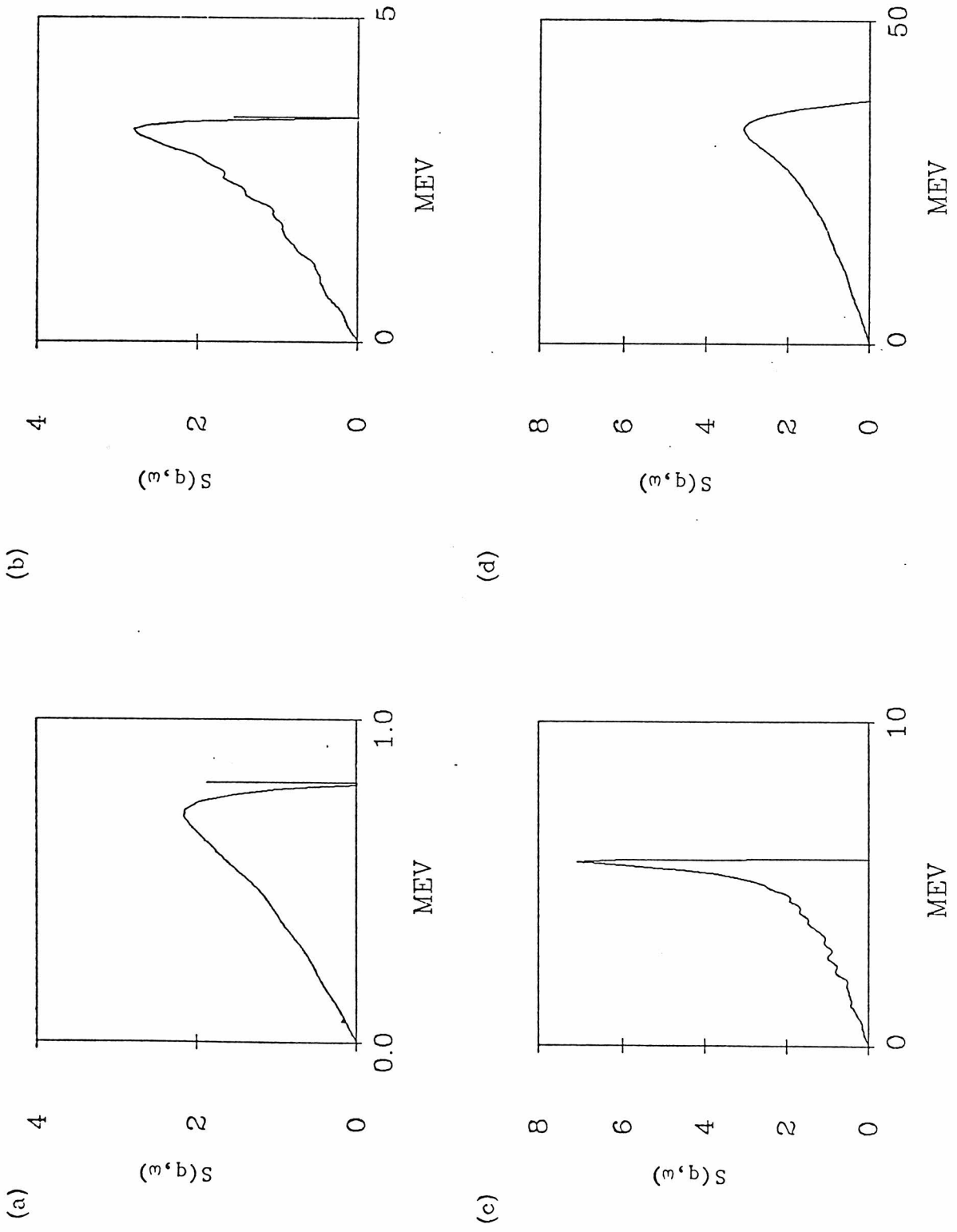
(a)
S(q,ω)
4
2
0
0.0
1.0
MEV
(b)
S(q,ω)
4
2
0
0
5
MEV
(c)
S(q,ω)
8
6
4
2
0
0
10
MEV
(d)
S(q,ω)
8
6
4
2
0
0
50
MEV

FIGURE 18

Figure 19

Results in (1,1) with Gogny d1

(a) $q = .007\ k_F$; (b) $q = .03\ k_F$; (c) $q = .05\ k_F$; (d) $q = .3\ k_F$.

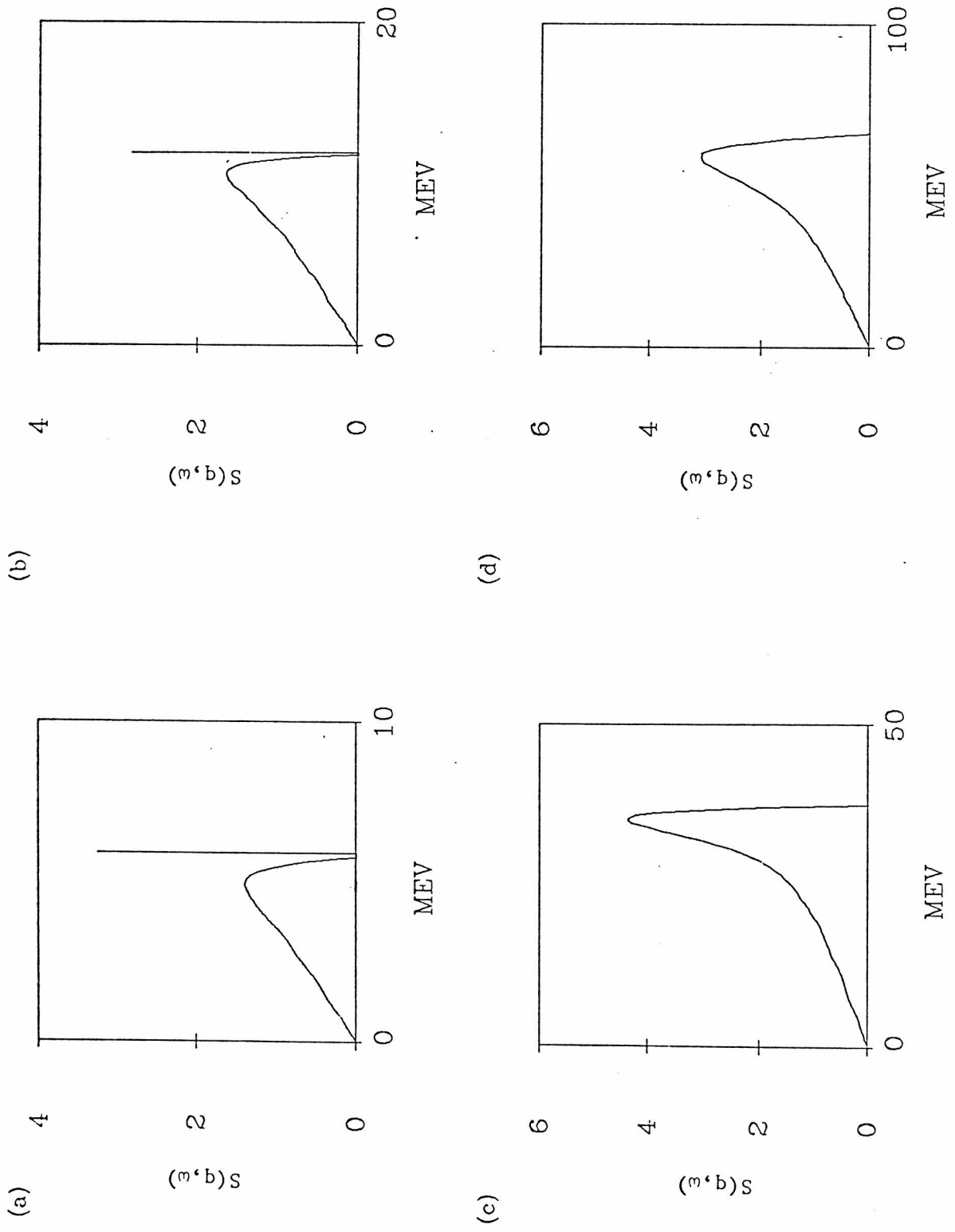
(a)
S(q,ω)
0
2
4
0
10
MEV
(b)
S(q,ω)
0
2
4
0
20
MEV
(c)
S(q,ω)
0
2
4
6
0
50
MEV
(d)
S(q,ω)
0
2
4
6
0
100
MEV

FIGURE 19

Figure 20

Evaluation of Local-Kernel Approximation

The local-kernel $S_2(q,\omega)$ (solid) is compared to the exact result (dashed) at the limit $q \to 0$ in (0,0) with the Gogny d1.

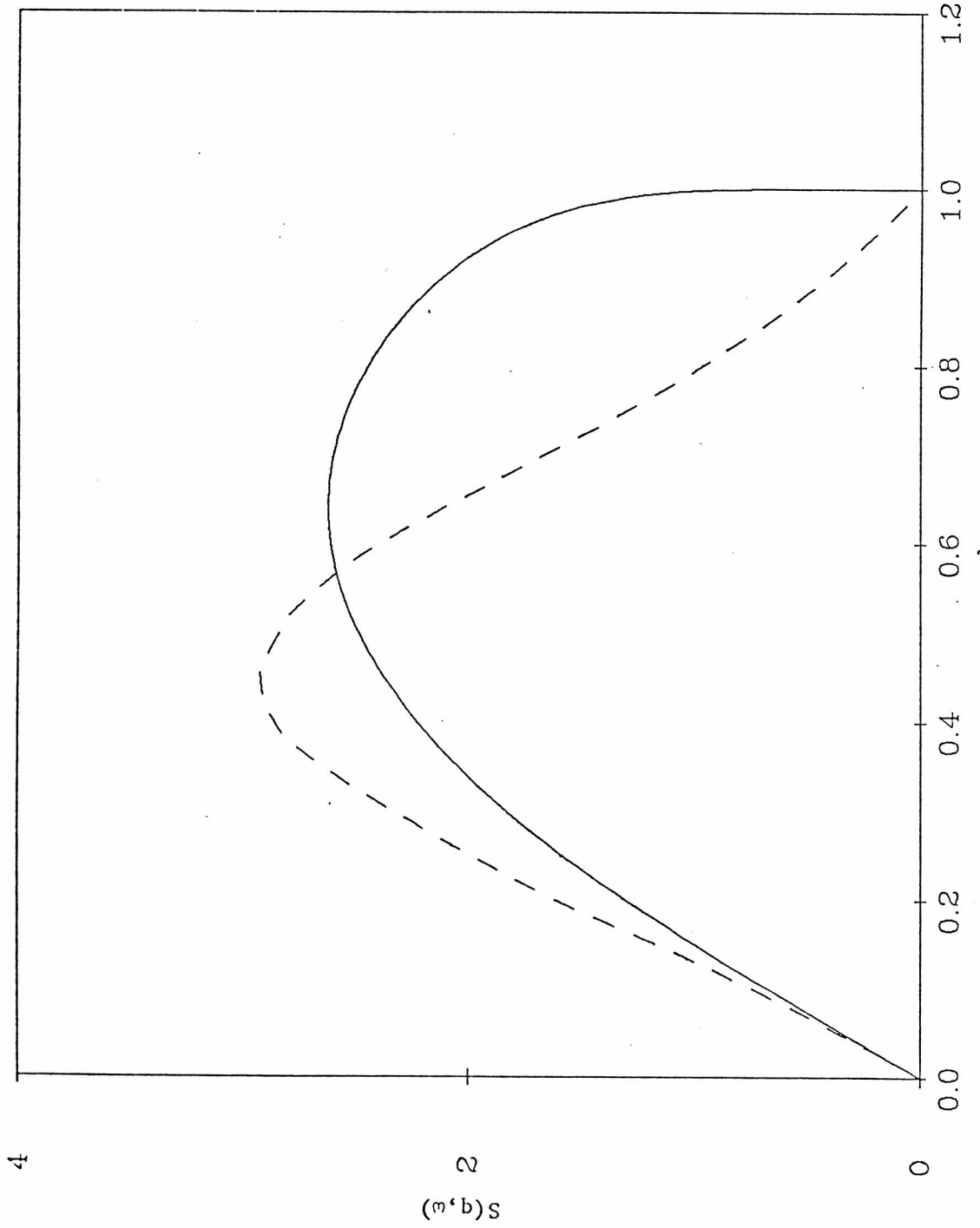

FIGURE 20

Figure 21

Evaluation of Local-Kernel-Approximation in (0,1)

$S_L(q,\omega)$ -- solid ; exact RPA $S(q,\omega)$ -- dashed.

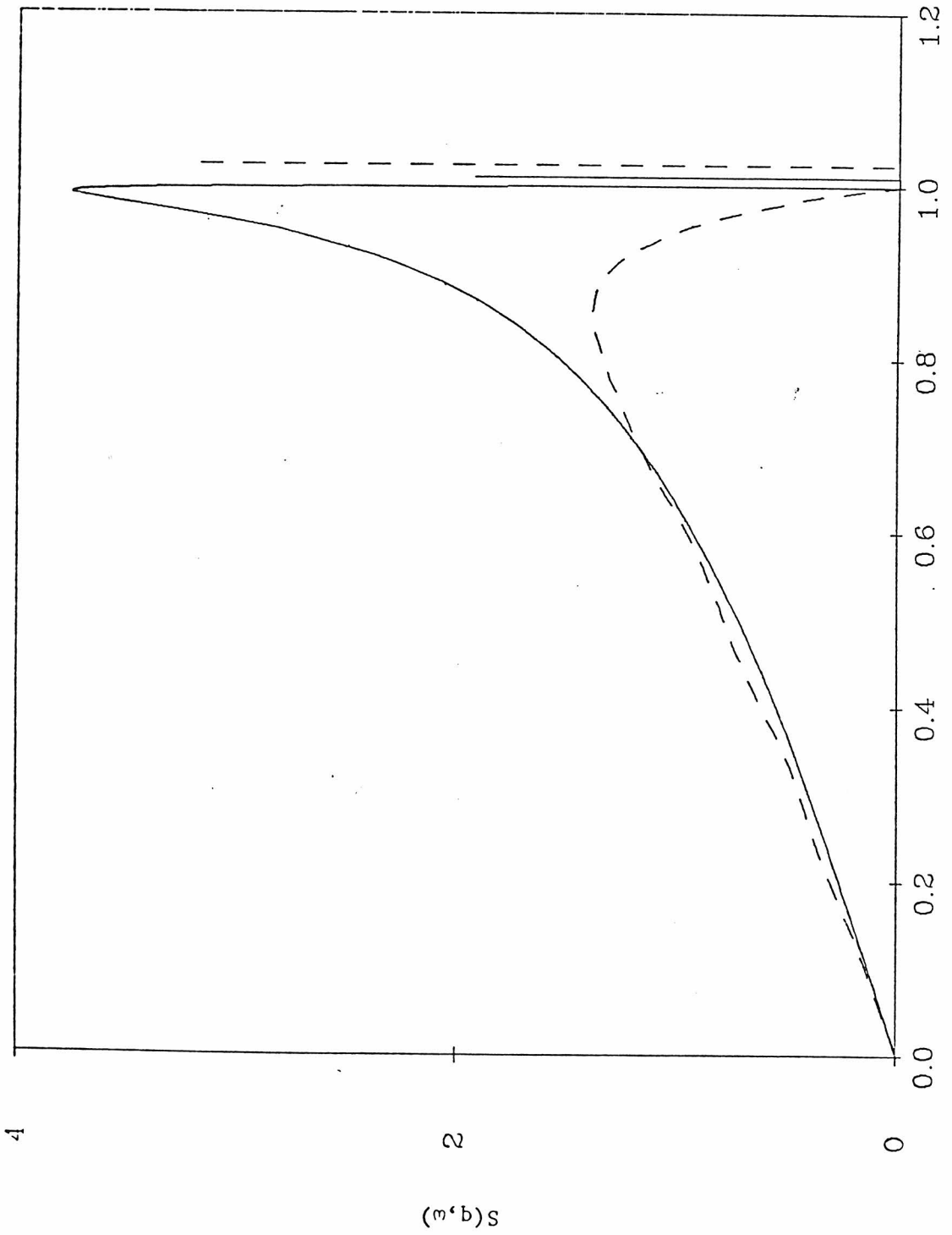

FIGURE 21

Figure 22

Results in (1,1) with Brown 1π-1ρ

The solid curve is the projection of $S(q,\omega)$ into the $\tilde{m}_s=0$ space and the dashed curve is the same for $\tilde{m}_s=1$ (or -1). The spike is set at $5x\frac{S_c}{\hbar\omega_c}$, $q=.1\ k_F$ and $f_\rho^2=4.86$.

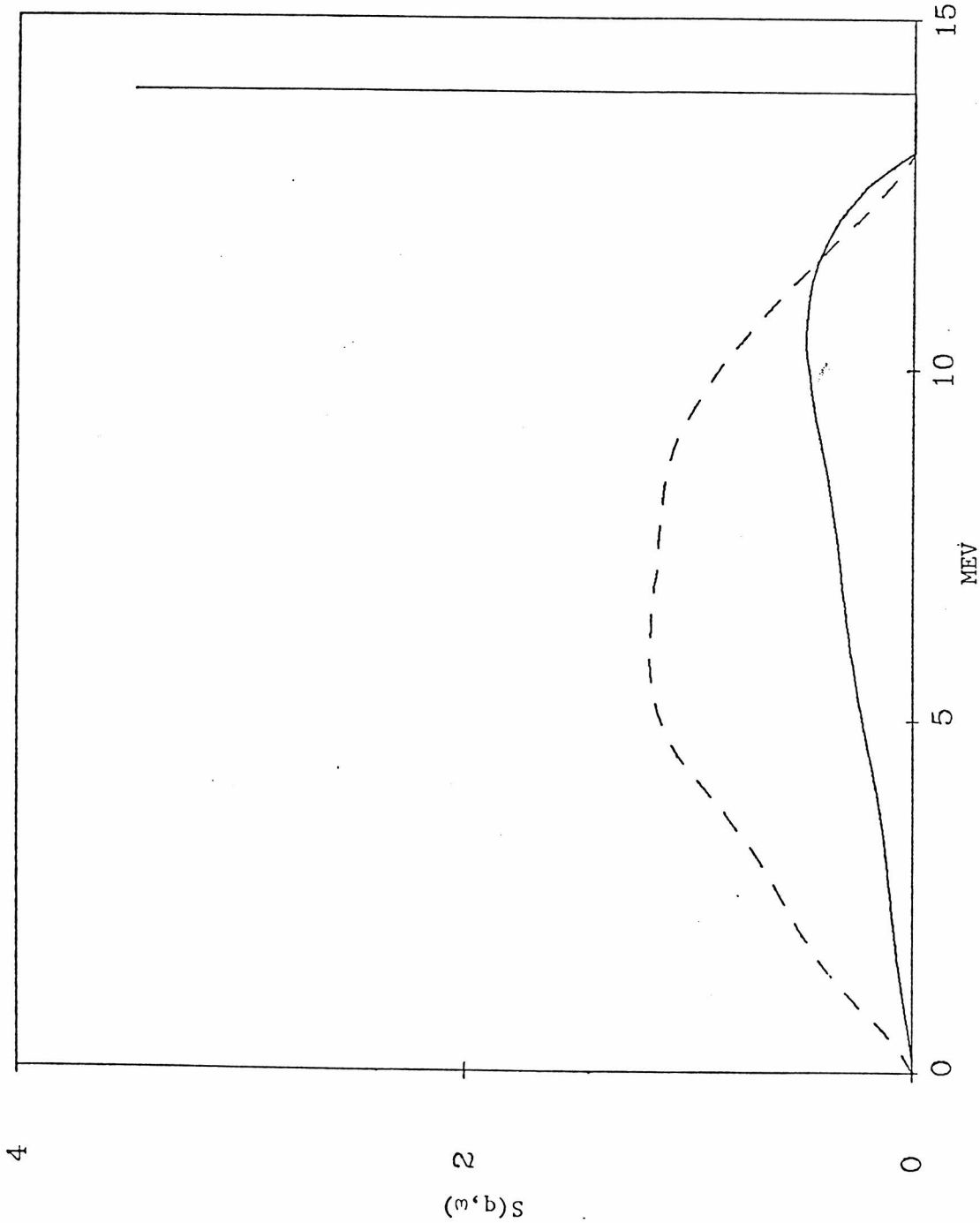

FIGURE 22

Figure 23

Results in (1,1) with Brown 1 π-1ρ

Except for $q = .5\ k_F$, all other labels are the same as for the previous figure.

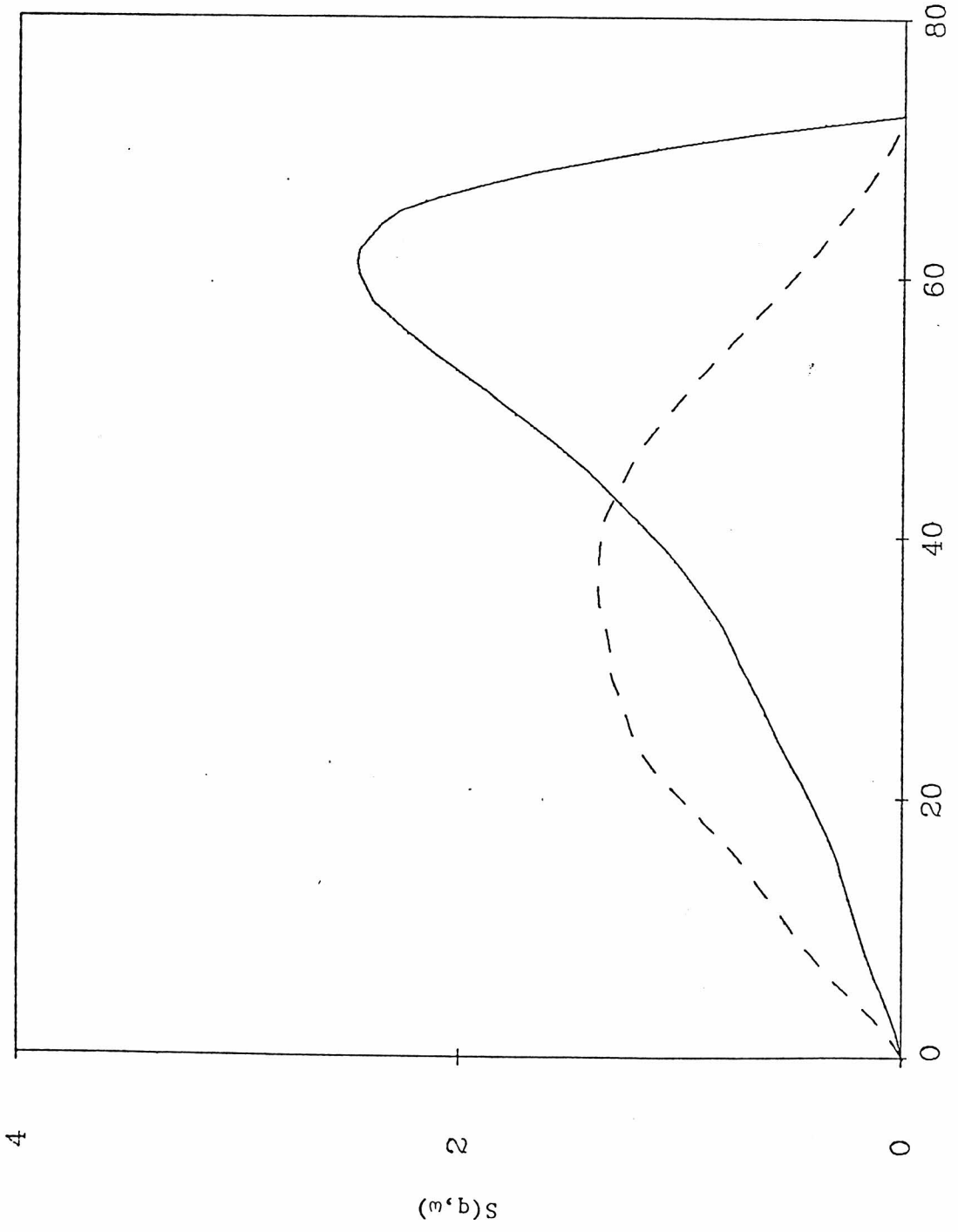

FIGURE 23

Figure 24

Results in (1,1) with Brown $1\pi-1\rho$

Here $f_\rho^2=1.86$ and $q=.1k_F$. Otherwise all labels are the same as for the previous figure.

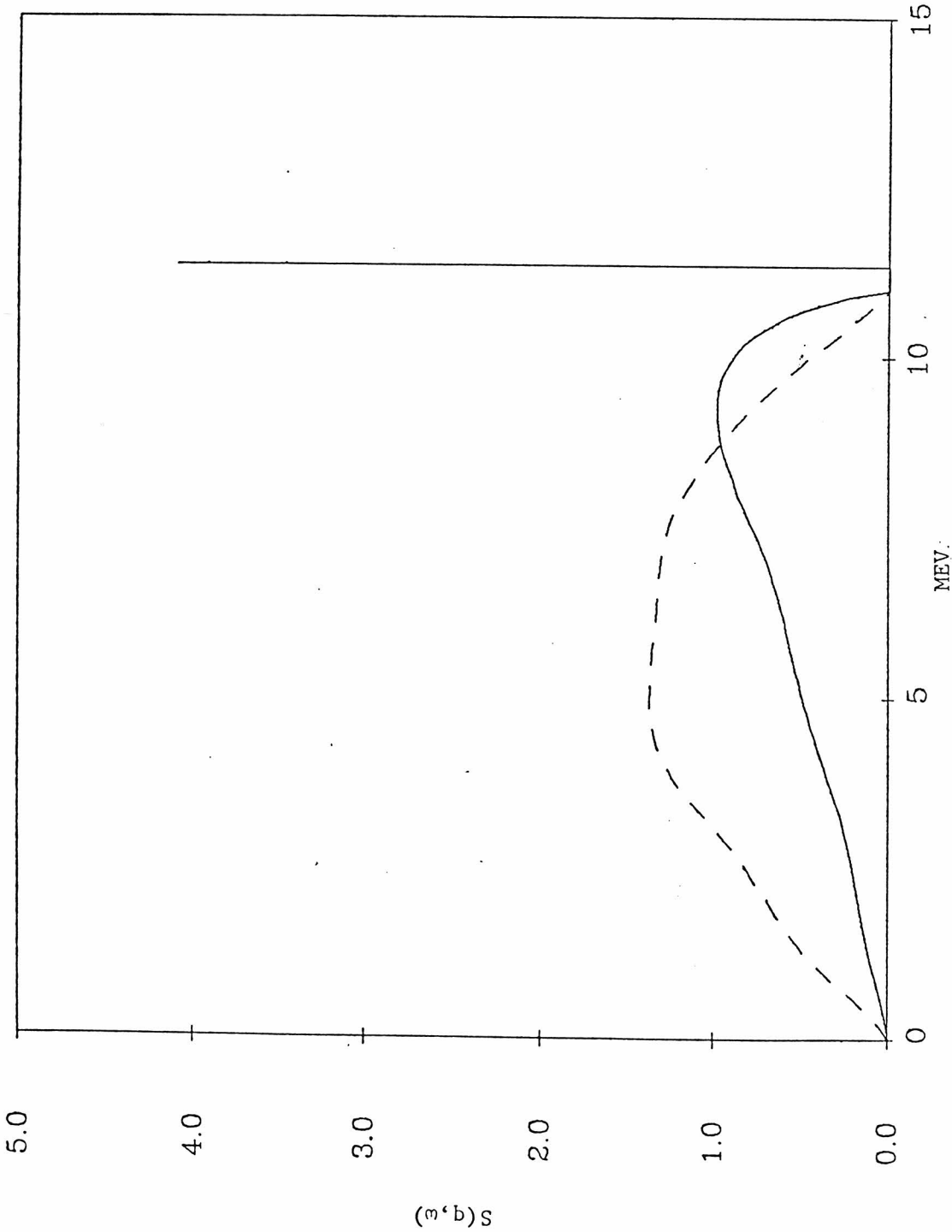

FIGURE 24

Figure 25

Results in (1,1) with Brown $1\pi-1\rho$

$q = .5\, k_F$. See the previous figure for explanation of symbols.

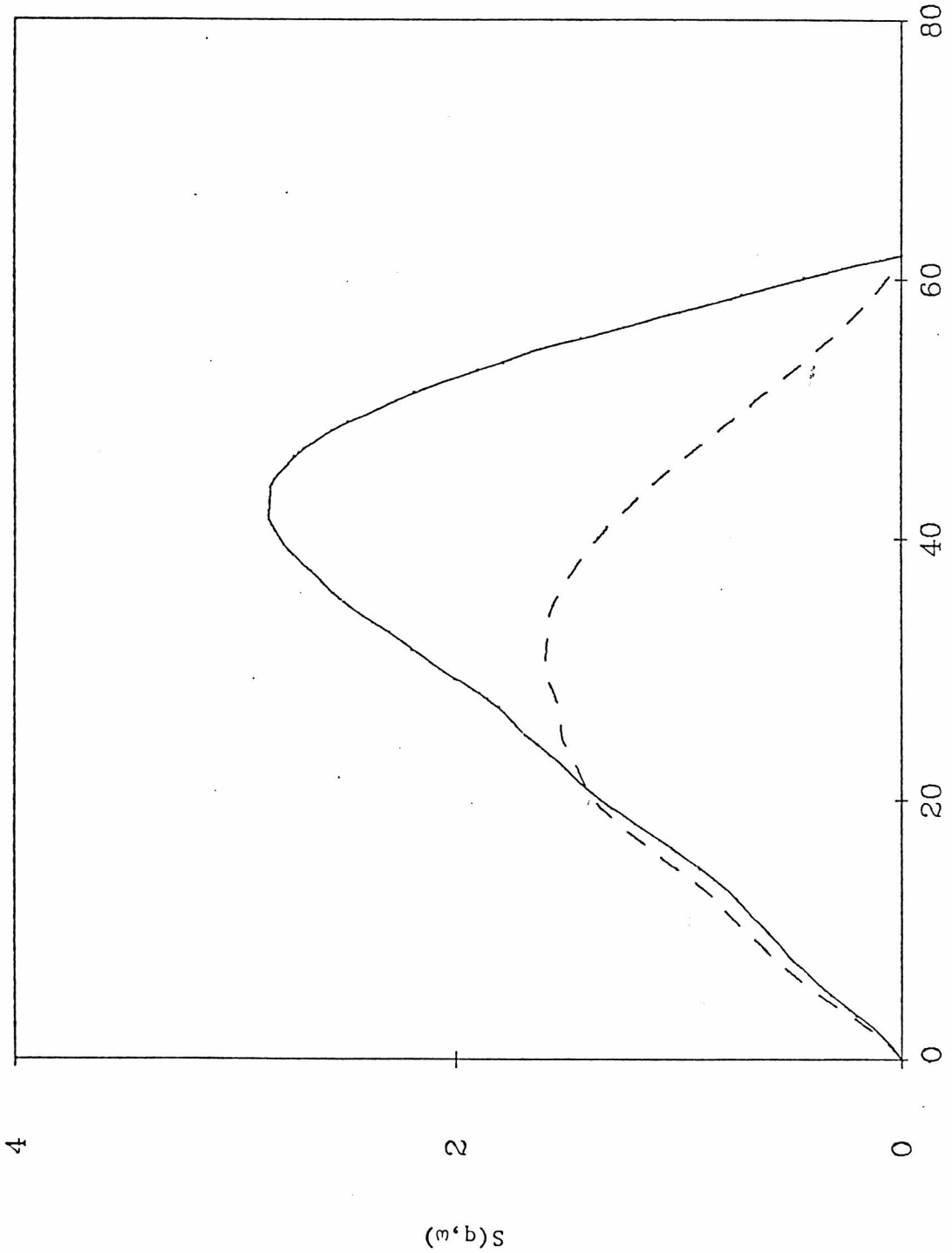

FIGURE 25

Figure 26

Cluster Diagrams

(a) $t = 12$ for this diagram.

(b) With an articulation point x, this graph is not allowed in the expansion for $g(12)$.

(c) Individually nodal, the chains form non-nodal graph.

(d) The singlest elementary graph.

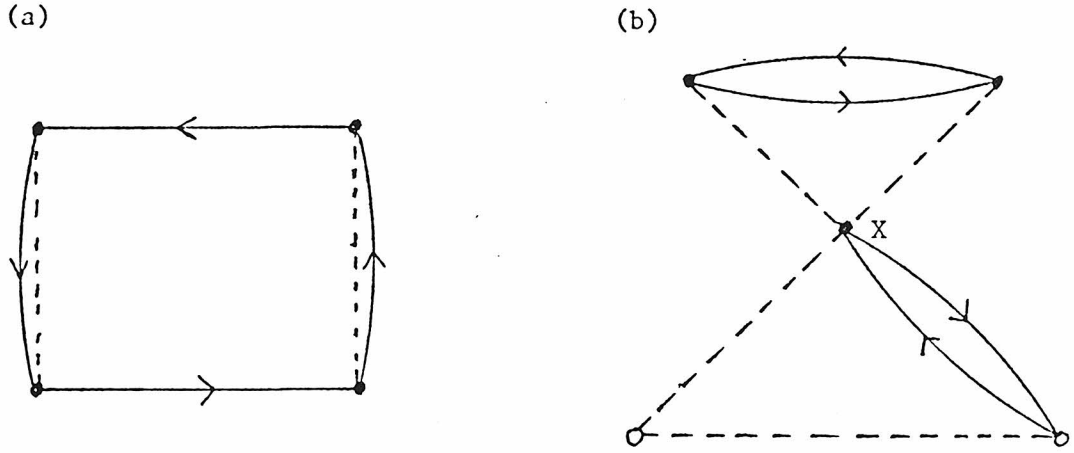

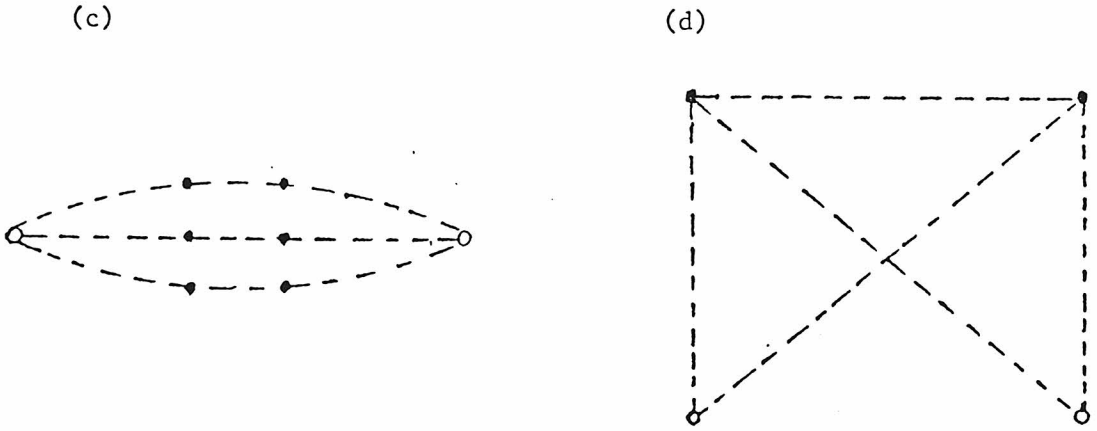

FIGURE 26

Figure 27

Cluster Diagrams

(a) Factorizable diagrams.

(b) A contribution to $V_h - V_h^{HF}$.

(a)

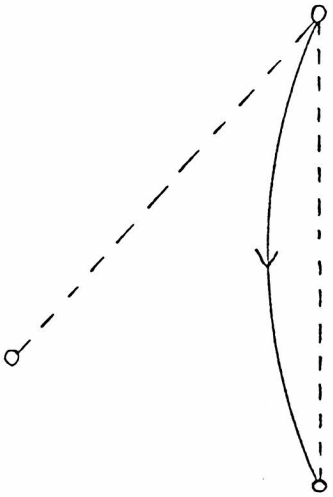

(b)

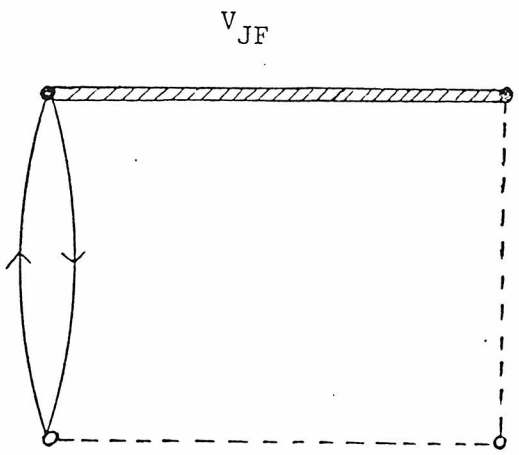

FIGURE 27

Figure 28

dd Distribution Functions

Γ_{dd} (solid) is used in FHNC while f^2 (dashed) is used in two-body calculations.

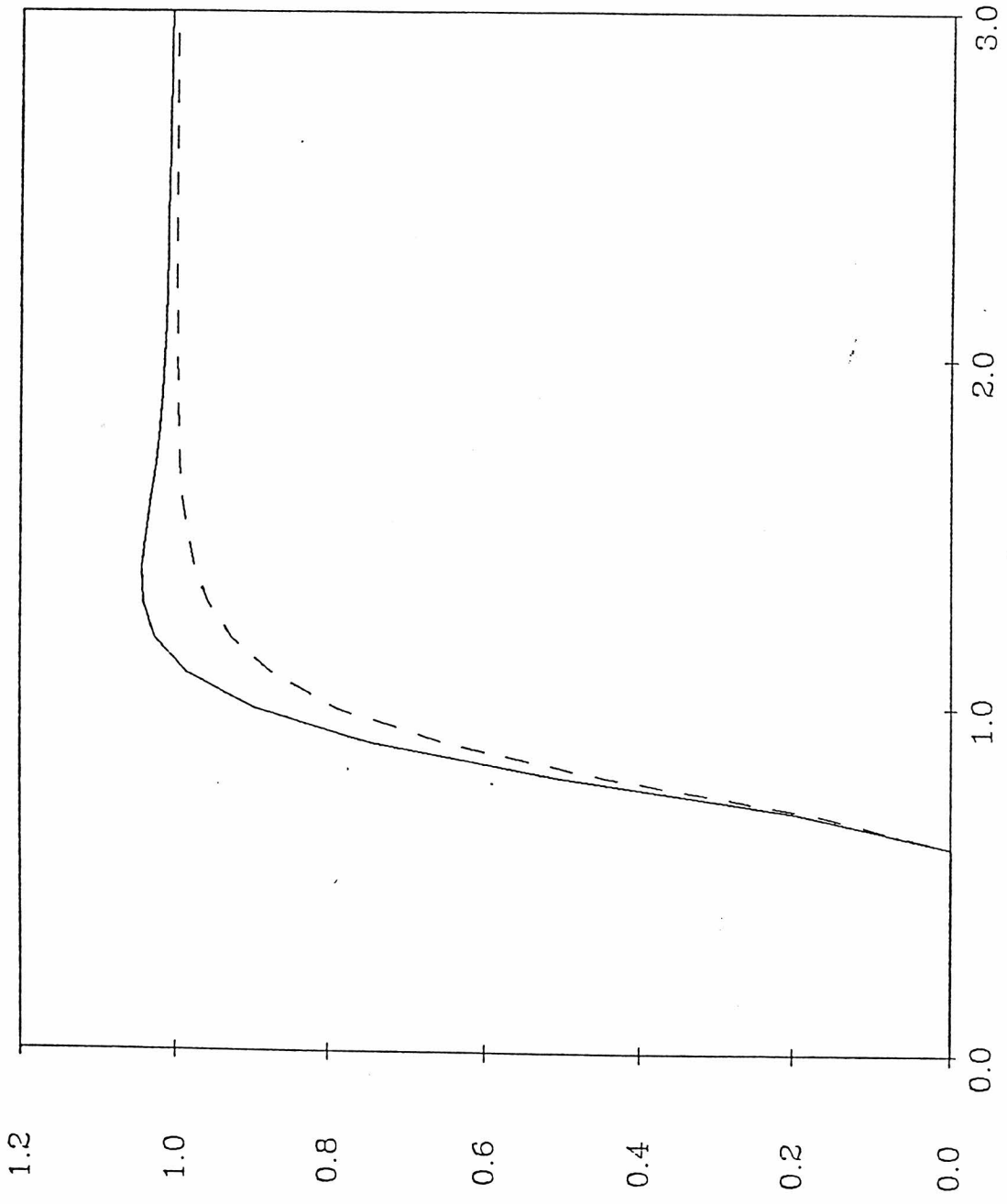

FIGURE 28

Figure 29

A Breakdown of $W(r)$

The highest solid line is $W(r)$. The lower solid curve and the dashed curve stand for $\Delta^2\Gamma_{dd}$ and Γ'_{dd} respectively. The dotted line is $V_h - V_h^{HF}$.

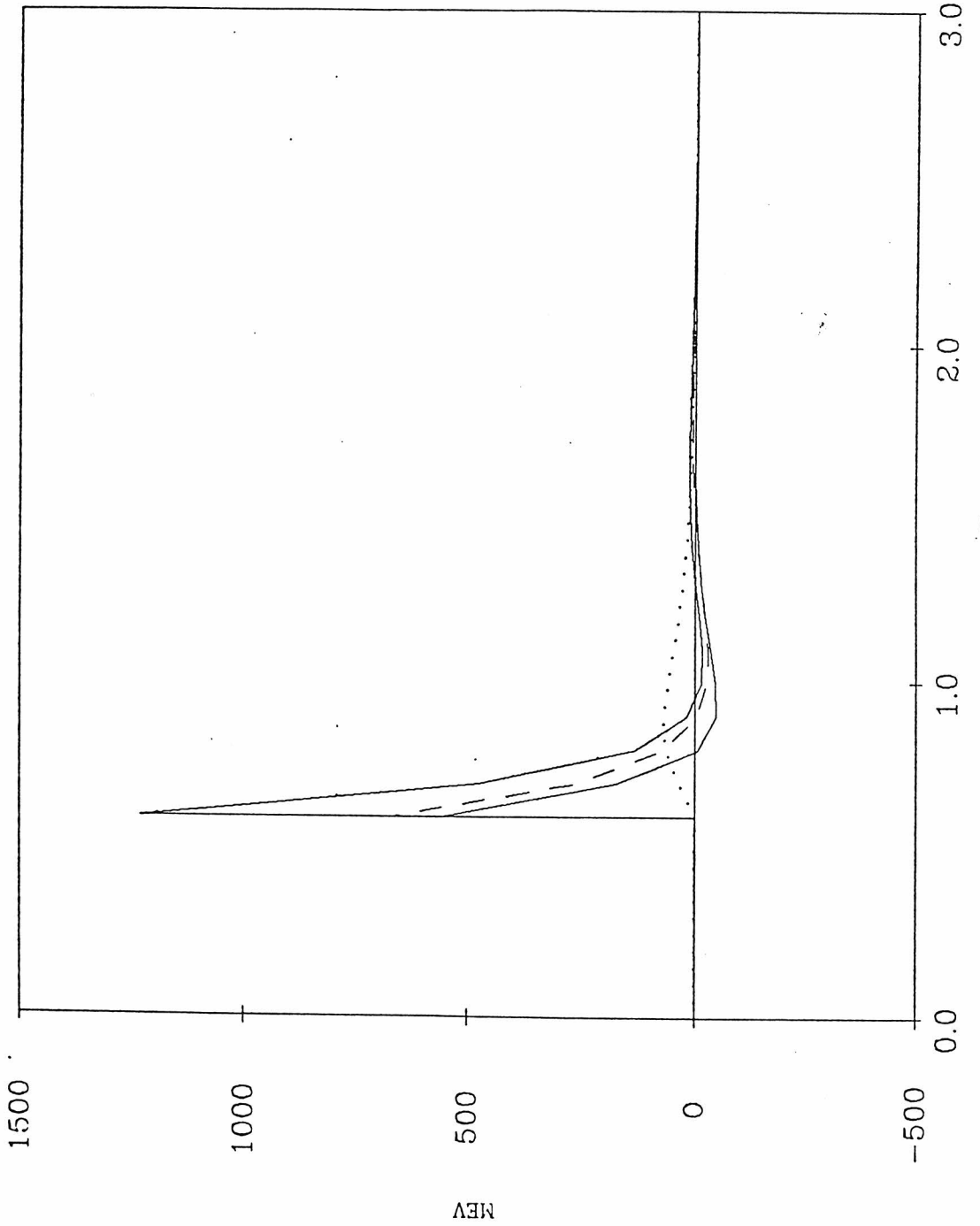

FIGURE 29

Figure 30

Comparison of Central Potentials

The 2-body radial potential : $\frac{\hbar^2}{m}|\nabla f|^2$ is compared to $W(r)$.

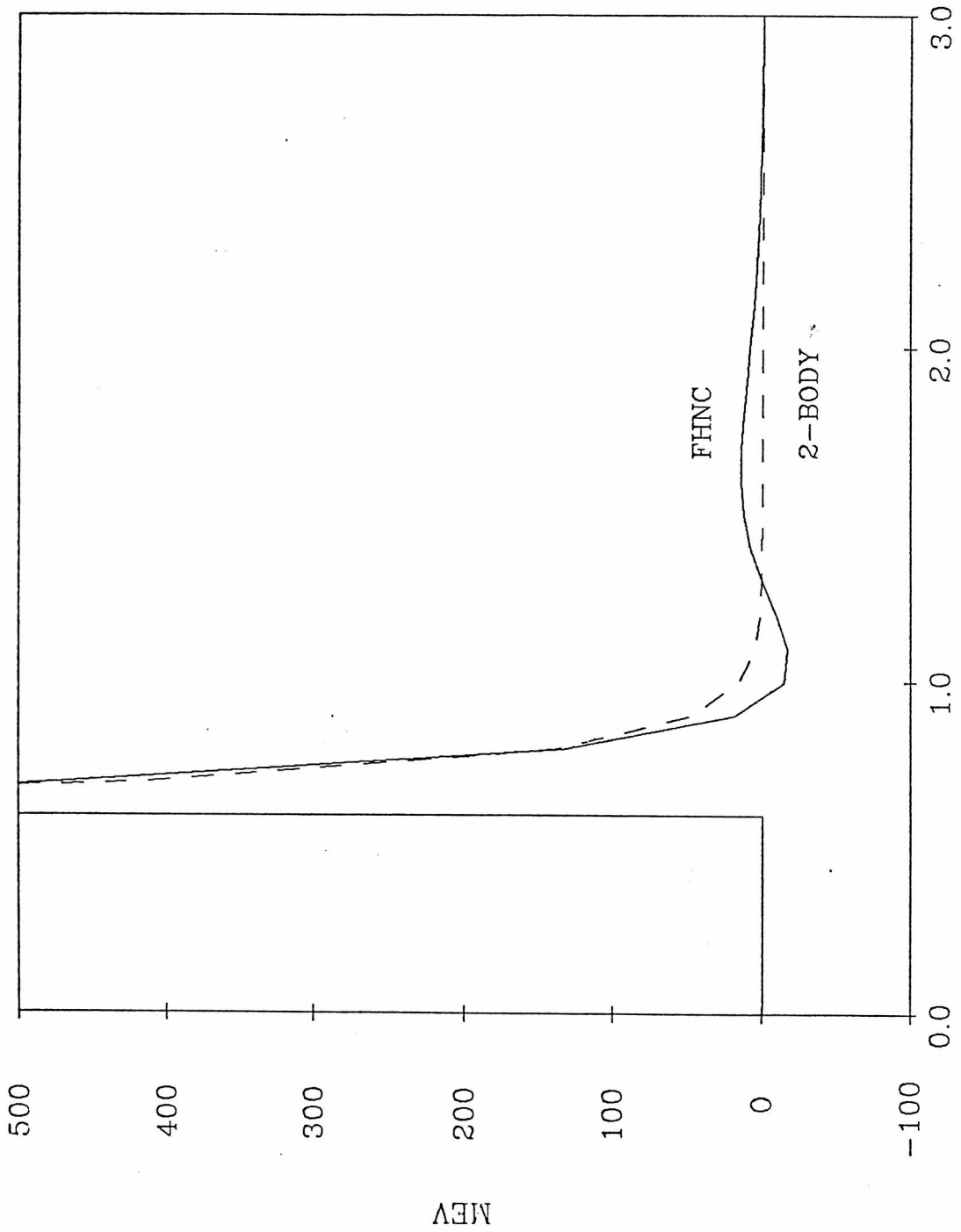

FIGURE 30

Figure 31

Particle-Hole Potentials in (0,0) with OMY

In this and the next three figures, the solid curves are FHNC curves and the dashed ones are 2-body approximations.

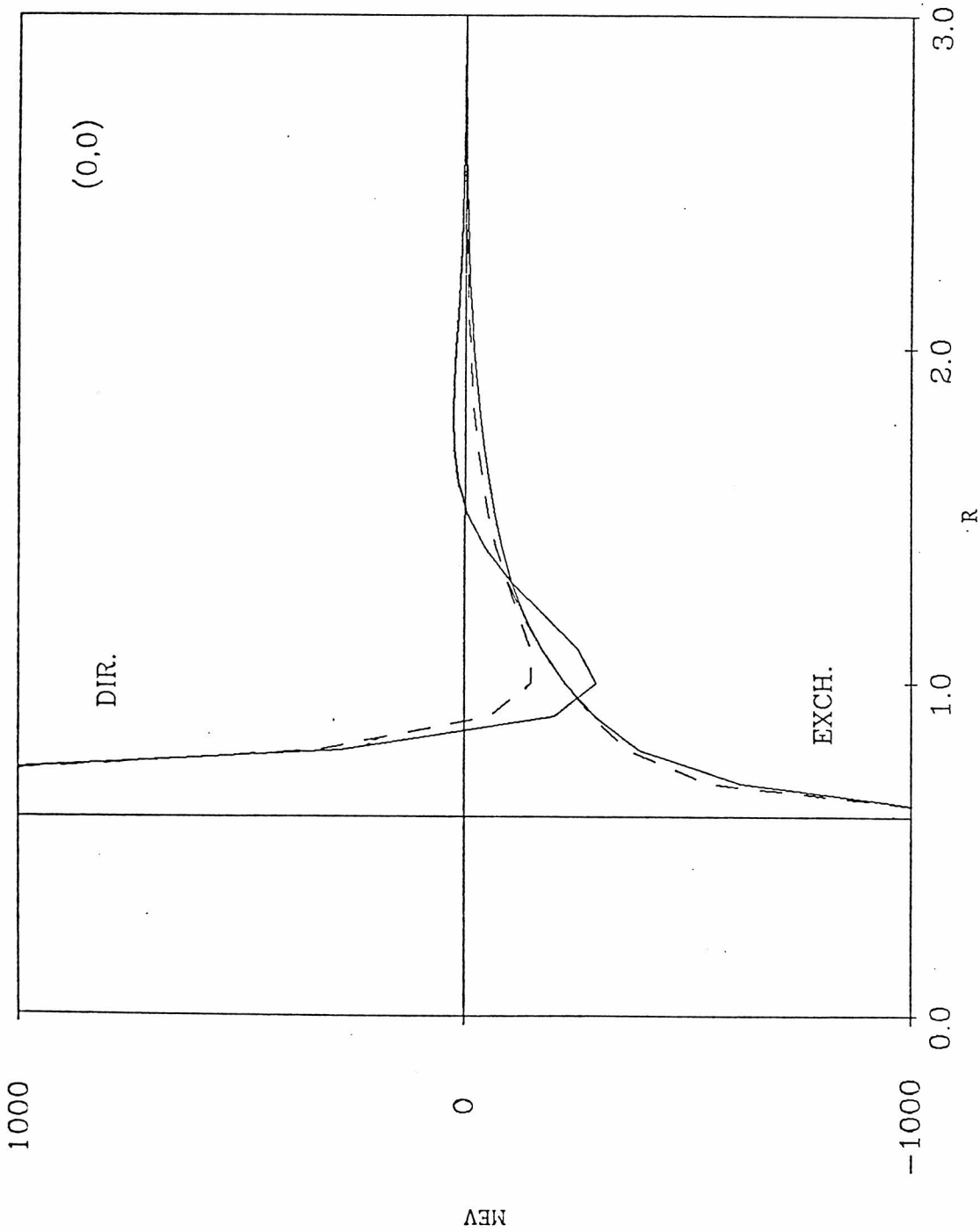

FIGURE 31

Figure 32

Particle-Hole Potentials in (0,1) with OMY

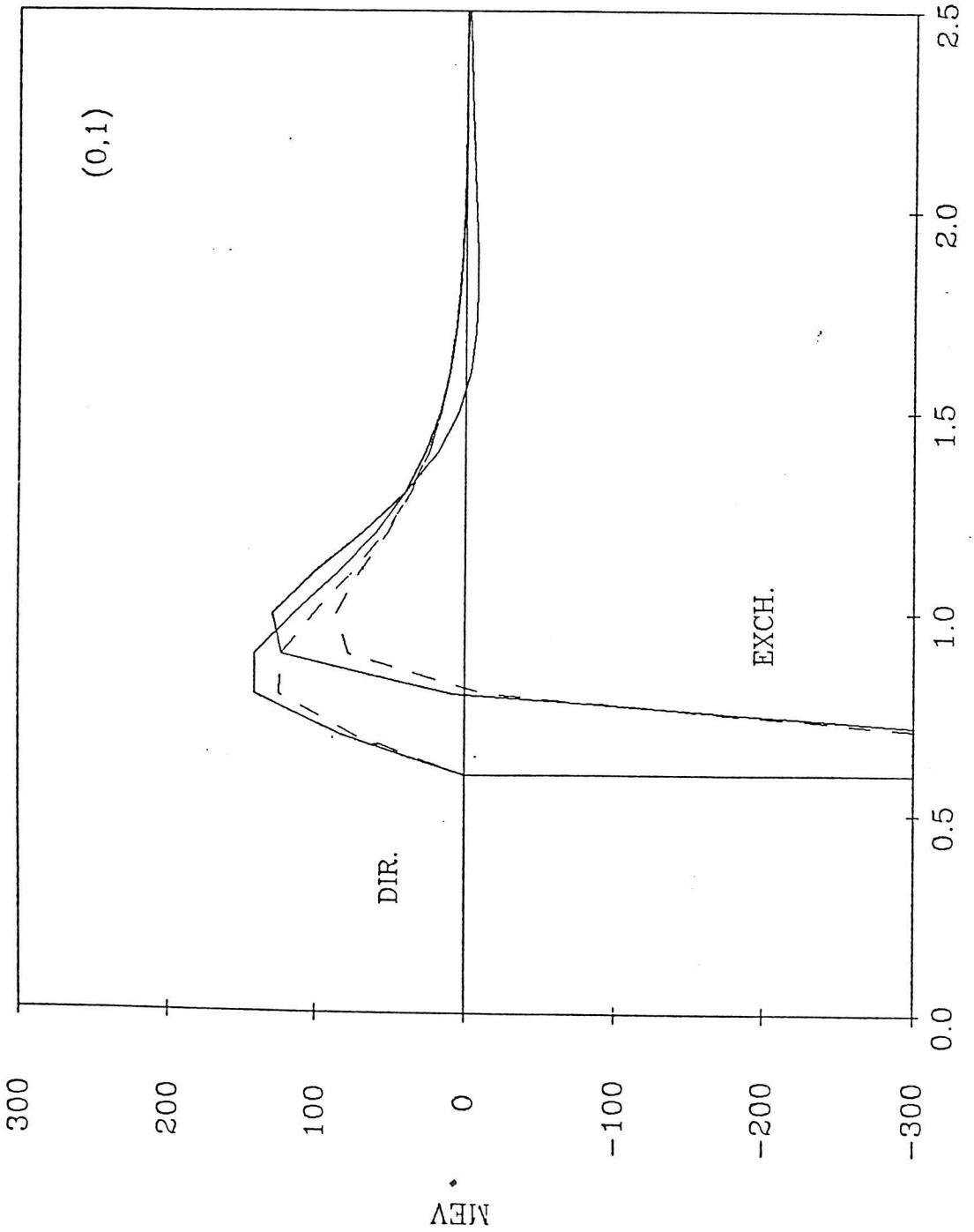

FIGURE 32

Figure 33

Particle-Hole Potentials in (1,0) with OMY

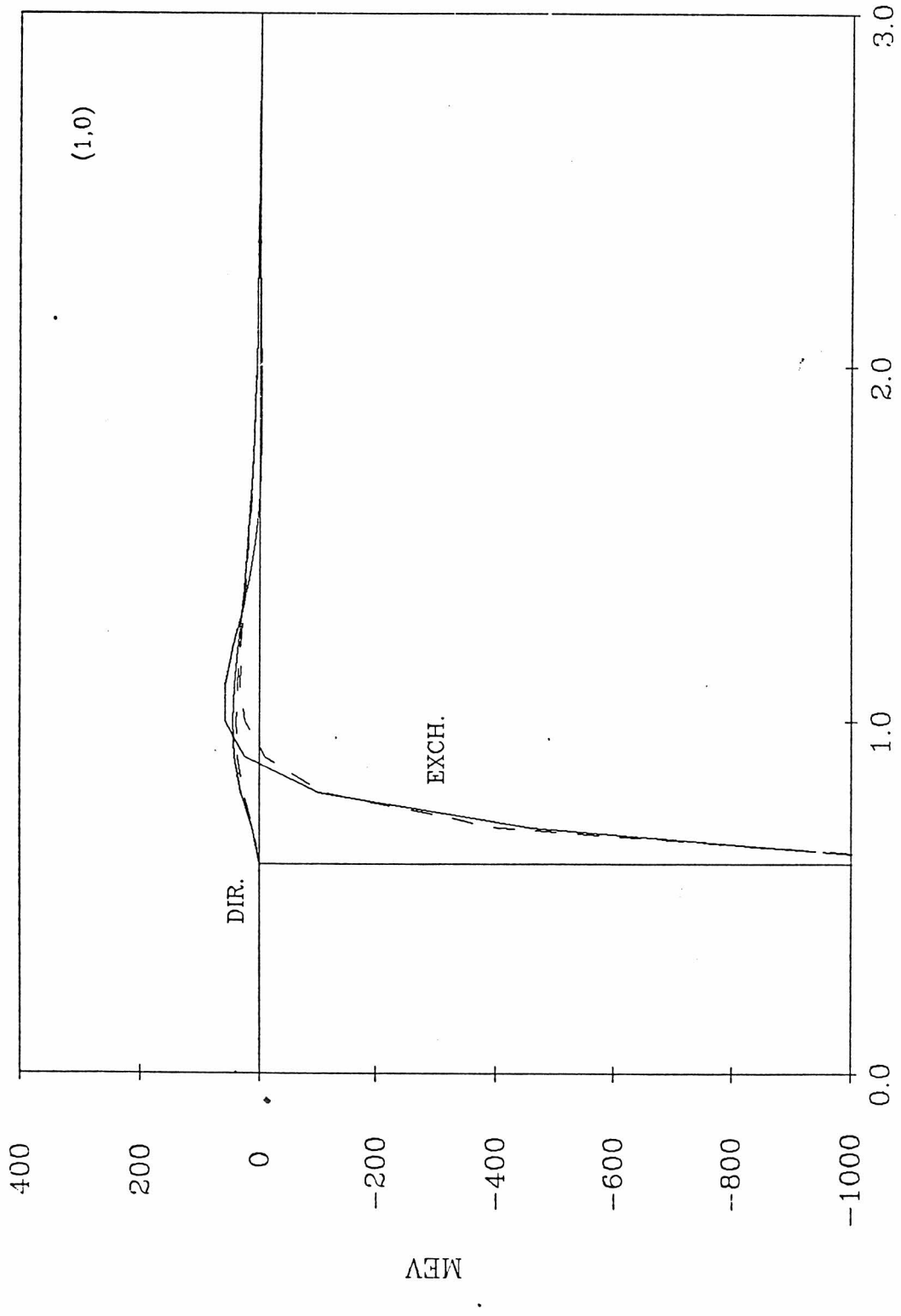

FIGURE 33

Figure 34

Particle-Hole Potentials in (1,1) with OMY

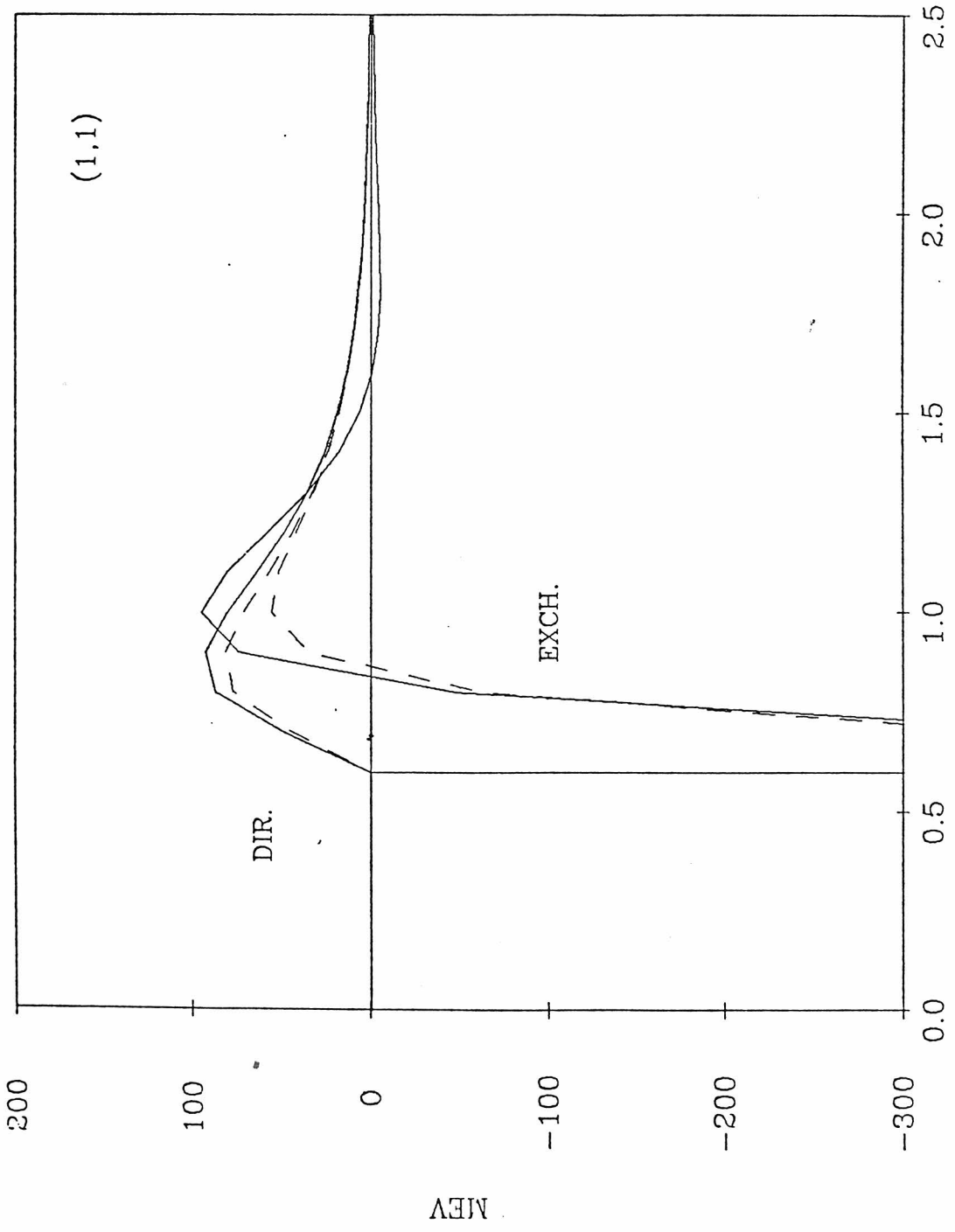

FIGURE 34

Figure 35

Comparison of 2-body and FHNC in (0,1)

In this and the next two figures, $q = .05\ k_F$ and the rule of assigning solid and dashed lines still applies.

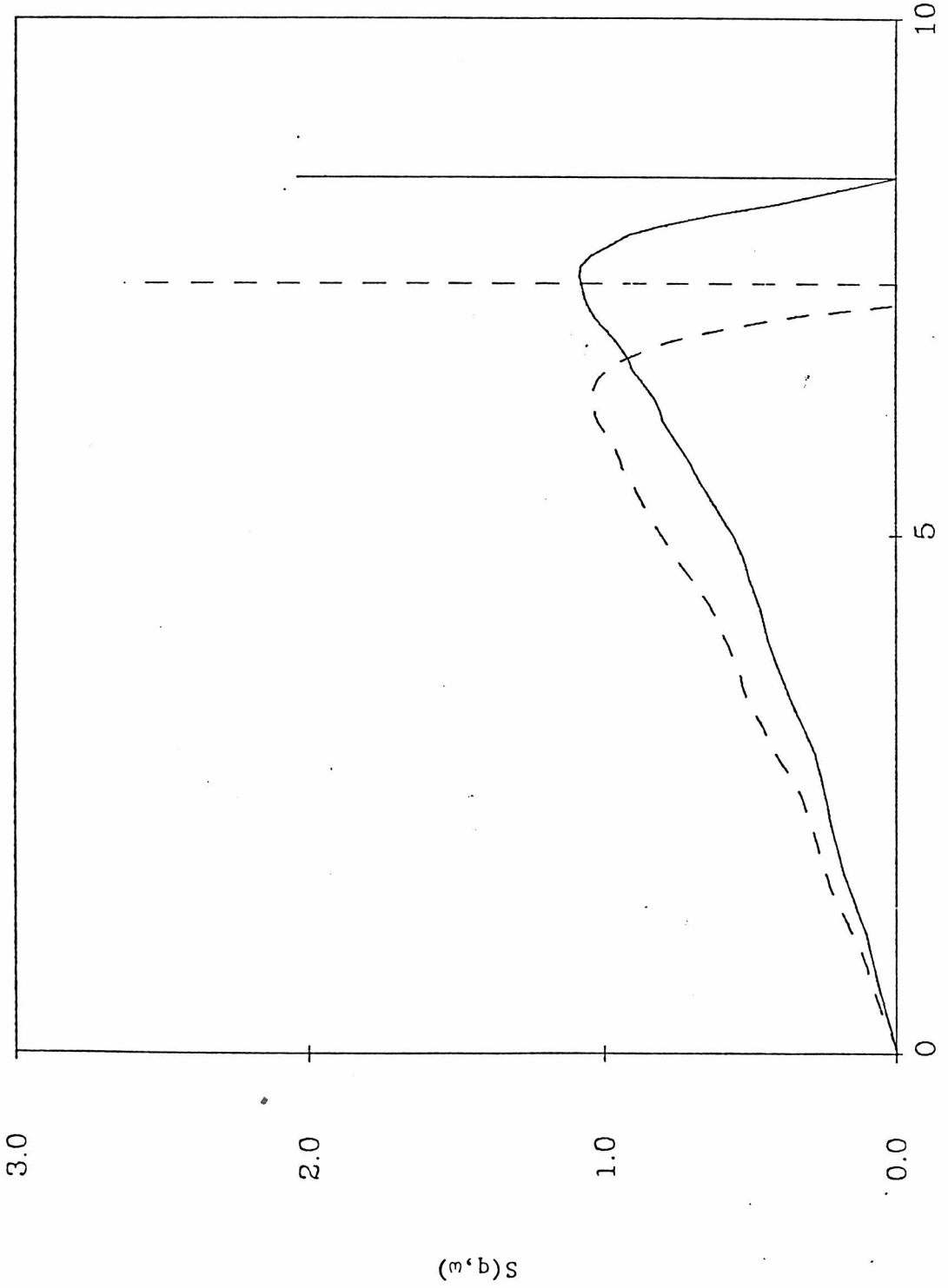

FIGURE 35

Figure 36

Comparison of 2-body and FHNC in (1,0)

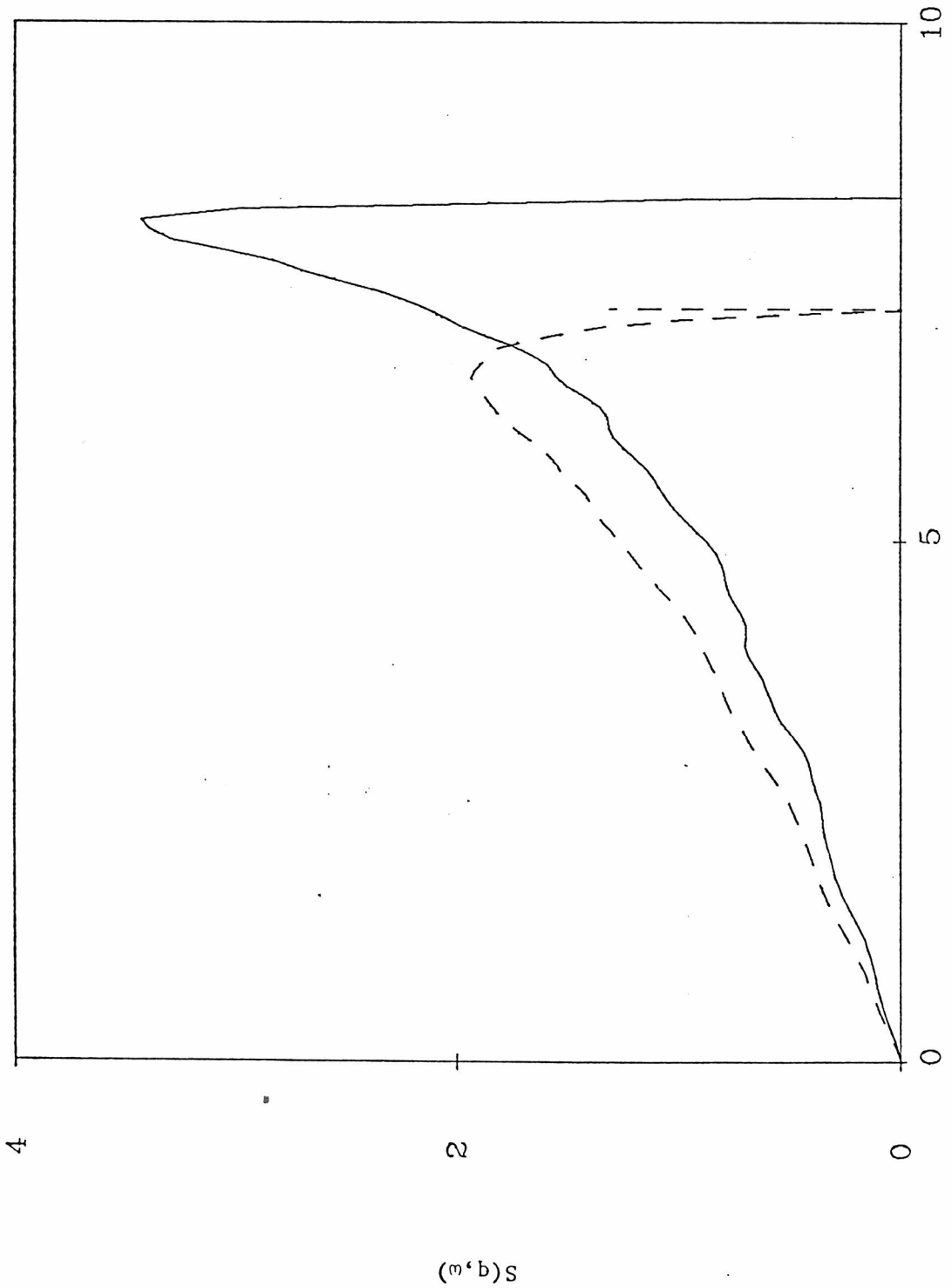

FIGURE 36

Figure 37

Comparison of 2-body and FHNC in (1,1)

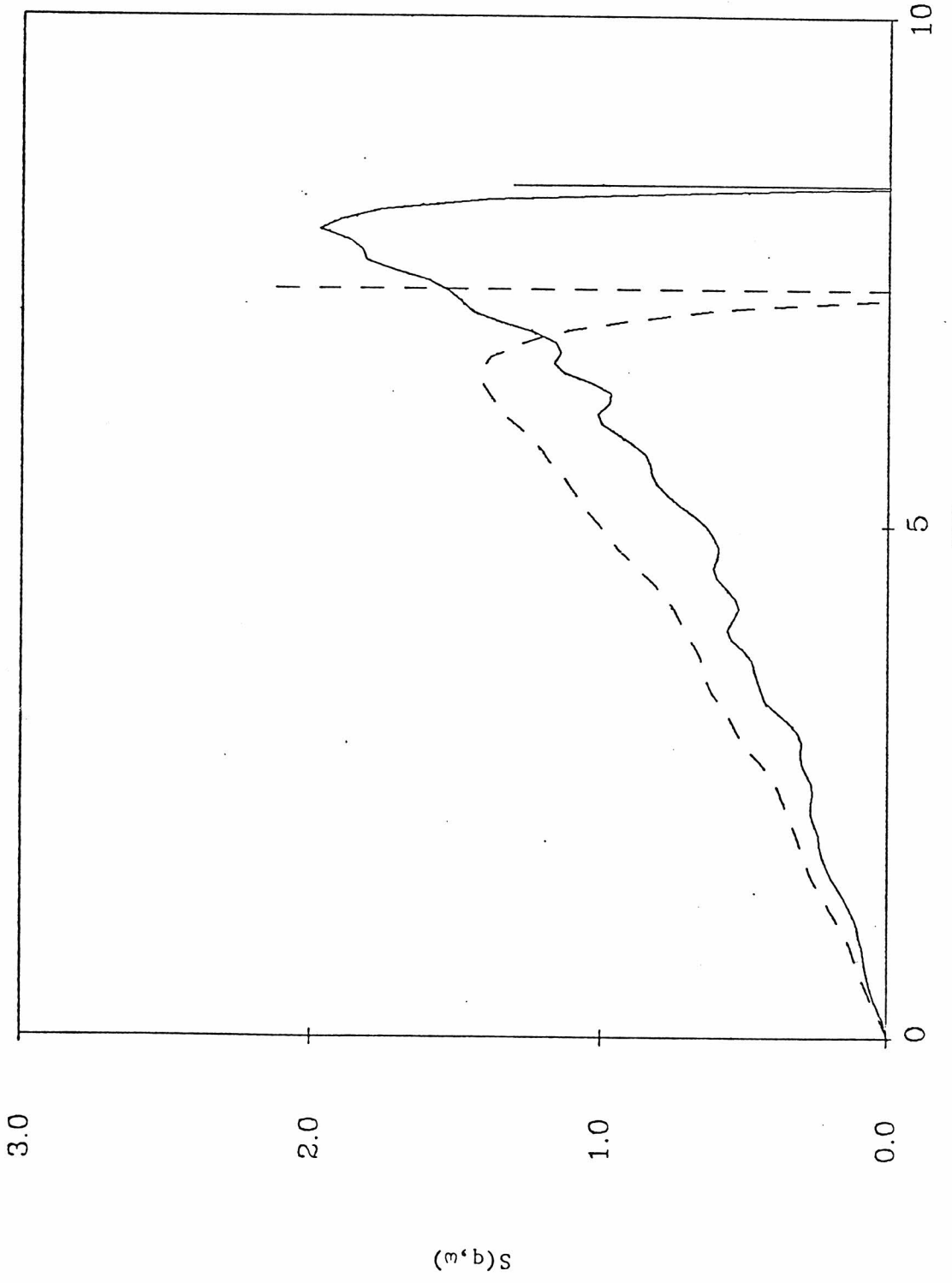

FIGURE 37